DOE/ID-10502

PM-ALPHA: A COMPUTER CODE FOR ADDRESSING THE PREMIXING OF STEAM EXPLOSIONS

W.W. Yuen and T.G. Theofanous

May 1995

Center for Risk Studies and Safety
Department of Chemical and Nuclear Engineering
University of California, Santa Barbara
Santa Barbara, CA 93106

Prepared for the
U. S. Department of Energy
Idaho Operations Office
Under ANL Subcontract No. 23572401

CRSS

ABSTRACT

This is a manual style documentation of computer code PM-ALPHA, developed for addressing the premixing phase of steam explosions. The documentation includes a description of the modelling approach, the complete formulation of the mathematical model, and all the details of the numerical solution procedure. Instructions for using the code, and a sample problem illustration are also provided.

The mathematical treatment is based on a general three-fluid model. The numerical treatment is rendered in two space dimensions (Cartesian or cylindrical geometry), and it allows for progressive changes in the fuel length scales, due to the processes of fragmentation and breakup. Verification and application aspects of the code are covered in a separate report.

TABLE OF CONTENTS

ABSTRACT iii
ACKNOWLEDGMENTS vii
NOMENCLATURE ix
1. INTRODUCTION 1-1
2. MODELLING APPROACH 2-1
3. MATHEMATICAL FORMULATION 3-1
3.1 Conservation Equations 3-1
3.2 Constitutive Laws 3-3
4. COMPUTATIONAL APPROACH AND NUMERICAL FORMULATION 4-1
4.1 General Numerical Approach 4-1
4.2 Basic Finite Difference Scheme 4-1
4.3 Numerical Formulation for Fuel and the Debris Equations 4-6
4.4 Implicit Coupling of the Liquid/Gas Continuity and Momentum 4-8
4.5 Numerical Formulation for the Liquid/Gas Energy Equations 4-15
4.6 Initial and Boundary Conditions 4-17
5. PROGRAM STRUCTURE AND CONTROL 5-1
5.1 Global Description 5-1
5.2 Description of Input Files 5-3
5.3 Description of Output Files 5-8
6. SAMPLE PROBLEM 6-1
7. REFERENCES 8-1
APPENDIX A. EFFECTIVE STEAM ABSORPTION IN AN ENCLOSURE A-1
APPENDIX B. EXCHANGE FACTORS FOR RADIATIVE HEAT TRANSFER . . . B-1
APPENDIX C. A HEAT CONDUCTION MODEL FOR FUEL PARTICLES C-1
APPENDIX D. SAMPLE PROBLEM INPUT DATA SET D-1
APPENDIX E. SAMPLE PROBLEM OUTPUT DATA SET E-1

ACKNOWLEDGEMENTS

The work on PM-ALPHA began under NRC sponsorship and continued after 1992 under DOE's ARSAP program (ANL subcontract No. 23572401). The authors are grateful to W. Pasedag and S. Sorrell for their cooperation and administrative/programmatic support, and to S. Additon for being available for intense technical interactions on all aspects of the ARSAP program at UCSB.

We are also pleased to acknowledge the contribution of Dr. W.H. Amarasooriya (SCIEN-TECH) who was responsible for PM-ALPHA during the early stages of development, and to Dr. S. Angelini, whose use of the code in conjunction with experiments in the MAGICO-2000 facility helped in both the development and verification efforts. The second author is also pleased to acknowledge the help and cooperation of Prof. W. Rivard on numerics of multiphase flows in general, through interactions that go back many years.

NOMENCLATURE

a	speed of sound, also absorption coefficient
A	dimensionless constant, Table 3.1, also area
A_{mn}	coefficients defined by Eqs. (4.28) to (4.31)
Ar	Archimedes number, Table 3.1
B	dimensionless constant, Table 3.1, constant in radiation model, Appendix A
B_k	coefficients defined by Eqs. (4.32) and (4.33)
Bo	Bond number, Eq. (3.75)
c_p	specific heat
C	dimensionless constant, Table 3.1, also normalization factor, Eq. (B34)
C_3	third radiation constant
C_d	drag coefficient
C_k	coefficients defined by Eqs. (4.34) and (4.35)
C_D	drag coefficient, Eqs. (3.16), (3.20), (3.21)
d	radiation model parameter, Eq. (A4)
d'	"modified" fuel diameter, Table 3.1
D	diameter, also residue
E	dimensionless constant, Table 3.1
E_d	empirical constant, Eq. (3.50)
$F(\vec{r},\vec{r}')$	radiative exchange factor, also dimensionless function, Appendix B
F_a	drag due to the added mass effect, Eq. (3.27)
F	interfacial friction factor, also dimensionless function, Appendix B
F^ℓ	laminar component of F
F^t	turbulent component of F
F_r	fragmentation rate
Fr	Froude number, Table 3.1
g	gravitational constant
$\mathbf{g}$	gravitational vector
gb	exchange factor between a volume element and an area element at the base wall
gg	exchange factor between volume elements
gs	exchange factor between a volume element and an area element at the side wall
gt	exchange factor between a volume element and an area element at the top wall
G	dimensionless function, Appendix B
h	specific enthalpy
h_c	convective heat transfer coefficient from fuel to liquid

H	dimensionless function, Appendix B
$H[J]$	Heaviside step function
I	specific internal energy
J	rate of mass transfer from liquid to gas (positive for evaporation)
J_m	characteristic mass transfer rate, Eq. (3.63)
k	thermal conductivity, absorption coefficient
$K_c(d')$	empirical function defined in Table 3.1
ℓ	length scale
L	total available fall distance, Eq. (3.79), also mean beam length
m_f	mass of one fuel particle
M	dimensionless constant, Table 3.1
n	number density
Nu_{fb}	Nusselt number for forced convective film boiling
Nu_p	Nusselt number for pool film boiling
p	pressure
Pr	Prandtl number
Q	scaler quantity
$\dot{q}$	interfacial convective heat transfer
$\dot{q}_r$	radiative heat transfer
$\dot{q}_a$	radiative self absorption
r	radial coordinate
R	dimensionless viscosity density ratio, interfacial heat transfer function
Re	Reynolds number
Re'	effective Reynolds number, Eq. (3.26)
Re''	effective Reynolds number, Eq. (3.46)
$\dot{S}$	source term for interfacial area transport
Sc	dimensionless subcooling parameter, Table 3.1
Sc'	modified dimensionless subcooling parameter, Table 3.1
Sc^*	modified dimensionless subcooling parameter, Table 3.1
Sp	dimensionless superheat parameter, Table 3.1
Sp'	modified dimensionless superheat parameter, Table 3.1
t	time
t_f	characteristic time for the complete fragmentation of one fuel particle
t_f^*	dimensionless complete fragmentation time of one fuel particle, Eq. (3.74)
T	temperature
$\hat{T}$	estimated advanced temperature

u	radial velocity (or horizontal in Cartesian coordinates)
$\mathbf{u}$	velocity vector
v	axial velocity (or vertical in Cartesian coordinates)
V	volume
We	Weber number
z	axial coordinate

Greek

α	void fraction
α^*	void fraction to switch from liquid iteration to vapor iteration
β	correlation constant in fuel fragmentation model, Eq. (3.74), also Eq. (3.79) also angular variable
δr	grid size in radial direction
δt	time step
δz	grid size in axial direction
ϵ	density ratio (ρ_f/ρ_i, $i = \ell$ or g) or convergence parameter
η	dimensionless integration variable, Appendix B
θ	volume fraction, also angular variable
λ	wavelength
λ_{max}	wavelength at which the Planck function is a miximum at T_f, Eq. (3.52)
μ	viscosity
ν	kinematic viscosity, also wave number in Appendix A
ρ	microscopic density
ρ'	macroscopic density, Eq. (3.1)
σ	Stefan-Boltzman constant, surface tension
τ	optical thickness, Eq. (B.45)
τ_e	time constant to bring the liquid to saturation, Eq. (3.63)
τ_g	time constant to bring the gas to equilibrium, Eq. (3.61)
τ_ℓ	time constant to bring the liquid to equilibrium, Eq. (3.62)
ϕ	"correction" factor to two-phase correlations due to presence of a third phase, Eq. (3.15),
ω	wave number

Subscript

a	absorption
b	breakup, also boiling
db	debris

e	emission
ex	exiting quantity
f	fuel, also fragmentation
fc	forced convection
g	vapor(steam)
i	instantaneous value
ij	between components i and j
i,j	grid location i,j
ℓ	liquid
m	minimum
s	interface, saturation
w	wall

Superscript

n	time step n

1. INTRODUCTION

This report presents the first formal documentation of the computer code PM-ALPHA, and is to serve also as a user's manual for it. The code is intended to simulate the premixing of steam explosions; that is, the thermohydraulic transient associated with the pouring of a high temperature melt into a pool of coolant (water, in the current version of the code). The result of main interest is mixing zone compositions and associated length scales. These compositions are expressed as volume fraction distribution maps, evolving in time. The resultant distributions can be used, with an appropriate trigger, in an escalation/propagation code, to compute a steam explosion. One such code is ESPROSE.m, documented in a companion report (DOE/ID 10501). In addition to the melt and coolant distribution, premixture constituents include coolant vapor and solidified melt particles produced as a result of the melt-coolant interaction. The vapor (void) introduces compressibility, which can affect both triggerability and propagation, while the quantity of solidified melt is important in that it cannot participate in the explosion.

PM-ALPHA is based on a multifield Eulerian treatment. There are three continuous fields (melt, coolant, and vapor—we call them fuel, liquid, and gas or fuel, water, and steam respectively). The mathematical formulation is given in Chapter 3, and the physical model from which it is derived is described in Chapter 2. The numerical model is rendered in two space dimensions with axial or planar symmetry—cylindrical (r,z) or Cartesian (x,z) geometries respectively—and is based on a special implementation of the well known ICE (Implicit, Continuous, Eulerian) method. This method is used to couple semi-implicitly the liquid and gas fields, while the fuel field is incorporated explicitly. The computational approach and detailed numerical formulation are provided in Chapter 4, while an overview of the computer program implementation (structure and control) is given in Chapter 5. The analysis of a sample problem with the code is presented in Chapter 6. Inputs and outputs for this sample run can be found in Appendices D and E respectively. Let us conclude this introduction by putting PM-ALPHA in the integral steam explosion assessment context.

The overall approach, with PM-ALPHA as one of the key elements, to assessing steam explosions in severe reactor accidents has been summarized by Theofanous et al. (1995). It involves a methodology, as outlined in Appendix A of Theofanous et al. (1994), and a set of codes, as illustrated in Table 1.1. With the exception of THIRMAL and ANACAPA/ABAQUS, the documents in this table should be studied in conjunction with each other. The following orientation-related remarks are offered.

1. The lead document (DOE/ID-10489) serves as an introduction to the problem and the analytical approach. Accordingly, it provides a discussion of the key physics, including previous literature and terminology, as well as sample results from PM-ALPHA and ESPROSE.m.

2. The type of analysis needed to assess melt pour conditions, the methodological framework employed in the utilization of these results, and the tie-in to the premixing calculations can be found in the two actual applications carried out so far, as listed under "initial conditions" in Table 1.1.

3. The manuals are restricted to documenting the codes and describing the mechanics of running them. The verification reports contain comparisons with analytical and experimental results that test key features of both the mathematical formulation and the numerical implementation. In addition to perspectives on strengths and limitations of the simulations, these special applications provide guidance (to the potential user) on how the codes are to be applied to various situations.

4. A full demonstration of the assessment methodology, including use of the simulation tools, is given in the two documents listed under "integration/application" in Table 1.1. Moreover, a first *ad hoc* demonstration of cavity (concrete) structural response under ESPROSE.m loads can be found in Rashid et al. (1995). Consideration of the above-listed material in its totality is crucial in appreciating the nature of the uncertainties involved, both in specifying initial conditions and in deploying the codes, as well as in gaining some perspectives on how one can compensate for these uncertainties. However, this material may not provide adequate guidance for other, new, applications; thus extreme caution needs to be exercised while broadening this experience base.

It should be noted that all these codes could be coupled into one computational package and, in fact, PM-ALPHA and ESPROSE.m could be condensed into one code. We have intentionally refrained from doing that. Besides better transparency and convenience in describing these tools independently, this is consistent with the ROAAM approach (Theofanous et al., 1995) in isolating the key physics and decomposing the problem in terms of these physics using a probabilistic framework.

Table 1.1 Steam Explosion Energetics and Structural Damage Potential

Introductory and Overall Approach		The Study–DOE/ID-10489[1]
Topical Element	**Codes**	**Documents**
Initial Conditions	Special Purpose Models	In-Vessel SE: DOE/ID-10505[2] Ex-Vessel SE: DOE/ID-10506[3]
Premixing	PM-ALPHA	Manual: DOE/ID-10502[4] Verification: DOE/ID-10504[5]
	THIRMAL	Manual: EPRI TR-103417[6]
Propagation	ESPROSE.m	Manual: DOE/ID-10501[7] Verification: DOE/ID-10503[8]
Structural Response	ANACAP-3D/ABAQUS	Manual:[9] Verification: ANA-89-0094[10]
Integration/Application		In-Vessel SE: DOE/ID-10505[2] Ex-Vessel SE: DOE/ID-10506[3]

(1) T.G. Theofanous, W.W. Yuen, S. Angelini and X. Chen, "The Study of Steam Explosions in Nuclear Systems," DOE/ID-10489, January 1995.

(2) T.G. Theofanous, W.W. Yuen, J.J. Sienicki and C.C. Chu, "The probability of a reactor pressure vessel failure by steam explosions in an AP600-like design," DOE/ID-10505.

(3) T.G. Theofanous, W.W. Yuen, J.J. Sienicki and C.C. Chu, "The probability of containment failure by steam explosions in an SBWR-like lower drywell," DOE/ID-10506.

(4) W.W. Yuen and T.G. Theofanous, "PM-ALPHA: A computer code for assessing the premixing of steam explosions," DOE/ID-10502.

(5) T.G. Theofanous and W.W. Yuen, "Premixing of steam explosions: PM-ALPHA verification studies," DOE/ID-10504.

(6) THIRMAL-1 Computer code for analysis of interactions between a stream of molten corium and a water pool. Vol. 1: Code Manual, EPRI TR-103417-V1, Project 3130-01, Final Report (December 1993). Vol. 2: User's Manual, EPRI TR-103417-V2, Project 3130-01, Final Report (December 1993).

(7) W.W. Yuen and T.G. Theofanous, "ESPROSE.m: A computer code to simulate the transient behavior of a steam explosion based on the microinteractions concept," DOE/ID-10501.

(8) T.G. Theofanous and W.W. Yuen, "Escalation and propagation of steam explosions: ESPROSE.m verification studies," DOE/ID-10503.

(9) H.D. Hibbit, et al., "ABAQUS Version 5.3," 1994.

(10) R.J. James, "ANACAP-3D — Three-dimensional analysis of concrete structures: theory, user's and verification manuals," ANATECH No. ANA-89-0094, 1989.

2. MODELLING APPROACH

The basic features of a premixing situation can be discussed with the help of Figure 2.1. Beginning with problem definition, it involves the pool-and-melt-pour geometry (including vent paths to the atmosphere, if any) and the thermodynamic states of the coolant and melt (including its material composition). A characterization of the melt stream must also be given. This requires velocity, mass pour rate, and characteristic length scale(s) at the inlet. These inlet conditions, in combination with the area specified for melt inlet (as part of the geometry) yield the melt inlet volume fraction. All of these will be referred to collectively as "initial conditions," and they must be supplied at the outset.

Upon entering the flow field, the melt stream, under the influence of gravity, accelerates downward, subject to flow resistances due to its interaction with the liquid pool and, to a much lesser extent, with the vapors in the space above it. In the liquid pool, the fuel-coolant momentum exchange sets the liquid in motion. The fuel/coolant energy exchange leads to the generation of a third fluid, vapor, by boiling. All processes of mass, momentum and energy transfer are coupled through the pressure field and must also obey the coolant equation of state. The insert in Figure 2.1 is an attempt to illustrate all these interactions and associated transfer mechanisms. The intimate coupling depicted is a strong function of the characteristic length scales of the premixture constituents. These length scales characterize the magnitude of the interfacial areas and hence the extent of interfacial interactions, while at the same time these interactions govern the interfacial instabilities that lead to breakup and fragmentation (for definitions, see below), and hence to the enhancement in interfacial areas. Our modelling approach intends to capture the basic features of this highly complex and coupled behavior.

The task is approached in two qualitatively different steps. The first step is to address the multifield aspects of the behavior, the main challenge being to describe the interfield interactions *given* the characteristic length scales. The second step is to address to the evolution of the length scales within various, specified, multifield environments. The extent to which this second step can be completed is inherently limited by the very nature of the process (superposition of multiple non-linearalities) and by the difficulties in observing the dynamics of the process under relevant experimental conditions. So far, PM-ALPHA has emphasized the first step. However, it includes the basic framework for the second step as well, so as to allow at least parametric studies along this degree of freedom. This framework will be ready to accommodate new, more definitive formulations as future progress allows. Each step is taken up in turn below.

The multifield treatment is comprised of the field (conservation) equations in a 2D formulation, and the constitutive laws that describe interfacial transfers. The fields are superposed in

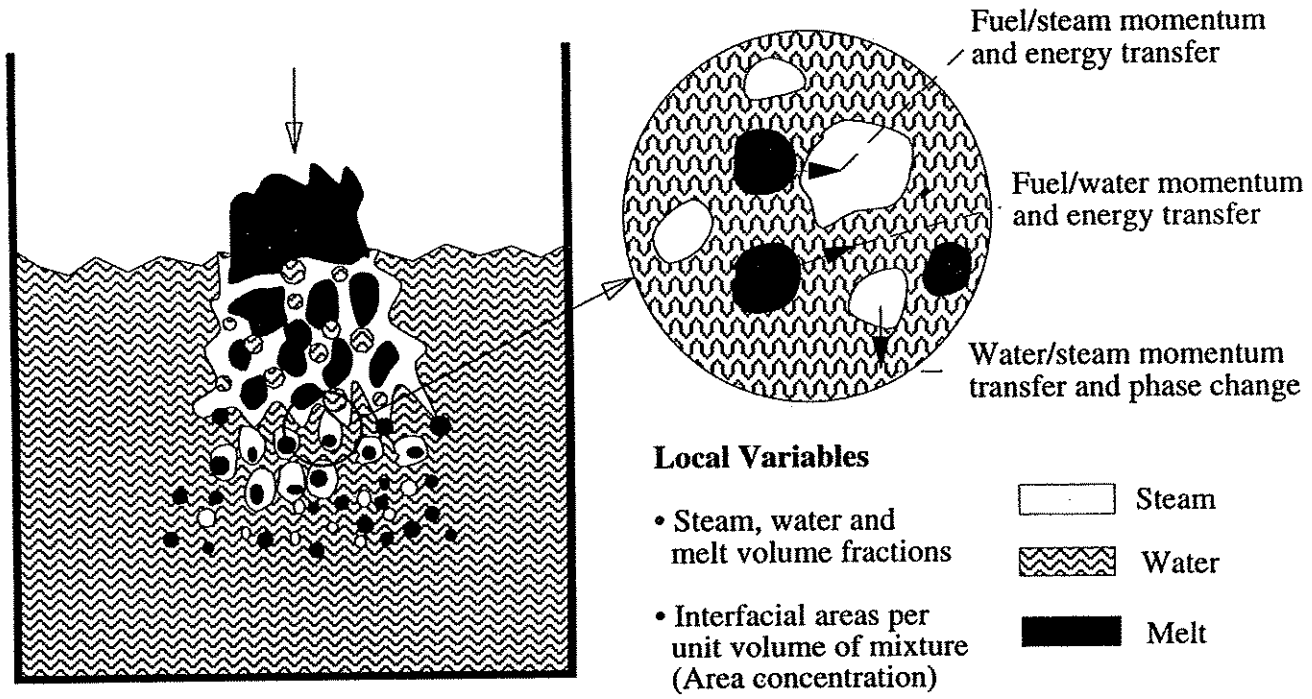

Figure 2.1. Schematic representation of a premixture, indicating key parameters of interest. The mixture is characterized locally by the volume fraction of the three phases, and the interfacial area concentration which depends on the local length scales.

a locally homogeneous manner, but the constitutive laws allow for inhomogeneities, as distinguished by applicable flow regimes. Two dimensionality is recognized as an outstanding feature of premixing, leading to qualitatively different behavior from a "forced" one-dimensional treatment. The latter is unrealistic in yielding much stronger contact, as the only way for coolant to escape is through the counterflowing melt particle cloud. Three-dimensionality, on the other hand, can have only a limited, by comparison, quantitative effect, as most of the flow-deflecting aspects of the behavior are already captured in two dimensions, and certainly in axisymmetric geometries.

The basic intent of the flow regimes consideration is to capture certain essential transitions in the behavior, as dictated primarily by which of the fields constitutes the continuous phase. In particular, we must distinguish between a highly dispersed, vapor-continuous coolant, obtained at high enough void fractions, from all other liquid-continuous (bubbly) or semi-continuous (churn-turbulent) regimes. The former flow regime allows vapor superheating and significant transparency to thermal radiation emitted from the melt. In the latter two flow regimes, essentially all emitted radiation is absorbed locally and the liquid-vapor mixture cannot deviate much from local thermodynamic equilibrium. Similarly, distinctions must be made relative to the liquid/vapor phase momentum coupling, which significantly diminishes from bubbly to churn turbulent, with a further more drastic reduction at the dispersed, vapor-continuous transition. The other key condition is obtained if the melt volume fraction becomes high enough for the process to resemble coolant flow through a "packed bed." This arises if solidified melt particles begin to accumulate at the bottom of the flow region.

The evolution of melt length scales must account for breakup and fragmentation which arise as a result of interfacial instabilities, as noted above. These instabilities are due to body forces and differential flow velocities with the surrounding two-phase coolant. A variety of different mechanisms is possible, as is a range of length scales for the disturbances that grow and detach. In a first approximation we recognize two scales: one fine enough to yield fragments that can be "captured" by the liquid field, and one large enough to continue with the fuel field. The two processes will be called "fragmentation" and "breakup" respectively. The effect of fragmentation is to provide an additional heat transfer mechanism to the coolant beyond radiation and film boiling. This process yields a corresponding quenching, and a gradual reduction in both the length scale and the volume fraction of the fuel phase. Breakup, on the other hand, is a "macroscopic" process in which fuel particles are broken up into particles with "smaller" (but of the same order of magnitude) length scale. In the current Eulerian formulation, the "new" particles are still considered as a part of the fuel phase and the reduction in length scale leads to enhancement in both the interfacial heat and momentum transfer. An interplay between the two

mechanisms is possible as breakup can set up, or promote, the more intense conditions required for fragmentation.

In relation to other premixing codes, PM-ALPHA and CHYMES (Fletcher and Thagaraja, 1991), developed independently but under very similar modelling philosophies, have led the way in the 2D multifield treatment of premixing. An excellent comparison between the two has been presented (Theofanous and Yuen, 1994) with coolant kept at saturation, as required by CHYMES. With the addition of subcooling, currently implemented in CHYMES, the two codes should be rather equivalent, while both share a very cautious approach to treating interfacial area evolution. More recently, the codes EVA, TRIO-MC, and IFCI are also being developed to simulate the premixing phenomenon, but it is too early to discuss comparisons with them. At the other extreme, we have the codes THIRMAL and FRECON. They place emphasis on the detailed description of melt jet breakup. We believe those two approaches are complementary to the 2D multifield treatment. The breakup/fragmentation framework provided in PM-ALPHA, as described above, has been designed to take advantage of results generated by these codes. Moreover, as indicated in Table 1.1, the THIRMAL code has been included in the assessment of premixing in conjunction with PM-ALPHA.

3. MATHEMATICAL FORMULATION

3.1 Conservation Equations

There are four phases allowed in the PM-ALPHA formulation: namely, water (liquid), steam (gas), fuel drops (fuel), and fragmented fuel (debris). The debris is assumed to be fully entrained by the liquid and the liquid/debris mixture is in thermal and hydrodynamic equilibrium. There are thus four continuity equations, three momentum equations, and three energy equations. In addition, there is a transport equation of fuel length scale to simulate the effect of fuel fragmentation and breakup. In the usual manner, the fields are allowed to exchange energy, momentum and mass with each other. With the definition of the macroscopic density ρ_i' of phase i,

$$\rho_i' = \theta_i \rho_i \qquad \text{for} \quad i = g,\, \ell,\, f, \text{and } db, \tag{3.1}$$

and the compatibility condition,

$$\theta_g + \theta_\ell + \theta_f + \theta_{db} = 1, \tag{3.2}$$

these equations can be written rather directly (Ishii, 1975).

- Continuity Equations.

  Gas:

$$\frac{\partial \rho_g'}{\partial t} + \nabla \cdot (\rho_g' \mathbf{u}_g) = J \tag{3.3}$$

  Liquid:

$$\frac{\partial \rho_\ell'}{\partial t} + \nabla \cdot (\rho_\ell' \mathbf{u}_\ell) = -J \tag{3.4}$$

  Fuel:

$$\frac{\partial \rho_f'}{\partial t} + \nabla \cdot (\rho_f' \mathbf{u}_f) = -F_r \tag{3.5}$$

  Debris:

$$\frac{\partial \rho_{db}'}{\partial t} + \nabla \cdot (\rho_{db}' \mathbf{u}_\ell) = F_r \tag{3.6}$$

- Momentum Equations.

  Gas:

$$\begin{aligned} \frac{\partial}{\partial t}(\rho_g' \mathbf{u}_g) + \nabla \cdot (\rho_g' \mathbf{u}_g \mathbf{u}_g) = & -\theta_g \nabla p - F_{g\ell}(\mathbf{u}_g - \mathbf{u}_\ell) - F_{gf}(\mathbf{u}_g - \mathbf{u}_f) \\ & + J(H[J]\mathbf{u}_\ell + H[-J]\mathbf{u}_g) + \rho_g' \mathbf{g} \end{aligned} \tag{3.7}$$

Liquid and debris:

$$\frac{\partial}{\partial t}((\rho'_\ell + \rho'_{db})\mathbf{u}_\ell) + \nabla \cdot ((\rho'_\ell + \rho'_{db})\mathbf{u}_\ell \mathbf{u}_\ell) = -(\theta_\ell + \theta_{db})\nabla p + F_{g\ell}(\mathbf{u}_g - \mathbf{u}_\ell) \quad (3.8)$$
$$- F_{\ell f}(\mathbf{u}_\ell - \mathbf{u}_f) - J(H[J]\mathbf{u}_\ell + H[-J]\mathbf{u}_g) + F_r \mathbf{u}_f + (\rho'_\ell + \rho'_{db})\mathbf{g}$$

Fuel:

$$\frac{\partial}{\partial t}(\rho'_f \mathbf{u}_f) + \nabla \cdot (\rho'_f \mathbf{u}_f \mathbf{u}_f) = -\theta_f \nabla p + F_{gf}(\mathbf{u}_g - \mathbf{u}_f)$$
$$+ F_{\ell f}(\mathbf{u}_\ell - \mathbf{u}_f) - F_r \mathbf{u}_f + \rho'_f \mathbf{g} \quad (3.9)$$

- Energy Equations:

Gas:

$$\frac{\partial}{\partial t}(\rho'_g I_g) + \nabla \cdot (\rho'_g \mathbf{u}_g I_g) = -p\left[\frac{\partial}{\partial t}(\theta_g) + \nabla \cdot (\theta_g \mathbf{u}_g)\right] \quad (3.10)$$
$$+ Jh_g - R_{gs}(T_g - T_s) + \dot{q}_{fg} + \dot{q}_{r,g}$$

Liquid and debris:

$$\frac{\partial}{\partial t}(\rho'_\ell I_\ell + \rho'_{db} I_{db}(T_\ell)) + \nabla \cdot [(\rho'_\ell I_\ell + \rho'_{db} I_{db}(T_\ell))\mathbf{u}_\ell] =$$
$$-p\left[\frac{\partial}{\partial t}(\theta_\ell + \theta_{db}) + \nabla \cdot ((\theta_\ell + \theta_{db})\mathbf{u}_\ell)\right] - Jh_\ell \quad (3.11)$$
$$+ F_r I_f - R_{\ell s}(T_\ell - T_s) + \dot{q}_{f\ell} + \dot{q}_{r,\ell}$$

Fuel:

$$\frac{\partial}{\partial t}(\rho'_f I_f) + \nabla \cdot (\rho'_f I_f \mathbf{u}_f) = -F_r I_f - \dot{q}_{fg} - \dot{q}_{f\ell} - \dot{q}_{r,f} \quad (3.12)$$

- Interfacial Area Transport Equation.

$$\frac{\partial}{\partial t}\left(\frac{\theta_f}{D_f}\right) + \nabla \cdot \left(\frac{\theta_f}{D_f}\mathbf{u}\right) = \dot{S}_f + \dot{S}_b \quad (3.13)$$

In the continuity equations we can identify the source/sink terms for phase change, J (positive for evaporation), and for fragmentation, F_r. The phase change leads to corresponding source/sink terms in the momentum equations, $J\mathbf{u}_\ell$ or $J\mathbf{u}_g$ (depending on the direction of phase change between the liquid and gas), and in the energy equations, Jh_g and Jh_ℓ (where h_g - h_ℓ corresponds to the latent heat for phase change). $H[J]$ is the Heaviside step function that

becomes unity for positive values of the argument and zero otherwise. The fragmentation, on the other hand, leads to the source/sink term $F_r \mathbf{u}_f$ for the momentum equations and $F_r I_f$ for the energy equations. The terms involving the F_{ij}'s in the r.h.s. of the momentum equations represent the pair-wise momentum coupling (drag) between the three fields. The term $\dot{q}_{r,f}$, in the fuel energy equation, represents the radiant energy loss (from the fuel field), and the $\dot{q}_{fg}$, $\dot{q}_{f\ell}$ are the interfield convective heat transfers. These last two terms appear in the gas and liquid energy equations, respectively, while the $\dot{q}_{r,g}$ and $\dot{q}_{r,\ell}$ represent the apportionment of the radiant energy loss from the fuel (the $\dot{q}_{r,f}$ term). While all the above terms involve interfield transfers (or couplings) the R terms in the liquid and gas energy equations represent bulk-to-the-interface transfers of energy, the interface being kept at saturation (T_s). The difference between these terms $[R_{\ell s}(T_s - T_\ell)$ and $R_{gs}(T_g - T_s)]$ provides the latent heat necessary for phase change. Finally, in the interfacial area transport equation, the $\dot{S}_f$ and $\dot{S}_b$ terms represent the sources/sinks of interfacial area due to the processes of fragmentation and breakup, respectively. More details on the physical meaning of these "source" and "interfacial coupling terms" in and between the three fields, and their explicit formulations—generically referred to as constitutive laws—are provided in the next section.

3.2 Constitutive Laws

The purpose of the constitutive laws is to define the interactions between the three fields, so that their motions, macroscopic densities (or concentrations), and thermodynamic states can be calculated by means of the conservation equations given in the previous section. These interactions include drag, heat transfer, and mass transfer either by phase change (gas $\leftrightarrow$ liquid) or by fragmentation (fuel$\leftrightarrow$liquid/debris). In addition, we need to describe the length scales of the three phases. For the liquid and gas we assume that their adjustment to local conditions (relative velocities) is instantaneous, so they can be obtained from Weber number stability criteria. For the fuel the time constant for length scale adjustment is much longer, and we wish to accommodate multiple length scales—as a minimum a macroscopic scale that is subjected to breakup, and a microscopic scale (the debris) as the product of fragmentation. Thus our approach to length scale changes is based on an interfacial area transport equation and constitutive laws for the "sink" terms in it, that are intended to describe these processes. Drag, heat transfer/phase change, and fragmentation/breakup are described in the following three subsections respectively.

3.2.1 Interfacial Drag

As can be seen from the momentum equations interfacial drag provides the coupling that moderates the slip between the three fields—with inertia, buoyancy forces and pressure gradient being the other factors influencing the different velocities. For a highly dispersed (locally

homogeneous) flow regime as is the case here, the slip depends primarily upon which is the continuous phase. Our basic position is that this can be decided on the basis of the volume fractions. Specifically, the phase with a volume fraction below 30% is considered dispersed. The fuel typically meets this criterion and is therefore considered always dispersed, while the gas or liquid are considered as the dispersed phase for void fractions below 30% or above 70% respectively. The intermediate range, $0.3 < \alpha < 0.7$, is considered as churn-turbulent, a special case of dispersed flow, as described below. The important physics to capture here is that, in the bubbly regime, the gas and liquid are strongly coupled together and their tendency to disengage increases substantially in churn flow and dramatically in droplet flow.

The Ishii–Zuber (1979) approach is used to describe the interactions between each pair of phases, as described in the following. The general expression for the F_{ij}'s in the drag terms is:

$$F_{ij} = \frac{3}{4}\theta_i \phi_{ij} \rho_j \frac{C_{Dij}}{\ell_i} \mid \mathbf{u}_i - \mathbf{u}_j \mid \tag{3.14}$$

The effect of the third phase is approximately taken into account by weighing the interfacial area between phases i and j with the factor

$$\phi_{ij} = \frac{\theta_j}{\theta_j + \theta_k}. \tag{3.15}$$

where θ_k is the volume fraction of the third phase. Physically, ϕ_{ij} is the relative volume fraction of phase j in the continuum mixture phase (j+k) and hence is a reasonable approximation of the fractional interfacial contact between phase i and phase j. This weighing factor has the correct value in the limits of $\theta_k \to 0$ and $\theta_j \to 0$.

- For droplet and bubbly flow, the gas-liquid drag coefficient is expressed as

$$C_{Dij} = \frac{2}{3}\ell_i \left\{ \frac{g\Delta\rho}{\sigma} \right\}^{1/2} \left\{ \frac{1 + 17.67\,[f(\alpha)]^{6/7}}{18.67 f(\alpha)} \right\}^2 \tag{3.16}$$

where

$$i = g, \quad j = \ell, \quad \alpha \leq 0.3 \qquad f(\alpha) = (1-\alpha)^{1.5} \tag{3.17}$$

$$i = \ell, \quad j = g, \quad \alpha > 0.7 \qquad f(\alpha) = \alpha^3 \tag{3.18}$$

and ℓ_i is obtained from

$$\frac{\rho_j \mid \mathbf{u}_\ell - \mathbf{u}_g \mid^2 \ell_i}{\sigma} = \mathrm{We}_{cr} \begin{cases} = 8 & \text{for } i,j = g,\ell \\ = 12 & \text{for } i,j = \ell,g \end{cases} \tag{3.19}$$

- For churn flow, the drag coefficient is expressed as

$$C_{Dij} = \frac{8}{3}(1-\alpha)^2 \tag{3.20}$$

where

$$i = g, \quad j = \ell, \qquad \ell_i = 4\left\{\frac{g\Delta\rho}{\sigma}\right\}^{-1/2}$$

- The $F_{f,g}$ and $F_{f,\ell}$ in fuel-coolant drag are again expressed by Eq. (3.14) with $i = f$, $j = \ell$ or g, $\ell_i = D_f$, and a drag coefficient given by an expression similar to Eq. (3.16), i.e.

$$C_{Dij} = 0.45\left\{\frac{1 + 17.67\,[f(\theta_f)]^{6/7}}{18.67 f(\theta_f)}\right\}^2 \tag{3.21}$$

with

$$i = f, \quad j = g,\ell, \quad f(\theta_f) = (1-\theta_f)^3 \tag{3.22}$$

A special case arises in computations where the fuel is allowed to fall and accumulate at the bottom boundary, i.e., yielding $\theta_f > 0.3$. The actual physics here may involve melt droplet coalescence, local capture of coolant within the melt, or between the melt and the wall, followed by superheat-driven microexplosions. These processes are outside the current scope of PM-ALPHA. In fact, the latter process is one of the commonly considered triggers of a steam explosion, and hence indicative that the PM-ALPHA-predicted configuration at this time should be continued with ESPROSE.m simulations into the explosion regime. On the other hand, benign accumulation may be allowed to continue if for some reason one wished to pursue the premixing zone at later times. For this situation the user may wish to continue to run PM-ALPHA with an increased fuel length scale (in the accumulation region). In PM-ALPHA, the fuel-coolant drag, when $\theta_f > 0.3$, is assumed to be solely due to gas flow through a densely packed bed. Concepts of laminar and turbulent permeabilities (Sissom and Pitts, 1972) are used as follows:

$$F_{gf} = F_{gf}^{\ell} + F_{gf}^{t} \tag{3.23}$$

where

$$F_{gf}^{\ell} = \begin{cases} 150 \frac{\theta_g \theta_f^2}{(1-\theta_f)^3} \frac{\mu_g}{D_f^2} & \text{for } \mathrm{Re}_g' < 1000 \\ 0 & \text{for } \mathrm{Re}_g' \geq 1000 \end{cases} \tag{3.24}$$

and

$$F_{gf}^{t} = \begin{cases} 1.75 \frac{\theta_g \theta_f}{(1-\theta_f)^3} \frac{\rho_g' |\mathbf{u}_g - \mathbf{u}_f|}{D_f} & \text{for } \mathrm{Re}_g' > 10 \\ 0 & \text{for } \mathrm{Re}_g' \leq 10, \end{cases} \tag{3.25}$$

with

$$\mathrm{Re}_g' = \theta_f \frac{\rho_g' D_f \mid \mathbf{u}_g - \mathbf{u}_f \mid}{\mu_g} \tag{3.26}$$

Finally, in the bubbly regime the added mass effect is included in the liquid-gas interfacial drag, as given by Wallis (1989)

$$F_a = \frac{\alpha}{3-\alpha} \rho_\ell \phi_{g\ell} \frac{1}{\mid \mathbf{u}_g - \mathbf{u}_\ell \mid} \mid \frac{\partial}{\partial t}(\mathbf{u}_g - \mathbf{u}_\ell) \mid \tag{3.27}$$

The schematic of the logic used in PM-ALPHA in deploying the above correlations is provided in Figures 3.1 and 3.2.

3.2.2 Interfacial Heat Transfer and Phase Change

The principal, in fact overwhelming, mechanism in premixing is heat transfer from fuel to coolant. This occurs primarily by radiation, but film boiling is also present and it can be important. Phase changes can occur when the liquid/vapor constituents of the premixture find themselves in local thermodynamic non-equilibrium. The main manifestations of this non-equilibrium is the presence of superheated or subcooled liquid. This leads to vaporization or condensation respectively. Since the void distribution is of major importance in characterizing premixtures, the accurate calculation of these phase change processes is one of the most critical tasks of the calculation.

In fact, due to the highly dispersive nature of the premixing zone, and the penetrative nature of radiative power, this set of rather complicated processes can be viewed in rather

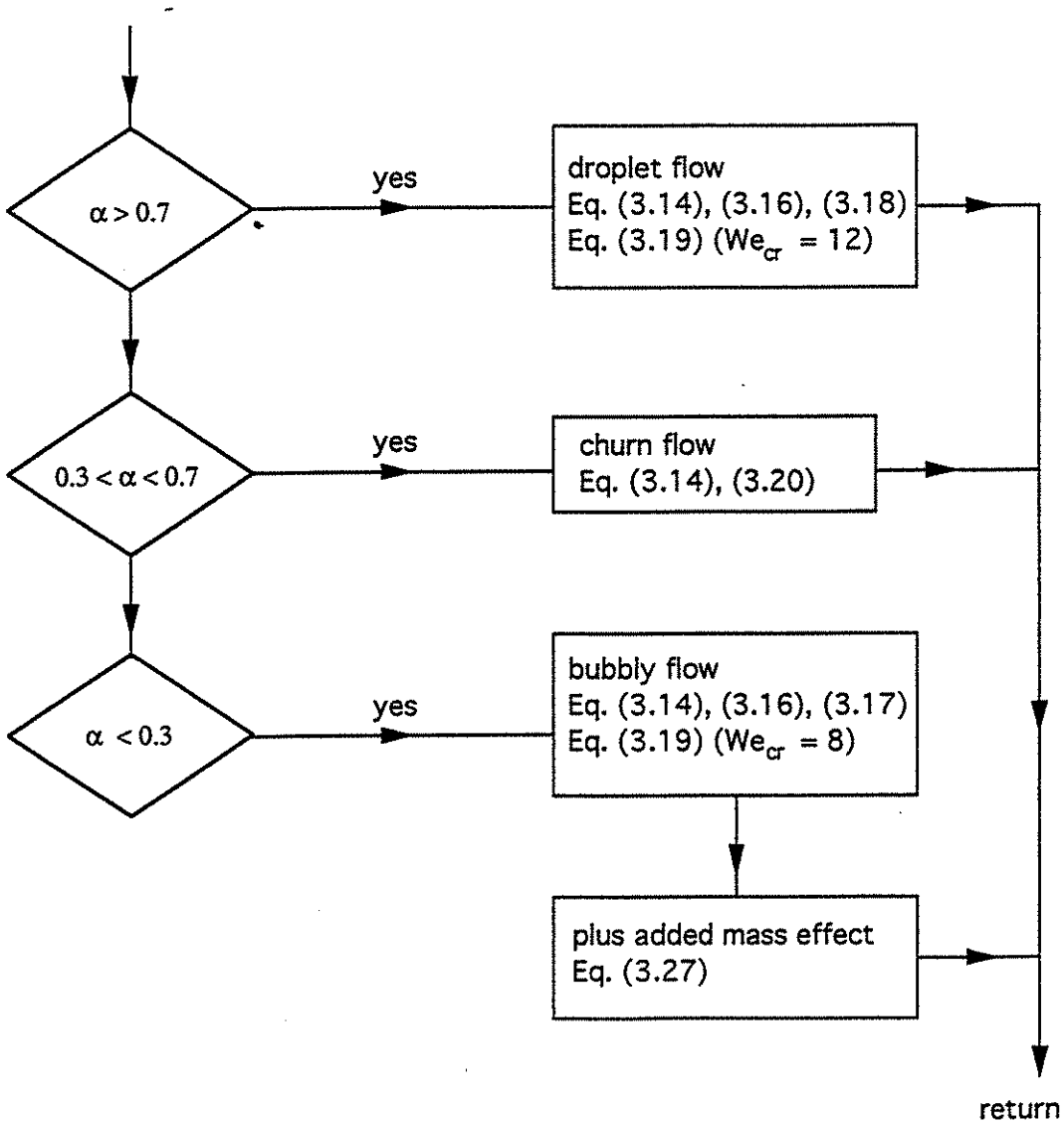

Figure 3.1. Schematic diagram for the calculation of gas-liquid interfacial momentum coupling.

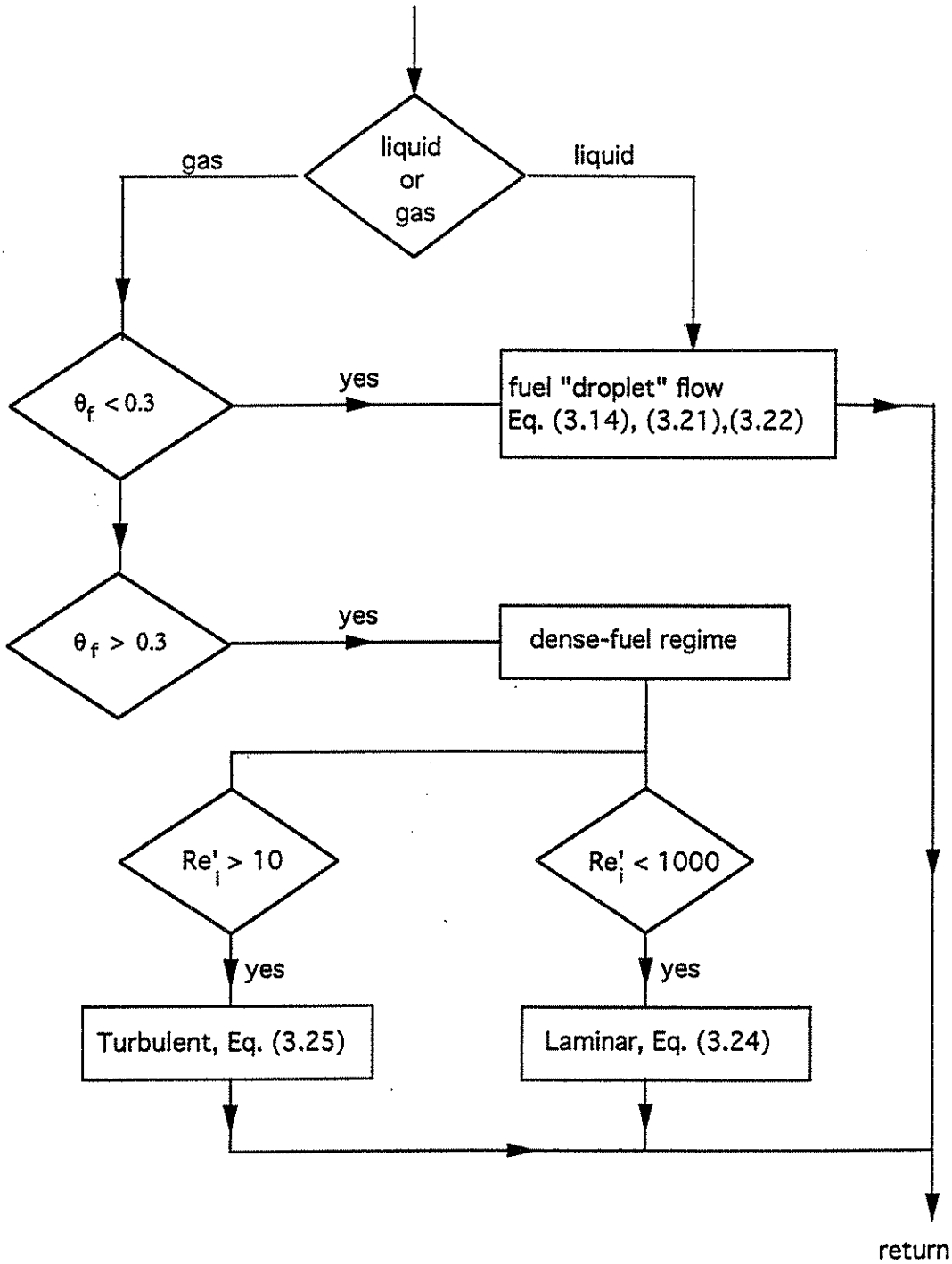

Figure 3.2. Schematic diagram for the calculation of fuel-coolant interfacial momentum coupling.

simple terms. Initially with a subcooled liquid in the bulk, vapor exists only around the melt particles. It is in the form of very thin blankets, and as such of negligible quantity. The coolant is effectively a "single phase" medium, and heat transfer by both radiation and (subcooled) film boiling is added directly to the liquid. Upon reaching saturation, any further heating leads to a vapor/liquid two-phase mixture, again in a highly dispersive process. There are, initially (upon reaching saturation) ample interfaces for phase change (around the previously thin vapor blankets), and more are created as the vapor generated by boiling detaches and mixes with the liquid. The actual paths for heat transfer in this regime are radiation mainly into the liquid bulk, and convection to vapor and from vapor to the liquid. The quantity of energy sustained in the vapor due to superheating is negligible, and the liquid cannot sustain any significant amount of superheat—both due to the extended interfacial area and turbulent mixing conditions that prevail. The whole process, therefore, can be represented quite simply by transferring the energy directly to the liquid and allowing it to produce an equivalent amount of vapor. In the original version of PM-ALPHA this was accomplished by imposing the appropriate phase change rates to drive the mixture to local thermodynamic equilibrium within a very short, specified, relaxation time constant. Presently, we have a more flexible scheme, that accomplishes the same thing within a non-equilibrium framework. Namely, the boiling/condensation rate is written as:

$$J = \frac{1}{h_g - h_\ell}[R_{gs}(T_g - T_s) + R_{\ell s}(T_\ell - T_s)] \tag{3.28}$$

where a negative value for J stands for condensation and the R quantities include the interfacial area per unit volume of mixture. Changes in pressure are accounted for, through corresponding changes in the saturation temperature T_s. Thus, to complete the formulation we need to determine these R's, as well as the rates of energy transfer discussed above. We begin with the latter.

3.2.2.1 Fuel-to-Coolant Convective Heat Transfer

For film boiling we make use of the correlations developed by Liu and Theofanous (1994), specifically for this purpose. All heat transfer goes to the liquid at a rate given by

$$\dot{q}_{f\ell} = \left(\frac{\mathrm{Nu}_{fb} k_g}{D_f}\right) n_f \pi D_f^2 (T_f - T_\ell) \tag{3.29}$$

where n_f is the number density of fuel particles given by

$$n_f = \frac{6\theta_f}{\pi D_f^3} \tag{3.30}$$

The film boiling Nusselt number depends on the flow regime, as follows:

- For subcooled or low void fraction ($\alpha < 0.3$) liquid, we use

$$Nu_{fb} = \left\{ \mathrm{Nu}_p^5 + [f(Fr)Nu_f]^5 \right\}^{\frac{1}{5}} \tag{3.31}$$

which can span conditions from low (pool boiling) to high relative velocities. The function of Froude number is defined as

$$f(\mathrm{Fr}) = 1 - \frac{0.2}{1 + \left| \mathrm{Fr}^{0.5} - 1 \right|} \tag{3.32}$$

where Fr is based on the relative velocity between fuel and liquid and given by

$$\mathrm{Fr} = \frac{|\mathbf{u}_f - \mathbf{u}_\ell|^2}{gD_f} \tag{3.33}$$

Nu_f and Nu_p are Nusselt numbers based on the forced convection and pool film boiling respectively. They can be obtained from

$$\frac{\mathrm{Nu}_p}{1 + \frac{2}{\mathrm{Nu}_p}} = K_c(d') \left(\frac{Ar}{Sp'} \right)^{\frac{1}{4}} M^{\frac{1}{4}} \tag{3.34}$$

and

$$\mathrm{Nu}_f = 0.5 Re_\ell^{1/2} \frac{\mu_\ell}{\mu_g} \left(\frac{\rho_\ell R^4}{\rho_g Sp'} \right)^{1/4} + 0.072\ \mathrm{Re}_\ell^{0.77}\ \mathrm{Pr}_\ell^{0.5} \frac{\mu_\ell}{\mu_g} \frac{Sc'}{Sp'} \tag{3.35}$$

The various dimensionless groups appearing in the above equations are summarized in Table 3.1. Physically, Sp' and Sc' are the superheating and subcooling parameters respectively, and Ar is the Archimedes parameter.

- For the two-phase region $0.3 < \alpha < 1$, we use

$$\mathrm{Nu}_{fb} = 0.55\ \mathrm{Re}_\ell^{\frac{1}{2}} \frac{\mu_\ell}{\mu_g} \left[\frac{R^4 \rho_\ell}{Sp' \rho_g} (1 - \alpha) \right]^{\frac{1}{4}} \tag{3.36}$$

This equation is supported by data up to void fractions of 95%, and it shows that $\mathrm{Nu}_{fb} \to 0$ as $\alpha \to 1$. In this limit the heat transfer from the fuel is due to forced convection to the gas and is appropriately given by (Bird et al. 1960)

$$\dot{q}_{fg} = \left(\frac{\mathrm{Nu}_g k_g}{D_f} \right) n_f \pi D_f^2 (T_f - T_g) \tag{3.37}$$

where

$$\mathrm{Nu}_g = 2 + 0.6\ \mathrm{Re}_g^{1/2}\ \mathrm{Pr}_g^{1/3} \tag{3.38}$$

Table 3.1. Summary of Dimensionless Groups Appearing in Constitutive Laws for Fuel-to-Coolant Convective Heat Transfer

$$d' = D_f \left[\frac{g(\rho_\ell - \rho_g)}{\sigma} \right]^{\frac{1}{2}} \qquad R = \left[\frac{\mu_g \rho_g}{\mu_\ell \rho_\ell} \right]^{\frac{1}{2}} \qquad \mathrm{Pr}_g = \frac{\mu_g c_{pg}}{k_g} \qquad \mathrm{Pr}_\ell = \frac{\mu_\ell c_{p\ell}}{k_\ell}$$

$$\mathrm{Ar} = \frac{g(\rho_\ell - \rho_g) D_f^3}{\rho_g \nu_g^2} \qquad \mathrm{Re}_\ell = \frac{|\,\mathbf{u}_f - \mathbf{u}_\ell\,|\, D_f}{\nu_\ell}$$

$$Sp = \frac{c_{pg}(T_f - T_s)}{[h_g(T_s) - h_\ell(T_s)] Pr_g}$$

$$Sp' = \frac{c_{pg}(T_f - T_s)}{[h_g(T_s) - h_\ell(T_s) + 0.5 c_{pg}(T_f - T_s)]\, Pr_g}$$

$$Sc = \frac{c_{p\ell}(T_s - T_\ell)}{[h_g(T_s) - h_\ell(T_s)] Pr_\ell}$$

$$Sc' = \frac{c_{p\ell}(T_s - T_\ell)}{[h_g(T_s) - h_\ell(T_s) + 0.5 c_{pg}(T_f - T_s)]\, Pr_\ell}$$

$$Sc^* = \frac{0.93 Pr_\ell^{0.22} c_{p\ell}(T_s - T_\ell)}{h_g(T_s) - h_\ell(T_s) + 0.5 c_{pg}(T_f - T_s)}$$

$$K_c(d') = 0.5 d'^{-\frac{1}{4}} \qquad \text{for} \qquad d' < 0.14$$

$$K_c(d') = \frac{0.86}{1 + 0.28 d'} \qquad \text{for} \qquad 0.14 < d' < 1.25$$

$$K_c(d') = \frac{2.4 d'}{1 + 3.0 d'} \qquad \text{for} \qquad 1.25 < d' < 6.6$$

$$K_c(d') = 0.47 d'^{\frac{1}{4}} \qquad \text{for} \qquad d' > 6.6$$

$$M = \frac{E^3}{\left[1 + \frac{E}{Sp' Pr_\ell}\right] (R Pr_\ell Sp')^2}$$

$$E = \left(A + CB^{\frac{1}{2}}\right)^{\frac{1}{3}} + \left(A - CB^{\frac{1}{2}}\right)^{\frac{1}{3}} + \frac{1}{3} Sc^*$$

$$A = \frac{1}{27} Sc^{*3} + \frac{1}{3} R^2 Sp' Pr_\ell Sc^* + \frac{1}{4} R^2 Sp'^2 Pr_\ell^2$$

$$B = -\frac{4}{27} Sc^{*2} + \frac{2}{3} Sp' Pr_\ell Sc^* - \frac{32}{27} Sp' Pr_\ell R^2 + \frac{1}{4} Sp'^2 Pr_\ell^2 + \frac{2}{27} \frac{Sc^{*3}}{R^2}$$

$$C = \frac{1}{2} R^2 Sp' Pr_\ell$$

with

$$\mathrm{Re}_g = \frac{\rho_g \mid \mathbf{u}_g - \mathbf{u}_f \mid D_f}{\mu_g} \tag{3.39}$$

A smooth transition to this unimportant, limiting regime ($\alpha \rightarrow 1$) is provided in the calculation by using the condition $\mathrm{Nu}_{fb} \leq \mathrm{Nu}_g$ to transit from Eqs. (3.29) and (3.36), to Eqs. (3.37) and (3.38).

For completeness, the heat transfer between fuel and liquid in the unimportant regime after rewetting ($T_f - T_s <\sim 150$ °C) is also prescribed. A combined forced convection and pool boiling correlation (Rohsenow and Hartnett, 1973) is utilized. It is

$$\dot{q}_{f\ell} = \dot{q}_{fc}\left(1 + \frac{\dot{q}_b}{\dot{q}_{fc}}\right)^{\frac{1}{2}} \tag{3.40}$$

with $\dot{q}_{fc}$ and $\dot{q}_b$ being the single-phase forced convective heat flux and pool boiling heat flux respectively.

The correlation for $\dot{q}_{fc}$ can be obtained by standard reference (Incropera and DeWitt, 1981) to be

$$\dot{q}_{fc} = \left(\frac{\mathrm{Nu}_{fc} k_\ell}{D_f}\right) n_f \pi D_f^2 (T_f - T_\ell) \tag{3.41}$$

where

$$\mathrm{Nu}_{fc} = 2 + 0.644\ \mathrm{Re}_\ell^{0.5}\ \mathrm{Pr}_\ell^{1/3} \tag{3.42}$$

For the pool boiling heat flux, the familiar correlation for nucleate boiling (Incropera and DeWitt, 1981) is used, up to the condition of critical heat flux, which occurs at $T_f - T_s \sim 50$ °C.

$$\dot{q}_b = \mu_\ell (h_g - h_\ell)\left[\frac{g(\rho_\ell - \rho_g)}{\sigma}\right]^{\frac{1}{2}}\left[\frac{c_{p\ell}(T_f - T_s)}{0.01(h_g - h_\ell)\ \mathrm{Pr}_\ell^{1.7}}\right]^3 \tag{3.43}$$

For the transition boiling regime, 50 °C $< T_f - T_s <$ 150 °C, a linear interpolation between the film boiling correlation (Eq. (3,34)) evaluated at 150 °C and the above nucleate boiling correlation evaluated at $T_f - T_s \sim$50 °C (i.e. the critical heat flux) is used to generate the approximate value of the pool boiling heat flux required by Eq. (3.40). The transition to the vapor dominated regime ($\alpha \rightarrow 1$) is applied in the same manner as described above.

Finally, for the special "dense" fuel regime ($\theta_f > 0.3$) discussed at the end of the previous section, we use Eq. (3.37) for $\dot{q}_{fg}$, but with

$$\mathrm{Nu}_g = 0.91\left(\frac{c_{pf}\rho_g' D_f}{k_g}\right) \mid \mathbf{u}_g - \mathbf{u}_f \mid\ \mathrm{Re}_g''^{-0.51}\ \mathrm{Pr}_g^{-2/3} \quad \text{for } \mathrm{Re}_g'' \leq 50 \tag{3.44}$$

$$\mathrm{Nu}_g = 0.61 \left(\frac{c_{pf} \rho_g' D_f}{k_g} \right) \mid \mathbf{u}_g - \mathbf{u}_f \mid \ \mathrm{Re}_g''^{-0.41} \ \mathrm{Pr}_g^{-2/3} \quad \text{for } \mathrm{Re}_g'' > 50 \tag{3.45}$$

where

$$\mathrm{Re}_g'' = \frac{\rho_g' D_f \mid \mathbf{u}_g - \mathbf{u}_f \mid}{6\theta_f \mu_g} \tag{3.46}$$

Schematics of the logic used in PM-ALPHA in deploying the above correlations are given in Figures 3.3 and 3.4.

3.2.2.2 Fuel-to-Coolant Radiative Heat Transfer

For radiation heat transfer, the objective is to properly estimate the total radiant power leaving the fuel and to deposit it throughout the coolant region. Since a complete treatment of radiation heat transfer is computationally intensive, two options are provided in PM-ALPHA.

In the first option, the gas phase is assumed to be non-absorbing, i.e.

$$\dot{q}_{r,g} = 0 \tag{3.47}$$

and, therefore,

$$\dot{q}_{r,f} = q_{r,\ell} \tag{3.48}$$

The absorption by liquid is assumed to be diffusion-like and occurs only in the local region surrounding the fuel. For $\alpha < 0.7$, we use

$$\dot{q}_{r,\ell} = n_f (1-\alpha) \pi D_f^2 \epsilon \sigma (T_f^4 - T_\ell^4) \tag{3.49}$$

In the droplet flow regime, the radiation heat transfer to liquid drops is approximated by

$$\dot{q}_{r,\ell} = min(n_\ell \pi \ell_\ell^2, n_f \pi D_f^2) E_d \epsilon \sigma (T_f^4 - T_\ell^4) \tag{3.50}$$

where E_d is an empirical constant accounting for the fraction of radiation that is actually absorbed by the liquid drops and n_ℓ is the number density of liquid drops given by

$$n_\ell = \frac{6\theta_\ell}{\pi \ell_\ell^3} \tag{3.51}$$

The above option, however, is inaccurate at high fuel temperature at which water becomes optically transparent. It also fails to account for the effect of steam absorption, which can become significant in premixing scenarios at high pressure. In such situations, we make use

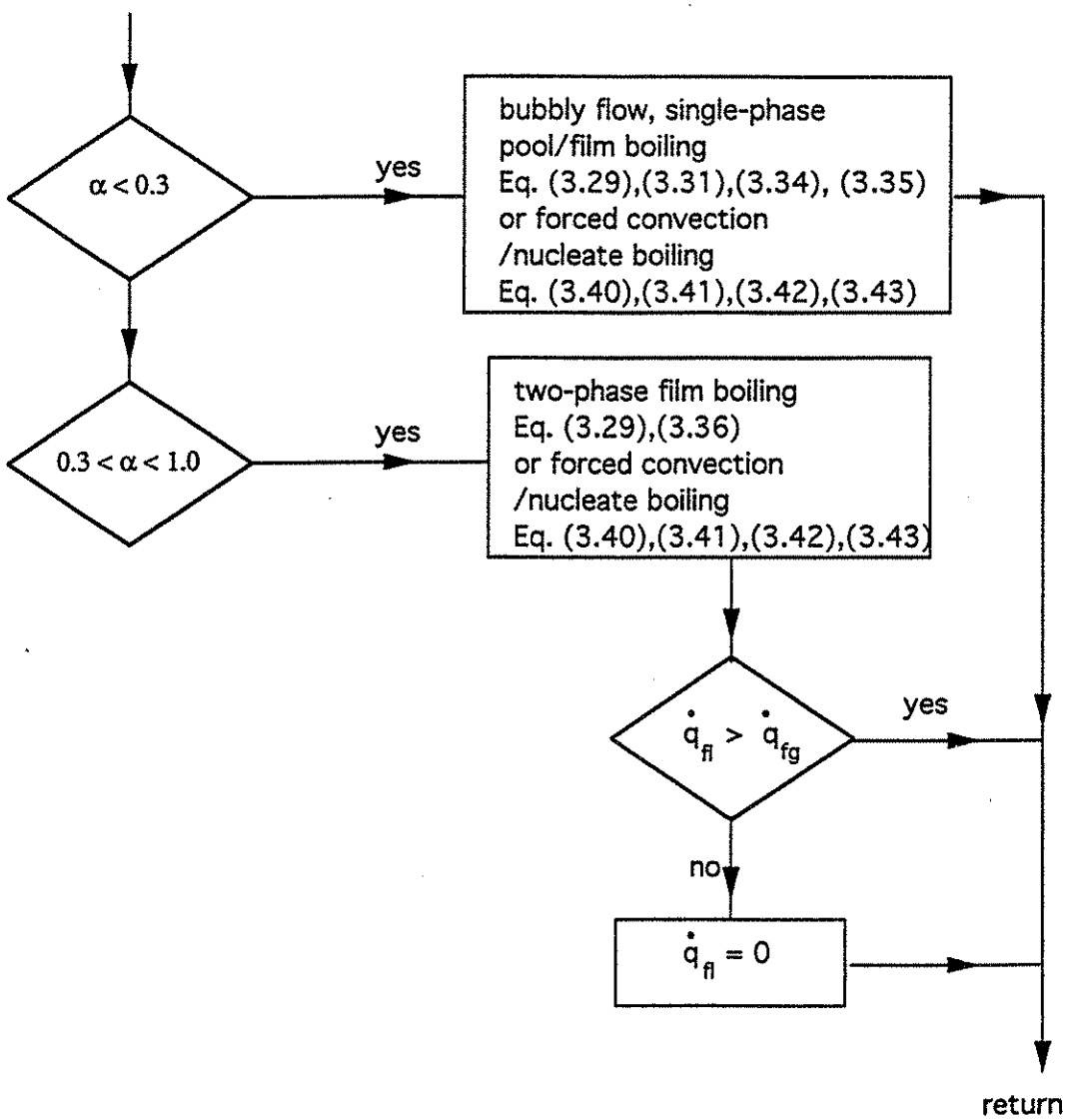

Figure 3.3. Schematic diagram for the calculation of convective heat transfer from fuel to liquid.

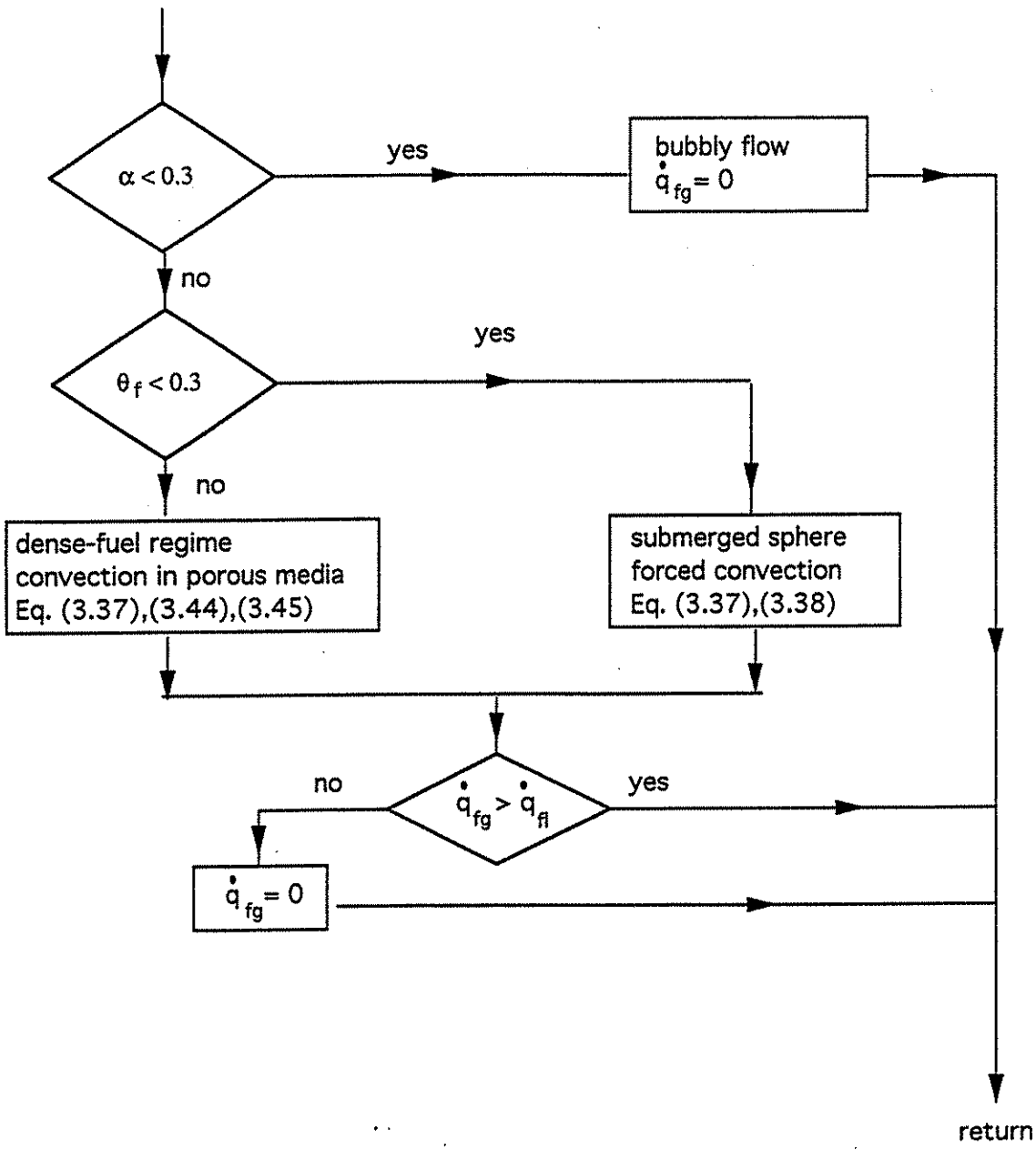

Figure 3.4. Schematic diagram for the calculation of convective heat transfer from fuel to gas.

of the zonal method (Hottel and Sarofim, 1967) which is extended to account for field internal inhomogeneities (Appendix B).

In the zonal method, the important physical properties required for the evaluation of radiation heat transfer are the absorption coefficients of the three primary components, water, vapor and fuel. For water, the absorption coefficient is evaluated at the peak wavelength of the blackbody spectrum at the fuel temperature, i.e.

$$\lambda_{max} = \frac{C_3}{T_f} \tag{3.52}$$

with C_3 being the third radiation constant (2898 μm K). The absorption coefficient for steam is estimated by evaluating the effective absorption of steam at the fuel temperature and a "typical" steam temperature using the Edwards wide band correlation (Edwards, 1976). For special situations (such as the FARO experiments) in which the domain allows radiation to reach the reflecting walls of the system boundary, the effect of multiple reflections is accounted for by an "effective" absorption coefficient for steam which is generated by a three-zone network analysis (Yuen, 1990, Appendix A) of the fuel-steam-boundary configuration prior to the penetration of the water surface. Finally, the "effective" absorption coefficient for fuel is estimated by the expression for a "dispersed" particle cloud in the geometric absorption limit (Siegel and Howell, 1992)

$$a_f = \frac{3}{2}\frac{\theta_f}{D_f} \tag{3.53}$$

The zonal method allows one to compute the radiant energy exchange between any two local regions (say, two computational cells) accounting for the absorption (radiative attenuation) that occurs in the medium in-between. The approach is based on an exchange factor $F(\mathbf{r}, \mathbf{r}')$ defined such that if $\dot{q}_{ex}(\mathbf{r}')$ is the net radiant power density exiting from a small volume at location $\mathbf{r}'$, the power $\dot{q}_{ex}(\mathbf{r}')F(\mathbf{r}, \mathbf{r}')a_i(\mathbf{r})dV'$ is absorbed by component i (with absorption coefficient $a_i(\mathbf{r})$) at position $\mathbf{r}$. The total energy absorbed by the liquid is then

$$\dot{q}_{r,\ell}(\mathbf{r}) = \dot{q}_{a,\ell}(\mathbf{r}) + \int_{\mathbf{r}' \neq \mathbf{r}} \dot{q}_{ex}(\mathbf{r}')F(\mathbf{r}, \mathbf{r}')a_\ell(\mathbf{r})dV' \tag{3.54}$$

where we have included also $\dot{q}_{a,\ell}(\mathbf{r})$, the absorption by liquid in the immediate neighborhood of $\mathbf{r}$ due to radiation from fuel within this neighborhood—this separation is convenient in the finite difference representation. Radiation absorbed by vapor is normally not important. However,

after evaluating Eq. (3.54), its inclusion involves only a trivial additional effort, while providing flexibility that has proven very convenient under some special circumstances—as in interpreting the FARO experiments where the melt is allowed to fall through a space occupied by high pressure steam. Similar to Eq. (3.54), then, we have

$$\dot{q}_{r,g}(\mathbf{r}) = \dot{q}_{a,g}(\mathbf{r}) + \int_{\mathbf{r}' \neq \mathbf{r}} \dot{q}_{ex}(\mathbf{r}') F(\mathbf{r}, \mathbf{r}') a_g(\mathbf{r}) dV' \tag{3.55}$$

Finally, the radiant energy leaving the fuel is obtained from

$$\dot{q}_{r,f}(\mathbf{r}) = n_f \pi D_f^2 \epsilon \sigma T_f^4 - \dot{q}_{a,f}(\mathbf{r}) - \int_{\mathbf{r}' \neq \mathbf{r}} \dot{q}_{ex}(\mathbf{r}') F(\mathbf{r}, \mathbf{r}') a_f(\mathbf{r}) dV' \tag{3.56}$$

where the last two terms have the same interpretation as that discussed above.

To evaluate these equations we need the local absorption, $\dot{q}_{a,\ell}(\mathbf{r})$, $\dot{q}_{a,g}(\mathbf{r})$, and $\dot{q}_{a,f}(\mathbf{r})$, the exiting radiant power density $\dot{q}_{ex}(\mathbf{r})$ and the exchange factor $F(\mathbf{r}, \mathbf{r}')$. Briefly, the local absorption is evaluated on the basis of the emitted radiation, after it has been corrected for self-absorption (self-shielding) of fuel particles and attenuation in the coolant within the host computational cell. The exiting radiant power is what is left over after the local absorption. The exchange factors on the other hand embody the geometric configuration ($\mathbf{r}$, $\mathbf{r}'$) and the attenuation along the vector $\Delta\mathbf{r} = \mathbf{r}' - \mathbf{r}$ which depends on the mixture composition and the absorption coefficient of the three phases along the same path. This already complex situation is further complicated when the code is run in a cylindrical geometry, where a computational cell is actually a ring in three dimensional space - radiation from one part of the ring to another must be accounted for in evaluating "local" absorption. The detailed treatment, that endeavors to approximately capture all these effects, is provided in Appendix B.

3.2.2.3 Phase Change

In addressing the R's in Eq. (3.28), the principal consideration is to properly represent convection (turbulence) in the continuous phase. From the point of view of heat transfer the churn regime is dominated by the liquid phase, hence it is lumped together with the bubbly regime. On the dispersed phase we use the simple conduction model Nu$\sim$2. For a volume fraction θ and length scale ℓ, the interfacial area per unit volume of mixture is $6\theta/\ell$, and the dispersed phase R is then

$$R_{is} = \frac{6\theta_i}{\ell_i}\left(\frac{2k_i}{\ell_i}\right) \tag{3.57}$$

where i is ℓ or g, whichever is the dispersed phase. When the continuous phase is the gas we have droplets in a gas flow at relatively high relative velocities, thus the usual correlation for forced convection from spheres is deemed appropriate and

$$R_{gs} = \frac{6\theta_\ell k_g}{\ell_\ell^2}\left(2 + 0.6\ \mathrm{Re}_g^{1/2}\ \mathrm{Pr}_g^{1/3}\right) \tag{3.58}$$

where the Reynolds number is based on the relative velocity and droplet length scale.

A similar approach can be taken, and is provided as an option to the code, when the liquid is the continuous phase, i.e.,

$$R_{\ell s} = \frac{6\theta_g k_\ell}{\ell_g^2}\left(2 + 0.6\ \mathrm{Re}_\ell^{1/2}\ \mathrm{Pr}_\ell^{1/3}\right) \tag{3.59}$$

However, the situation here can be more intricate, especially at the very low void fractions characterized by low interfacial areas and relative velocities. Under such conditions, Eq. (3.59) will underestimate heat transfer, as heat transfer is actually dominated by turbulence created by the melt particles. An approach that accounts in a direct way for liquid turbulence at the liquid-vapor interface, as used by Liu and Theofanous (1994) for subcooled film boiling, yields

$$R_{\ell s} = 0.25\frac{6\theta_f}{D_f}\rho_\ell c_{p\ell} Pr_\ell^{-1/2}\left[\frac{0.066\nu_\ell \mid \mathbf{u}_\ell - \mathbf{u}_f \mid^3}{D_f}\right]^{1/4} \tag{3.60}$$

Recalling that the physics of the process dictate that liquid superheat is very limited, the coding in PM-ALPHA chooses the higher value among the two approaches.

Finally, we have to be concerned about special and extreme cases that may lead to highly non-equilibrium cases, whose relaxation cannot be captured by the above formulation. Such situations include rapid changes in pressure that produce superheated liquid and/or subcooled vapor. PM-ALPHA allows a mechanism to handle these situations through a formulation that drives the system to local equilibrium with a specified time constant. Namely:

$$R_{gs} = \frac{\rho_g'(I_{s,g} - I_g)}{(T_s - T_g)\tau_g} \qquad \text{when} \qquad T_s > T_g \tag{3.61}$$

and

$$R_{\ell s} = \frac{\rho_\ell'(I_\ell - I_{s,\ell})}{(T_\ell - T_s)\tau_\ell} \qquad \text{when} \qquad T_\ell > T_s \tag{3.62}$$

Physically, the boiling/condensation rate should decrease as the liquid approaches saturation. While this effect is implicit in the definition of J, it can lead to severe time step restriction, particularly in regions with high heat transfer coefficients. To improve the robustness of the

code while maintaining the correct physics, the phase change rate is assumed to be limited by a characteristic rate given by

$$J_m = \frac{\rho_g'}{\tau_e}\left[\left(\frac{p_s(T_\ell)}{p}\right)^{\frac{1}{\gamma}} - 1\right] \tag{3.63}$$

Physically, the above expression is the estimated boiling/condensation rate which will cause the liquid to become saturated in a characteristic time τ_e. τ_e is assumed to be proportional to the computational time step. Experience shows that this restriction in J improves significantly the robustness of the code and its effect diminishes in the limit of small time step. The corresponding limits on R's are

$$R_{gs,m} = \left|\frac{J_m}{J}\right| R_{gs} \tag{3.64}$$

$$R_{\ell s,m} = \left|\frac{J_m}{J}\right| R_{\ell s} \tag{3.65}$$

whenever $|J| > |J_m|$.

A schematic of the logic in PM-ALPHA deploying the above correlations is provided in Figures 3.5, 3.6 and 3.7.

3.2.3 Fuel Breakup and Fragmentation

The processes of breakup and fragmentation, as introduced in Section 2, are responsible for the two source terms that appear on the r.h.s. of the fuel length scale transport equation (Eq. 3.13). In order to relate physically to these source terms, and to obtain their general form, it is best to begin with the interfacial area transport equation, written in conservative form, per unit volume of the total flow field, as

$$\frac{\partial A_f}{\partial t} + \nabla \cdot (A_f \mathbf{u}_f) = \dot{S}_f' + \dot{S}_b' \tag{3.66}$$

In this equation $\dot{S}_f'$ and $\dot{S}_b'$ correspond to interfacial area source/sink terms due to fragmentation and breakup respectively, again, per unit volume of mixture. Fragmentation leads to a loss of mass from the fuel field, hence its effect would be to reduce the fuel particle (assuming the same shape) surface area. Breakup, on the other hand, is due to subdivision of a fixed mass, hence it should produce an increase in surface area. The above equation can be derived, in the usual manner, by using the Reynolds transport theorem and Green's theorem for a "material" volume in the fuel field, including the source terms in the statement of conservation, and letting the volume shrink to infinitesimally small dimensions.

Now, assuming that the interfacial area of the fuel can be characterized by that of a cloud of spherical particles with a single, effective length scale, the A_f can be written as

$$A_f = n_f \pi D_f^2 \tag{3.67}$$

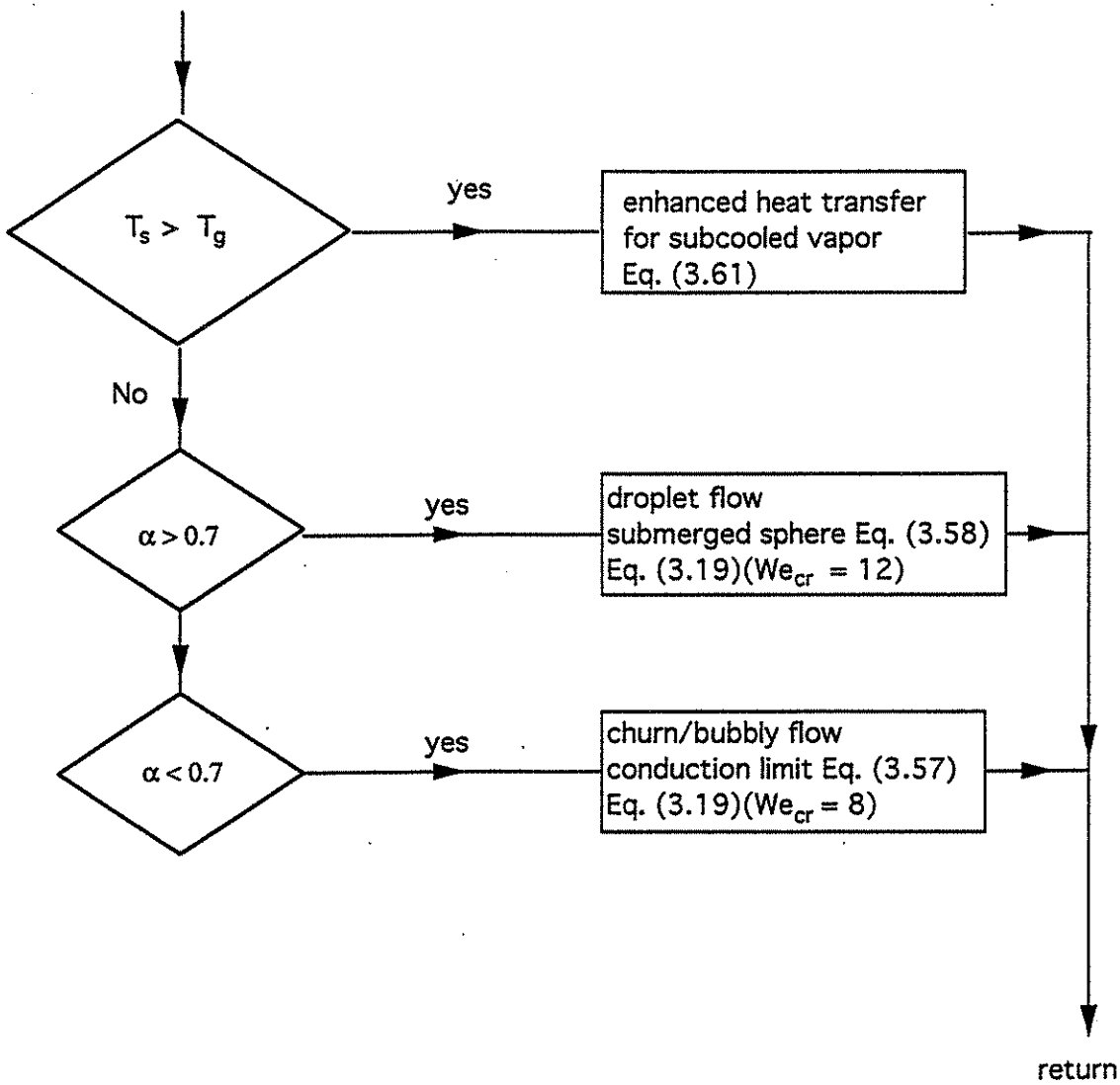

Figure 3.5. Schematic diagram for the calculation of vapor-interface heat transfer coefficient.

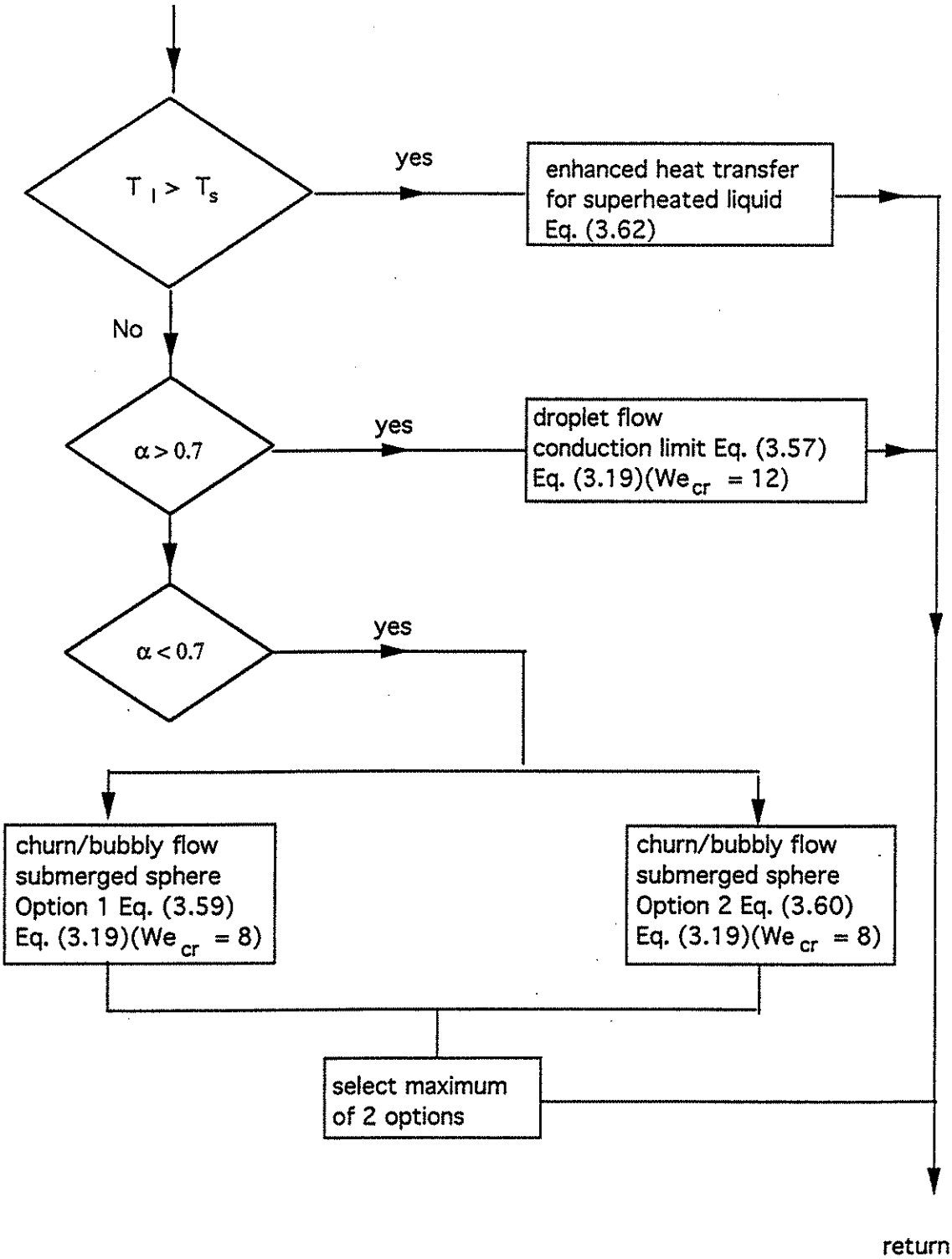

Figure 3.6. Schematic diagram for the calculation of liquid-interface heat transfer coefficient.

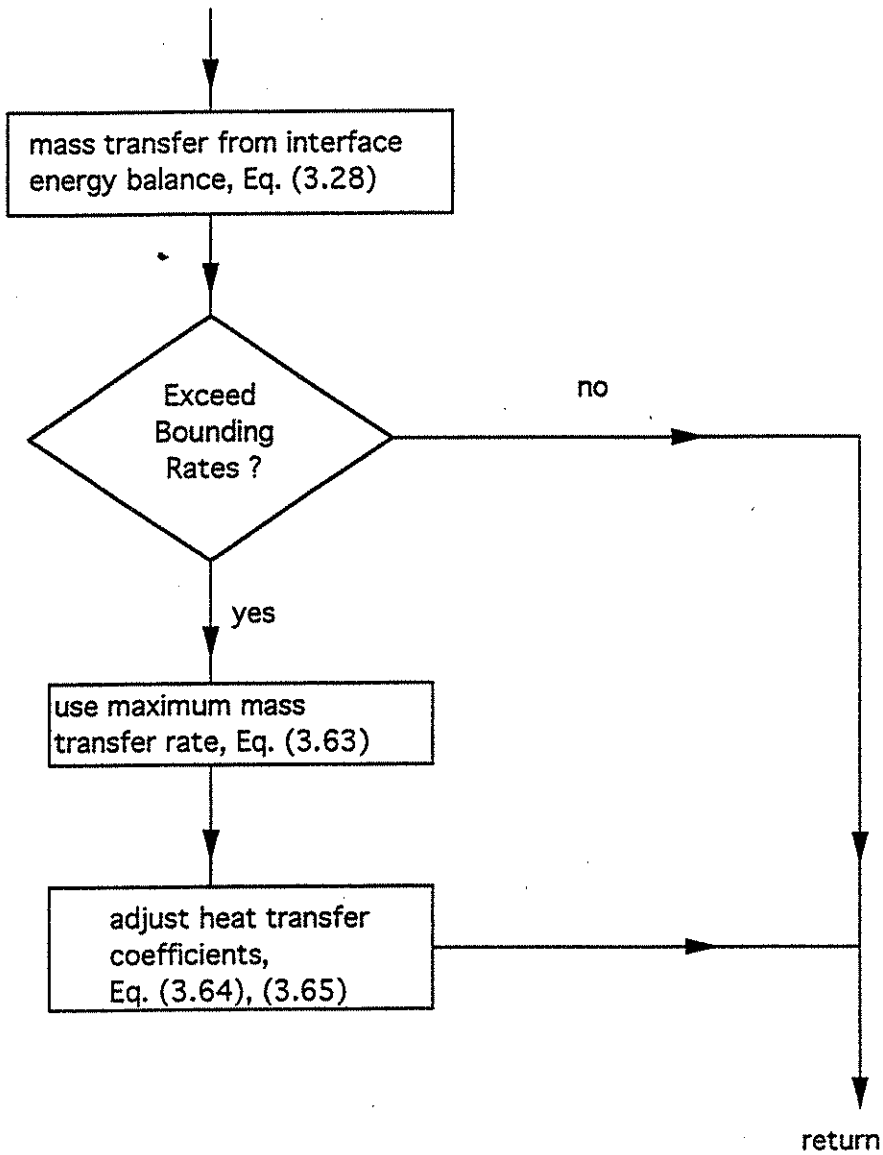

Figure 3.7. Schematic diagram for the calculation of the mass transfer rate between liquid and gas.

where n_f is the number density of particles and, therefore, relates to the particular volume fraction and length scale by

$$\theta_f = n_f \frac{1}{6} \pi D_f^3 \tag{3.68}$$

From these equations we obtain

$$A_f = \frac{6\theta_f}{D_f} \tag{3.69}$$

In the material volume mentioned above, the changes in A_f (and hence the source terms) can be obtained by simple differentiation for fragmentation and breakup respectively as:

$$\dot{S}'_f \equiv 6\dot{S}_f \equiv \left(\frac{dA_f}{dt}\right)_f = \frac{6}{D_f}\frac{d\theta_f}{dt} - \frac{6\theta_f}{D_f^2}\left(\frac{dD_f}{dt}\right)_f \tag{3.70}$$

and

$$\dot{S}'_b \equiv 6\dot{S}_b \equiv \left(\frac{dA_f}{dt}\right)_b = -\frac{6\theta_f}{D_f^2}\left(\frac{dD_f}{dt}\right)_b \tag{3.71}$$

Since the fragmentation is assumed to be occurring without affecting the particle number density, but only their size, the first term on the r.h.s. of Eq. (3.70) can be written (using Eq. 3.68) as:

$$\frac{6}{D_f}\frac{d\theta_f}{dt} = \frac{18\theta_f}{D_f^2}\left(\frac{dD_f}{dt}\right)_f \tag{3.72}$$

and collecting Eqs. (3.69) to (3.72) into Eq. (3.66) we finally obtain:

$$\frac{\partial}{\partial t}\left(\frac{\theta_f}{D_f}\right) + \nabla \cdot \left(\frac{\theta_f}{D_f}\mathbf{u}_f\right) = \frac{\theta_f}{D_f^2}\left\{2\left(\frac{dD_f}{dt}\right)_f - \left(\frac{dD_f}{dt}\right)_b\right\} \tag{3.73}$$

The first term on the r.h.s. (negative) can be seen to produce a reduction in interfacial area (sink), while the second term produces an increase due to particle subdivision (reduction in length scale). To complete the formulation we need to express the derivatives on the r.h.s. in terms of field variables, and this is done next.

Fragmentation is the fundamental mechanism that drives the steam explosion, after it has been triggered, and it has been, therefore, mainly discussed in this context (Yuen et al., 1994, Theofanous and Yuen, 1994). In premixing, the flow field is characterized mainly by low pressures, relatively low relative velocities, and fuel particles that are separated from the liquid by vapor—at subcooled conditions this is as thin vapor blankets; after saturation the vapor occupies a significant fraction of the flow field and is able to flow, especially where $\alpha > 0.3$, macroscopically through the mixing zone. None of the available data are appropriate for these conditions—they primarily address two phase, gas-liquid systems, although some liquid-liquid data are also

available (Patel and Theofanous, 1981; Yuen et al., 1994; Bürger et al., 1993). Moreover, all data are for drops with small millimeter length scales, while in premixing the length scales begin orders of magnitude larger than that. Recognizing this limitation, the treatment is considered, at this stage, as parametric in purpose, and we follow the instantaneous Bond number formulation of Yuen et al. (1994). It consists of defining a total fragmentation time, t_f^*, correlating it to the instantaneous Bond number, and assuming that the instantaneous fragmentation rate is given by the ratio of the current droplet volume to the instantaneous breakup time. Namely,

$$t_{fi}^* \equiv \frac{\mid \mathbf{u}_f - \mathbf{u}_i \mid t_{fi}}{D_f} \epsilon^{-1/2} = \beta_f \mathrm{Bo}^{-1/4} \tag{3.74}$$

with

$$\mathrm{Bo}_i \equiv \frac{3C_d \rho_c D_f \mid \mathbf{u}_f - \mathbf{u}_i \mid^2}{16\sigma} \quad \epsilon = \frac{\rho_f}{\rho_i} \quad i = \ell, g \tag{3.75}$$

and

$$\left[\frac{d}{dt}\left(\frac{\pi}{6} D_f^3\right)\right]_i \equiv \frac{\pi D_f^3}{6 t_{fi}} \tag{3.76}$$

The derivative we are looking for can be obtained from the last equation as

$$\left(\frac{dD_f}{dt}\right)_f = \frac{1}{3}\frac{D_f}{t_{fi}} \tag{3.77}$$

The two-phase character of the coolant is then approximately taken into account by weighting the above result by the vapor and liquid volume fraction to obtain the final result:

$$\left(\frac{dD_f}{dt}\right)_f = \frac{1}{3} D_f \left\{\frac{\alpha}{t_{fg}} + \frac{1-\alpha}{t_{f\ell}}\right\} \tag{3.78}$$

For breakup, the limitations due to lack of experimental evidence are even more severe, for here we are looking for the splitting up of large masses. The operative mechanisms are Rayleigh-Taylor instabilities at the interfaces, but also bulk phase motions and associated inertia. The latter aspect has not been discussed previously; it requires some further explanation, which can be made in terms of the following key observations:

1. At large length scales surface tension forces are negligible and macroscopic bulk motions can lead quite readily to breakup.

2. Coherent melt masses of macroscopic scale can lead to macroscopic vapor blankets, which can be unstable, especially under subcooled conditions. The collapse of such blankets is a dynamic phenomenon accompanied by macroscopic collisions, of melt and coolant masses,

with significant energy to affect the bulk flow behaviors. Under highly subcooled conditions such phenomena can supply effective triggers to initiate steam explosions.

3. Under the conditions mentioned above, and with the possible participation of local fragmentation phenomena, a premixing zone can provide an effective medium for multi-length scale interactions; that is, flow oscillations from one region of the zone to another, with associated breakup and fragmentation phenomena that continue to feed the dynamics.

As a consequence, a parametrics-oriented approach is utilized at this time. For an order of magnitude, the breakup process is taken to be controlled by the melt length scale, D_f, with a characteristic time constant obtained from the melt velocity, through a specified fall distance, taken as the smaller of the actual fall distance or $\beta_b D_f$.

$$\left(\frac{dD_f}{dt}\right)_b = \max\left\{\frac{|\,\mathbf{u}_f\,|}{\beta_b},\ \frac{D_f}{L}\,|\,\mathbf{u}_f\,|\right\} \tag{3.79}$$

where β_b is an input-specified parameter greater than unity, and L is the total available fall distance. Physically, the breakup should cease when the length scale has reached the so-called capillary length. Accordingly, the breakup process is terminated in the calculation by the condition

$$\left(\frac{dD_f}{dt}\right)_b = 0 \qquad \text{when} \qquad D_f \sim \sqrt{\frac{\sigma}{g(\rho_f - \rho_\ell)}} \tag{3.80}$$

By varying β_b as a constant we can explore wide ranges of breakup behavior. By making β_b to vary in space, or with flow conditions, additional dimensions of these phenomena can be explored. Because of the compensating effects discussed by Theofanous et al. (1995) these parametric evaluations can be quite focused and fruitful.

The source terms in the fuel/debris continuity equations, Eqs. (3.5) and (3.6), can be obtained in a similar fashion. We begin by recognizing that F_r is the fragmentation rate per unit volume of mixture, and in a material volume it can be obtained by simply differentiating the macroscopic fuel density, ρ_f. That is:

$$F_r \equiv \frac{d\rho_f'}{dt} = \rho_f \frac{d\theta_f}{dt} = \rho_f' \left\{\frac{\alpha}{t_{fg}} + \frac{1-\alpha}{t_{f\ell}}\right\} \tag{3.81}$$

where we have made use also of Eqs. (3.68), (3.77) and (3.78).

4. COMPUTATIONAL APPROACH AND NUMERICAL FORMULATION

4.1 General Numerical Approach

In devising a numerical scheme for the eleven partial differential equations described above, we placed robustness and simplicity (in implementation) at a premium, while, within practical limits of course, the speed (economics) of the computation was considered secondary. We determined that the key to robustness is accommodating the rapid phase change dynamics, and we chose to implicitly couple the liquid and gas continuity and momentum equations for this purpose. We already had extensive experience with the Los Alamos approach known as Implicit Continuous Eulerian (ICE) (Amsten and Harlow, 1971), and we had available a particular solver as found in the KFIX code (Rivard and Torrey, 1977). Thus, we build PM-ALPHA "around it." This means incorporating the fuel and debris equations explicitly, and solving the liquid and gas energy equations implicitly, but uncoupled from the continuity–momentum iteration (they are coupled in KFIX). The length scale transport equation is also advanced explicitly. We found that these explicit elements do not have a significant effect on the roubustness or speed of typical computations because the time step is already quite limited by the large source/sink terms (phase change dynamics), which turns out to be even more restrictive than the Courant stability criteria. As for ICE, we expect that PM-ALPHA is appropriate for all flow speeds.

A schematic of the general solution procedure used in PM-ALPHA is shown in Figure 4.1, and the implicit solution box in it is explained in Figure 4.2. Finally, details of the iteration box in Figure 4.2 are provided in Figure 4.7, to be found later in the text together with the explanation. The complete formulation of the finite difference equations and the details of the numerical procedure are provided below.

4.2 Basic Finite Difference Scheme

The basic finite difference solution procedure is an extension of the two phase flow procedure (K-FIX program, Rivard and Torrey, 1977) developed for pressurized water reactor safety analysis. This procedure embodies both the Simplified Marker-and-Cell method (SMAC, Amsden and Harlow, 1970) for low speed flow and the Implicit Continuous Flow Eulerian method (ICE, Harlow and Amsden, 1971; Rivard et al., 1974) for high speed chemically reactive flow.

The conservation equations in Section 3 are solved in two-dimensional plane or axisymmetric coordinates. The finite difference mesh used consists of rectangular cells of fixed width δr (or δx for rectangular coordinate) and height δz. [The fluid volumes corresponding to each cell in the axisymmetric case are rectangular tori.] The mesh region containing fluid is composed of IB cells in the r-direction (x-direction for rectangular coordinate), labelled with the index i, and

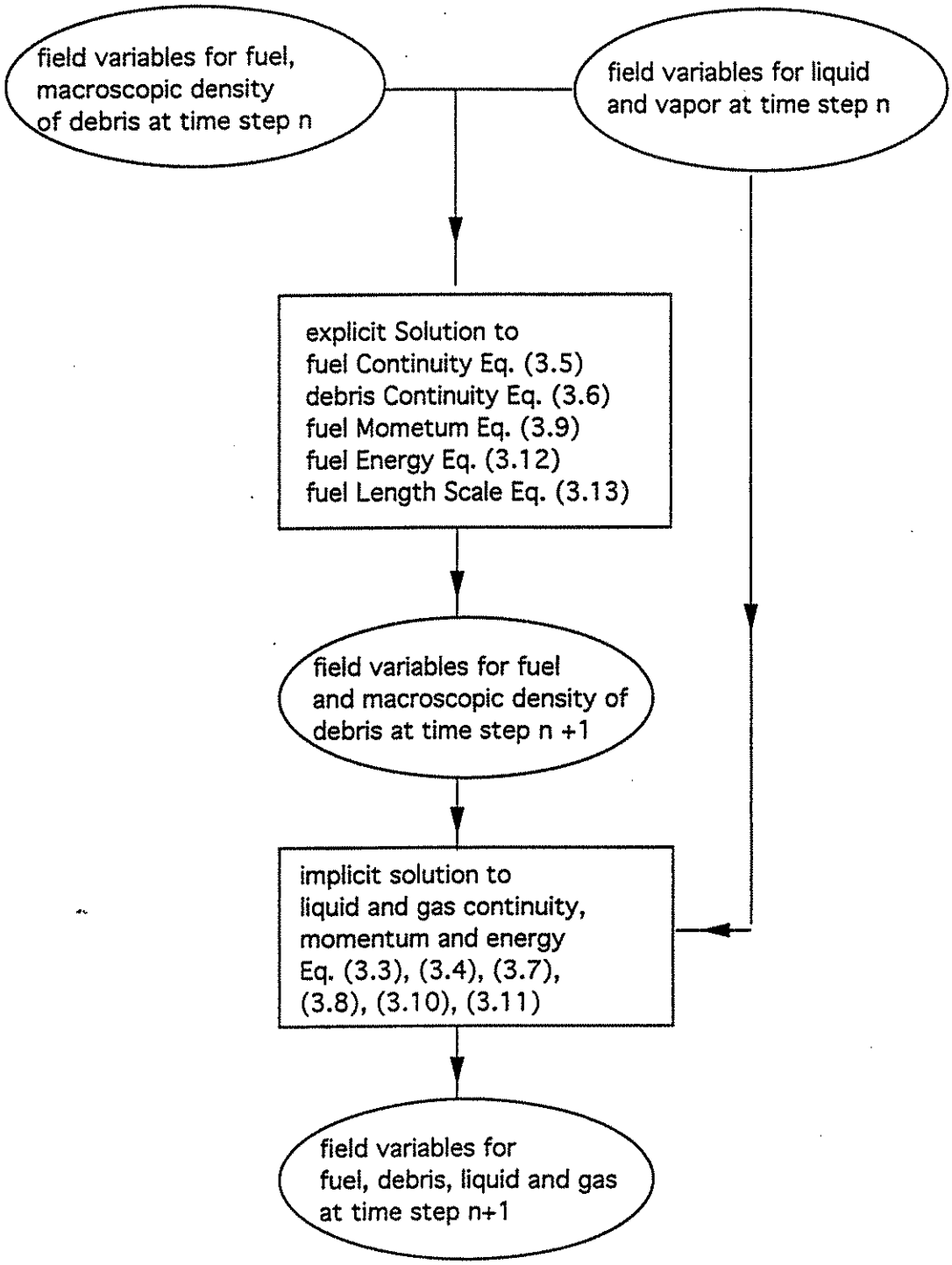

Figure 4.1. Schematic diagram of the hybrid explicit/implicit solution algorithm.

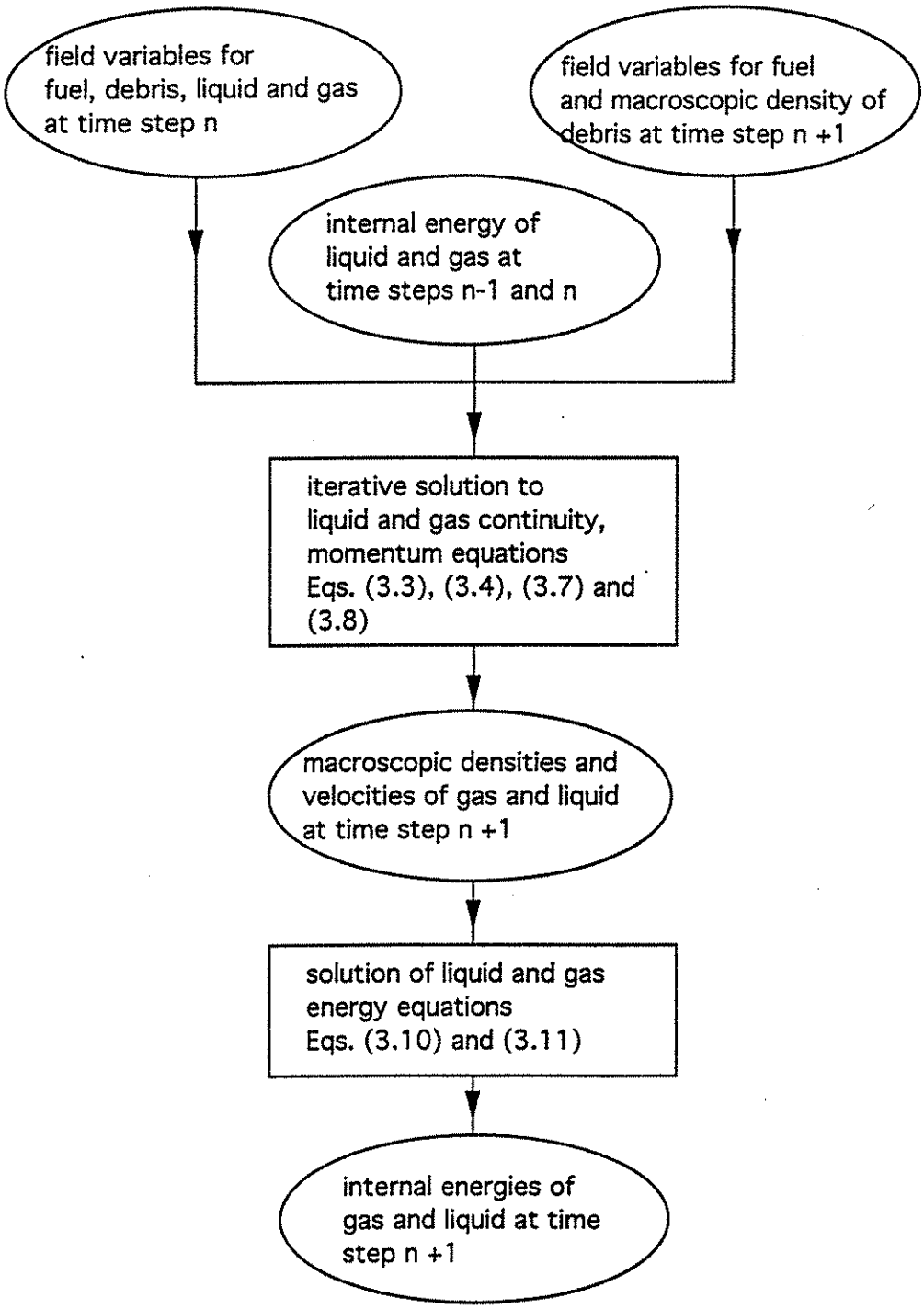

Figure 4.2. Schematic diagram of the implicit solution algorithm for the continuity, momentum and energy equation for liquid and gas in PM-ALPHA.

JB cells in the z-direction, labelled with index j. The fluid region is surrounded by a single layer of fictitious cells (or phantom or boundary cells) so that the cells in the complete mesh total IB2 = IB +2 by JB2 = JB +2 (see Figure 4.3). Boundaries of the rectangular computational region can be chosen (1) as rigid walls with free-slip, (2) as specified inflow or outflow boundaries, (3) as boundaries of specified pressure. Internal obstacles can also be added. The computation is carried out for a fixed time step δt, labelled with index n.

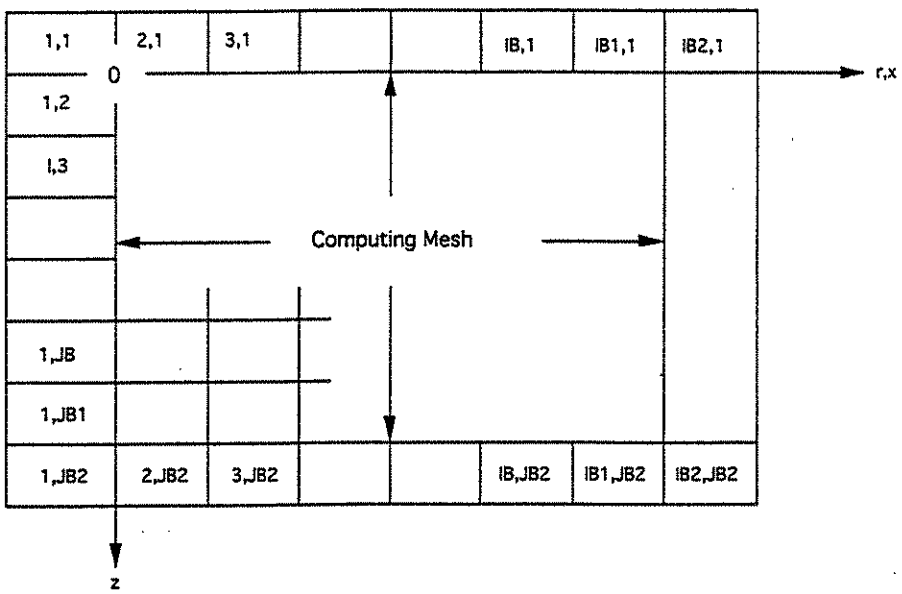

Figure 4.3. Computing mesh and surrounding fictitious cells.

Scalar quantities such as pressure and fluid density and vector quantities such as velocities are located in "staggered" cell positions as shown in Figure 4.4: u-velocity at the middle of the vertical sides of a cell, v-velocity at the middle of the horizontal sides and pressure (and other scalar variables) at the cell center. The finite difference notation involves subscripts for cell location and superscripts for the time level at which quantities are evaluated. That is,

$Q^n_{i,j}$ = scalar quantity Q at center of cell (i,j) at time level n

$u^n_{i+\frac{1}{2},j}$ = r-direction (or x-direction) velocity at middle of right side of cell (i,j) at time level n

$v^n_{i,j+\frac{1}{2}}$ = z-direction velocity at middle of top side of cell (i,j) at time level n

The staggered grid derives from staggering the control volume for momentum as illustrated in Figure 4.5. Values at half-grid points are obtained by averaging values at neighboring cells. [Note: Since in FORTRAN fractional indices are not allowed, in the code. $u^n_{i+\frac{1}{2},j}$ and $v^n_{i,j+\frac{1}{2}}$ are written as $u^n(i.j)$ and $v^n(i,j)$ respectively.

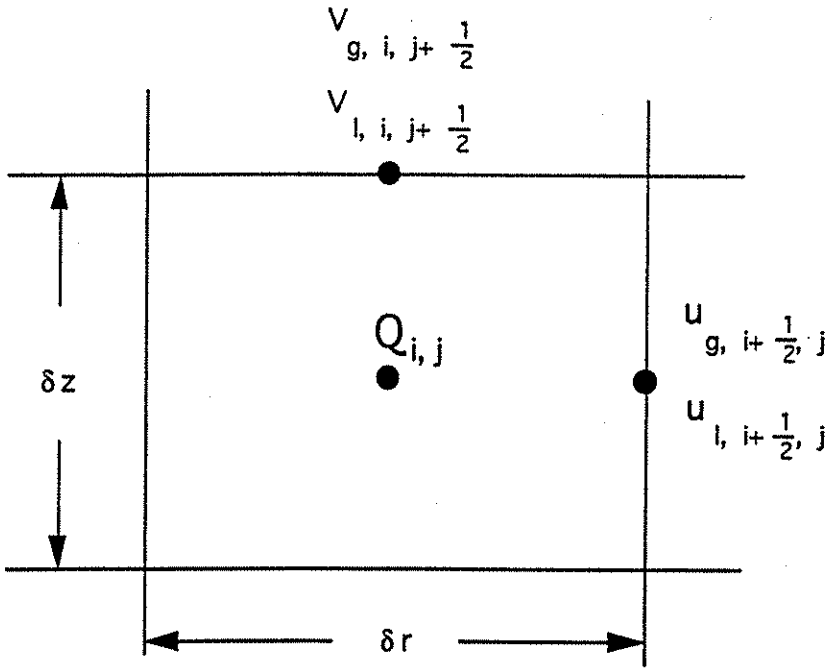

Figure 4.4. Locations of variables in the finite difference equations for a typical cell.

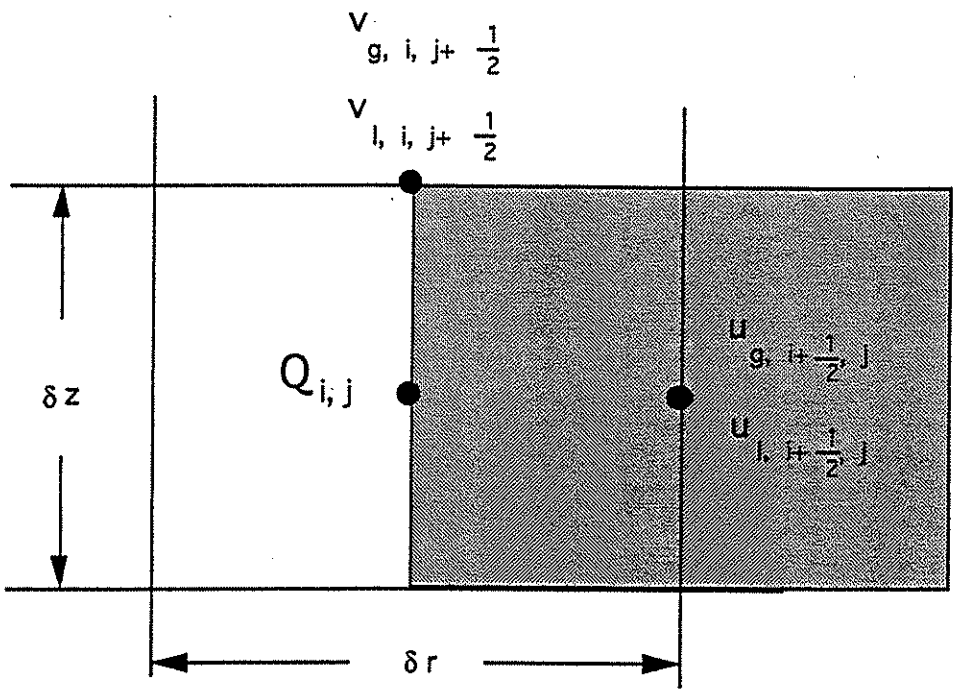

Figure 4.5. Momentum control volume in relation to the main control volume for scalar variables.

All illustrations, of the numerical procedure, that follow are given for the axisymmetric case. In writing the finite difference equations we make use of the notation $< Qur >$ and $< Qv >$ to express differences in flux quantities of the scalar Q, as follows:

$$< Qv >_{i,j} = < Qv >^{+}_{i,j} - < Qv >^{-}_{i,j} \tag{4.1}$$

The quantities on the r.h.s. of this equation are, in turn, written out using donor-cell differencing, as follows

$$< Qv >^{+}_{i,j} = v_{i,j+1/2} \begin{cases} Q_{i,j} & \text{if } v_{i,j+1/2} > 0. \\ Q_{i,j+1} & \text{if } v_{i,j+1/2} \leq 0. \end{cases} \tag{4.2}$$

$$< Qv >^{-}_{i,j} = v_{i,j-1/2} \begin{cases} Q_{i,j-1} & \text{if } v_{i,j-1/2} > 0. \\ Q_{i,j} & \text{if } v_{i,j-1/2} \leq 0. \end{cases} \tag{4.3}$$

In the special case that Q involves a velocity component, we have momentum fluxes, which have to be written in terms of fractional indices. Similarly then, for example, when $Q = \rho'_f u_f$, we have:

$$< Qv >_{i+1/2,j} = < Qv >^{+}_{i+1/2,j} - < Qv >^{-}_{i+1/2,j} \tag{4.4}$$

where

$$< Qv >^{+}_{i+1/2,j} = v_{i+1/2,j+1/2} \begin{cases} Q_{i+1/2,j} & \text{if } v_{i+1/2,j+1/2} > 0. \\ Q_{i+1/2,j+1} & \text{if } v_{i+1/2,j+1/2} \leq 0. \end{cases} \tag{4.5}$$

$$< Qv >^{-}_{i+1/2,j} = v_{i+1/2,j-1/2} \begin{cases} Q_{i+1/2,j-1} & \text{if } v_{i+1/2,j-1/2} > 0. \\ Q_{i+1/2,j} & \text{if } v_{i+1/2,j-1/2} \leq 0. \end{cases} \tag{4.6}$$

4.3 Numerical Formulation for Fuel and the Debris Equations

As shown in Figure 4.1, the first step at the beginning of a new computational cycle is to advance the solution of the debris continuity equation, the length scale transport equation, and all three fuel conservation equations by the time step δt. This is done by using an explicit formulation of the finite difference equations, so that the unknown quantities at the end of the time step $(n+1)$ can be computed directly in terms of quantities known from time step n. Specifically, we are dealing with Eqs. (3.5), (3.6), (3.9), (3.12) and (3.13), and we solve for ρ'_f, ρ'_{db}, $\mathbf{u}_f$, I_f, and D_f. From the macroscopic densities the respective volume fractions can be obtained directly from the definitions (Eq. 3.1).

The finite difference equations are:

$$(\rho'_f)^{n+1}_{i,j} = (\rho'_f)^{n}_{i,j} - \delta t \left[\frac{< \left(\rho'_f\right)^n u^n_f r >_{i,j}}{r_i \delta r} + \frac{< \left(\rho'_f\right)^n v^n_f >_{i,j}}{\delta z} + (F_r)^n_{i,j} \right] \tag{4.7}$$

$$(\rho'_{db})^{n+1}_{i,j} = (\rho'_{db})^{n}_{i,j} - \delta t \left[\frac{< (\rho'_{db})^n u^n_\ell r >_{i,j}}{r_i \delta r} + \frac{< (\rho'_{db})^n v^n_\ell >_{i,j}}{\delta z} - (F_r)^n_{i,j} \right] \tag{4.8}$$

$$\begin{aligned}
(\rho'_f u_f)^{n+1}_{i+1/2,j} &= \left(\widetilde{\rho'_f u_f}\right)_{i+1/2,j} \\
&+ \delta t \Bigg\{ -\theta^n_{f,i+1/2,j} \frac{(p^n_{i+1,j} - p^n_{i,j})}{\delta r} + F^n_{gf,i+1/2,j} \left[(u_g)^n_{i+1/2,j} - (u_f)^n_{i+1/2,j} \right] \\
&\quad + F^n_{\ell f,i+1/2,j} \left[(u_\ell)^n_{i+1/2,j} - (u_f)^n_{i+1/2,j} \right] \Bigg\}
\end{aligned} \tag{4.9}$$

$$\begin{aligned}
(\rho'_f v_f)^{n+1}_{i,j+1/2} &= \left(\widetilde{\rho'_f v_f}\right)_{i,j+1/2} \\
&+ \delta t \Bigg\{ -\theta^n_{f,i,j+1/2} \frac{(p^n_{i,j+1} - p^n_{i,j})}{\delta z} + F^n_{gf,i,j+1/2} \left[(v_g)^n_{i,j+1/2} - (v_f)^n_{i,j+1/2} \right] \\
&\quad + F^n_{\ell f,i,j+1/2} \left[(v_\ell)^n_{i,j+1/2} - (v_f)^n_{i,j+1/2} \right] \Bigg\}
\end{aligned} \tag{4.10}$$

$$\begin{aligned}
(\rho'_f I_f)^{n+1}_{i,j} = (\rho'_f I_f)^{n}_{i,j} - \delta t \Bigg[& \frac{< \left(\rho'_f\right)^n I^n_f u^n_f r >_{i,j}}{r_i \delta r} + \frac{< \left(\rho'_f\right)^n I^n_f v^n_f >_{i,j}}{\delta z} \\
& + (\dot{q}_{fg})^n_{i,j} + (\dot{q}_{f\ell})^n_{i,j} + (\dot{q}_{r,f})^n_{i,j} + (F_r I_f)^n_{i,j} \Bigg]
\end{aligned} \tag{4.11}$$

$$\begin{aligned}
\left(\rho'_f \frac{1}{D_f}\right)^{n+1}_{i,j} = \left(\rho'_f \frac{1}{D_f}\right)^{n}_{i,j} - \delta t \Bigg[& \frac{< \left(\rho'_f\right)^n \frac{1}{D_f}^n u^n_f r >_{i,j}}{r_i \delta r} + \frac{< \left(\rho'_f\right)^n \frac{1}{D_f}^n v^n_f >_{i,j}}{\delta z} \\
& + \left(\frac{\rho'_f}{D_f^2}\right)^n_{i,j} \left\{ 2 \left(\frac{dD_f}{dt}\right)^n_{f,i,j} - \left(\frac{dD_f}{dt}\right)^n_{b,i,j} \right\} \Bigg]
\end{aligned} \tag{4.12}$$

where

$$\begin{aligned}
\left(\widetilde{\rho'_f u_f}\right)_{i+1/2,j} &= (\rho'_f u_f)^n_{i+1/2,j} \\
&+ \delta t \left\{ -(F_r u_f)^n_{i+1/2,j} - \frac{< \left(\rho'_f\right)^n u^n_f u^n_f r >_{i+1/2,j}}{r_{i+1/2} \delta r} - \frac{< \left(\rho'_f\right)^n u^n_f v^n_f >_{i+1/2,j}}{\delta z} \right\}
\end{aligned} \tag{4.13}$$

$$\left(\widetilde{\rho'_f v_f}\right)_{i,j+1/2} = \left(\rho'_f v_f\right)^n_{i,j+1/2} \tag{4.14}$$

$$+\,\delta t\left\{\rho'^{\,n}_{f\,i,j+1/2}g - \left(F_r v_f\right)^n_{i,j+1/2} - \frac{<\left(\rho'_f\right)^n v^n_f u^n_f r>_{i,j+1/2}}{r_i\delta r} - \frac{<\left(\rho'_f\right)^n v^n_f v^n_f>_{i,j+1/2}}{\delta z}\right\}$$

4.4 Implicit Coupling of the Liquid/Gas Continuity and Momentum

Following the procedure shown schematically in Figure 4.1, the next task in the computations is to advance the solution for the liquid and gas fields. This is done in two steps, as illustrated in Figure 4.2. The first step, which is discussed here, involves the coupling (implicitly) of the liquid/gas continuity and momentum equation, to obtain velocities, and macroscopic densities, at the end of time step $n+1$. This is done by means of an iterative scheme as described below. However, fluid compressibility is now important and the procedure must also involve the equation of state and volume fraction. That is, we have six equations in six unknowns (ρ'^{n+1}_ℓ, ρ'^{n+1}_g, $\mathbf{u}^{n+1}_\ell$, $\mathbf{u}^{n+1}_g$, p^{n+1}, θ^{n+1}_g). Since internal energies are advanced outside of the iteration scheme—the second step described in the next subsection—the effect of energy change is captured by using the previous and current energy values (time step $n-1$ and n) in the evaluation of microscopic densities at time step n and $n+1$, i.e.,

$$\rho^n_g = \rho_g(p^n, I^{n-1}_g), \qquad \rho^n_\ell = \rho_\ell(p^n, I^{n-1}_\ell) \tag{4.15}$$

$$\rho^{n+1}_g = \rho_g(p^{n+1}, I^n_g), \qquad \rho^{n+1}_\ell = \rho_\ell(p^{n+1}, I^n_\ell) \tag{4.16}$$

We first present the iteration scheme and then provide details of the calculation.

4.4.1 Description of the Iteration Scheme

A successive overrelaxation technique with pressure as the primary iteration variable is used. The object is to find the pressure that produces locally (each cell) flow-and-density conditions that satisfy the continuity equation of the gas *or* the liquid. This is determined by the mass "residues" obtained from the continuity equations as

$$D_\ell = \left(\rho'_\ell\right)^{(n+1)}_{i,j} - \left(\rho'_\ell\right)^n_{i,j} + \delta t\left[\frac{<\left(\rho'_\ell\right)^{(n+1)} u^{(n+1)}_\ell r>_{i,j}}{r_i\delta r} + \frac{<\left(\rho'_\ell\right)^{(n+1)} v^{(n+1)}_\ell>_{i,j}}{\delta z} + J^n_{i,j}\right] \tag{4.17a}$$

$$D_g = \left(\rho'_g\right)^{(n+1)}_{i,j} - \left(\rho'_g\right)^n_{i,j} + \delta t\left[\frac{<\left(\rho'_g\right)^{(n+1)} u^{(n+1)}_g r>_{i,j}}{r_i\delta r} + \frac{<\left(\rho'_g\right)^{(n+1)} v^{(n+1)}_g>_{i,j}}{\delta z} - J^n_{i,j}\right] \tag{4.17b}$$

and their approach to zero. [The $(n+1)$ designation in the above is to indicate that these are trial quantities for the solution of time step $n+1$—they become that, when the residue is sufficiently close to zero—how to obtain these trial solutions from the trial pressures, $p_{i,j}^{(n+1)}$, introduced in the next paragraph, is described in the next subsection.] In the computation the residues are compared to a specified small parameter, the convergence criterion, called CONV. To properly "scale" the level of acceptable residue we make use of the macroscopic densities, and employ the liquid continuity for high liquid fraction cells and the vapor continuity for high vapor fraction cells. That is,

$$CONV_{i,j} = \begin{cases} \epsilon_\ell \left(\rho'_\ell\right)_{i,j}^n & \text{for } \alpha_{i,j} < \alpha^* \\ \epsilon_g \left(\rho'_g\right)_{i,j}^n & \text{for } \alpha_{i,j} \geq \alpha^* \end{cases} \tag{4.18}$$

where ϵ_g and ϵ_ℓ are small parameters (typically of order 10^{-5}). The actual value of α^* utilized is not important, and a value of 0.5 is recommended.

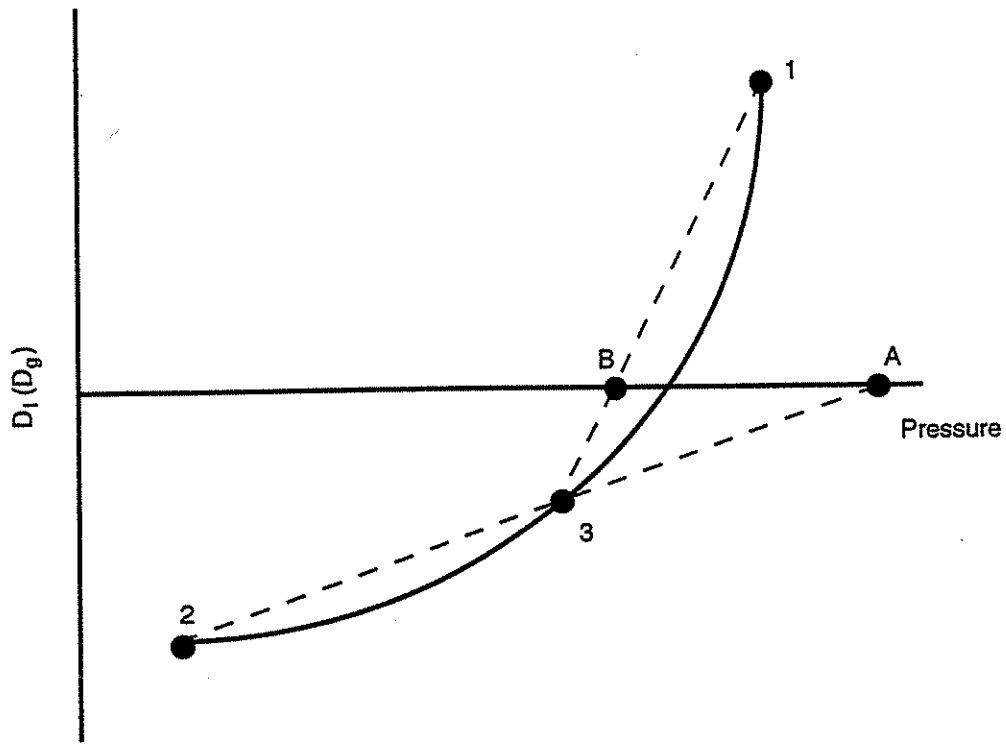

Figure 4.6. Pressure adjustment technique used in PM-ALPHA.

At each iteration cycle, a pressure adjustment is made, by using a constrained, two-sided secant method (as shown in Figure 4.6), until the residue meets the convergence criteria described above. At each cycle we must come up with two pressures (p_1 and p_2) that bound the solution (how to obtain the first two estimates is explained below); that is, giving residues of opposite sign in Figure 4.6, the pressure p_3 is then obtained from

$$p_3 = \frac{D(p_1)p_2 - D(p_2)p_1}{D(p_1) - D(p_2)} \tag{4.19}$$

and the p_A and p_B are found by the straight-line extrapolations as shown in Figure 4.6. The new estimate of the pressure (a trial value of $p_{i,j}^{n+1}$) is then computed as $p_{i,j}^{(n+1)} = (p_A + p_B)/2$. [If the pressure p_A should lie outside the interval p_1 to p_3, it is given the value $(p_1 + p_3)/2$.] If the convergence criterion is not met, one of the p_1, p_2, and p_3 is discarded so that the remaining two provide an improved bound for the next pressure estimate by repeating the above procedure.

To initiate this process (to find the first two pressures that bound the solution), we make use of the recurrence relations

$$p_{i,j} = p_{i,j} - \frac{D_\ell}{\left(\frac{dD_\ell}{dp}\right)} \tag{4.20}$$

or

$$p_{i,j} = p_{i,j} - \frac{D_g}{\left(\frac{dD_g}{dp}\right)} \tag{4.21}$$

Mathematically, the exact expressions for $\frac{dD_\ell}{dp}$ and $\frac{dD_g}{dp}$, calculated from Eqs. (4.17a) and (4.17b), are quite complicated. Since the purpose of these expressions is to generate the two bounding pressures, approximate expressions generated from pure two-phase continuity equations (i.e., ignoring the pressure of fuel and debris) are utilized in PM-ALPHA. They are

$$\begin{aligned}
\frac{dD_\ell}{dp} = {} & \frac{1-\alpha_{i,j}^n}{a_\ell^2} \\
& + \frac{(\rho_\ell)_{i,j}^n \alpha_{i,j}^n}{(\rho_g)_{i,j}^n a_g^2} + \left(\frac{\delta t}{\delta z}\right)^2 \left(2 + \alpha_{i,j}^n (\rho_\ell)_{i,j}^n \left\{ \frac{\alpha_{i,j+1/2}^n}{(\rho_g')_{i,j+1/2}^n + \delta t F_{g\ell,i,j+1/2}} \right.\right. \\
& \qquad \left.\left. + \alpha_{i,j-1/2}^n \left[(\rho_g')_{i,j-1/2}^n + \delta t F_{g\ell,i,j-1/2} \right] \right\} \right) \\
& + \left(\frac{\delta t}{\delta r}\right)^2 \left(r_{i+1/2} + r_{i-1/2} + \frac{\alpha_{i,j}^n (\rho_\ell)_{i,j}^n}{r_i} \left\{ \frac{r_{i+1/2}\alpha_{i+1/2,j}^n}{(\rho_g')_{i+1/2,j}^n + \delta t F_{g\ell,i+1/2,j}} \right.\right. \\
& \qquad \left.\left. + \frac{r_{i-1/2}\alpha_{i-1/2,j}^n}{(\rho_g')_{i-1/2,j}^n + \delta t F_{g\ell,i-1/2,j}} \right\} \right), \qquad \text{for } \alpha_{i,j}^n < \alpha^*
\end{aligned} \tag{4.22}$$

and

$$\frac{dD_g}{dp} = \frac{\alpha_{i,j}^n}{a_g^2} + \frac{1}{2} \times$$
$$\left\{ \left(\frac{\delta t}{\delta r}\right)^2 \frac{r_{i+1/2}\left(\alpha_{i,j}^n + \alpha_{i+1,j}^n\right) + r_{i-1/2}\left(\alpha_{i,j}^n + \alpha_{i-1,j}^n\right)}{r_i} \right.$$
$$\left. + \left(\frac{\delta t}{\delta z}\right)^2 \left[2\alpha_{i,j}^n + \alpha_{i,j+1}^n + \alpha_{i,j-1}^n\right] \right\}, \qquad \text{for } \alpha_{i,j}^n \geq \alpha^* \tag{4.23}$$

Equations (4.20) and (4.21) are applied repeatedly until we get a residual of opposite sign. For an initial value of $p_{i,j}$ we use $p_{i,j}^n$.

4.4.2 Procedure for Field Variables Evaluation in an Iteration Step

As mentioned above, at each iteration cycle the evaluation of the residues involves trial field quantities for the $n+1$ time step. They are obtained from the trial pressures, $p_{i,j}^{(n+1)}$, by solving the "other" (than that chosen for the residue) continuity equation, and the two momentum equations. The procedure, depicted in Figure 4.7, is explained below.

A first *estimate* of the void fraction is generated by solving the gas continuity equation with the latest values of the other variables. The finite-difference forms of the momentum equations, Eqs. (3.7) and (3.8), can then be solved to obtain the trial velocities, in closed form. For example, the values at a cell right and top boundaries can be written as:

$$(u_\ell)_{i+1/2,j}^{(n+1)} = \frac{B_1 A_{22,i+1/2,j} - B_2 A_{12,i+1/2,j}}{A_{11,i+1/2,j} A_{22,i+1/2,j} - A_{21,i+1/2,j} A_{12,i+1/2,j}} \tag{4.24}$$

$$(u_g)_{i+1/2,j}^{(n+1)} = \frac{-B_1 A_{21,i+1/2,j} + B_2 A_{11,i+1/2,j}}{A_{11,i+1/2,j} A_{22,i+1/2,j} - A_{21,i+1/2,j} A_{12,i+1/2,j}} \tag{4.25}$$

$$(v_\ell)_{i,j+1/2}^{(n+1)} = \frac{C_1 A_{22,i,j+1/2} - C_2 A_{12,i,j+1/2}}{A_{11,i,j+1/2} A_{22,i,j+1/2} - A_{21,i,j+1/2} A_{12,i,j+1/2}} \tag{4.26}$$

$$(v_g)_{i,j+1/2}^{(n+1)} = \frac{-C_1 A_{21,i,j+1/2} + C_2 A_{11,i,j+1/2}}{A_{11,i,j+1/2} A_{22,i,j+1/2} - A_{21,i,j+1/2} A_{12,i,j+1/2}} \tag{4.27}$$

where

$$A_{11,i,j} = (\rho_\ell')_{i,j}^{(n+1)} + (\rho_{db}')_{i,j}^{n+1} + \delta t \left[F_{g\ell,i,j}^n + F_{\ell f,i,j}^n + J_{i,j}^n H(J_{i,j}^n)\right] \tag{4.28}$$

$$A_{12,i,j} = \delta t \left[-F_{g\ell,i,j}^n + J_{i,j}^n H(-J_{i,j}^n)\right] \tag{4.29}$$

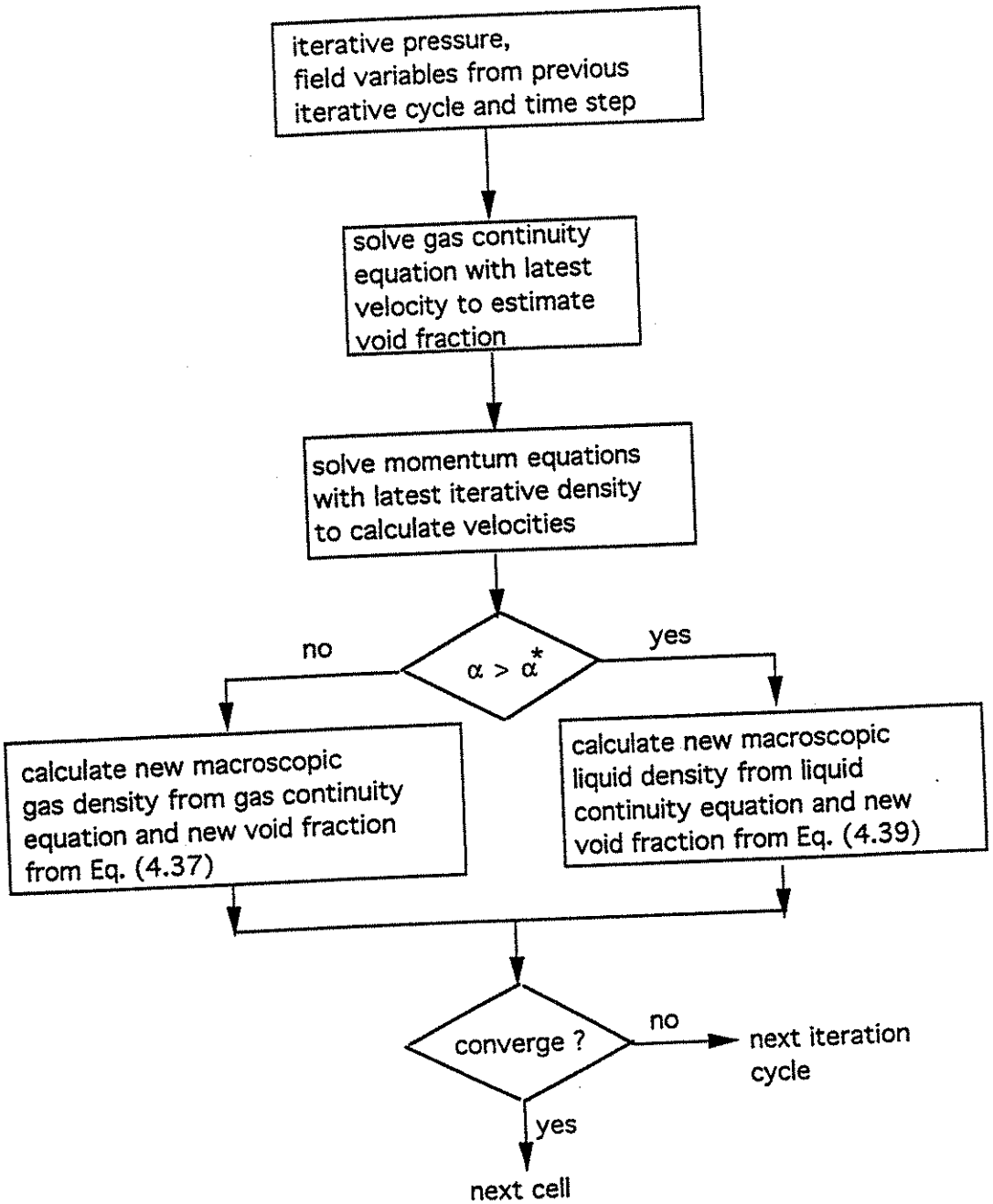

Figure 4.7. Schematic of one iteration cycle in the solution of the gas and liquid continuity and momentum equations.

$$A_{21,i,j} = -\delta t \left[F^n_{g\ell,i,j} + J^n_{i,j} H(J^n_{i,j}) \right] \tag{4.30}$$

$$A_{22,i,j} = \left(\rho'_g\right)^{(n+1)}_{i,j} + \delta t \left[F^n_{g\ell,i,j} + F^n_{gf,i,j} + J^n_{i,j} H(-J^n_{i,j}) \right] \tag{4.31}$$

$$\begin{aligned} B_1 = \left[(\rho'_\ell + \widetilde{\rho'_{db}})\, u_\ell \right]_{i+1/2,j} - \delta t \Bigg\{ & \left[\left(1 - \theta^{n+1}_{f,i+1/2,j} - \theta^{n+1}_{db,i+1/2,j} \right) \left(1 - \alpha^{(n+1)}_{i+1/2,j} \right) \right. \\ & \left. + (\theta_{db})^{n+1}_{i+1/2,j} \right] \frac{p^{(n+1)}_{i+1,j} - p^{(n+1)}_{i,j}}{\delta r} \\ & - \left[F^n_{\ell f,i+1/2,j} + F^n_{r,i+1/2,j} \right] (u_f)^{n+1}_{i+1/2,j} \Bigg\} \end{aligned} \tag{4.32}$$

$$\begin{aligned} B_2 = \left(\widetilde{\rho'_g u_g} \right)_{i+1/2,j} - \delta t \Bigg\{ & \left(1 - \theta^{n+1}_{f,i+1/2,j} - \theta^{n+1}_{db,i+1/2,j} \right) \alpha^{(n+1)}_{i+1/2,j} \frac{p^{(n+1)}_{i+1,j} - p^{(n+1)}_{i,j}}{\delta r} \\ & - F^n_{gf,i+1/2,j} (u_f)^{n+1}_{i+1/2,j} \Bigg\} \end{aligned} \tag{4.33}$$

$$\begin{aligned} C_1 = & \left[(\rho'_\ell + \widetilde{\rho'_{db}})\, v_\ell \right]_{i,j+1/2} \\ & - \delta t \Bigg\{ \left[\left(1 - \theta^{n+1}_{f,i,j+1/2} - \theta^{n+1}_{db,i,j+1/2} \right) \left(1 - \alpha^{(n+1)}_{i,j+1/2} \right) \right. \\ & \left. + (\theta_{db})^{n+1}_{i,j+1/2} \right] \frac{p^{(n+1)}_{i,j+1} - p^{(n+1)}_{i,j}}{\delta z} - \left[(\rho'_\ell)^{(n+1)}_{i,j+1/2} + (\rho'_{db})^{n+1}_{i,j+1/2} \right] g \\ & - \left[F^n_{\ell f,i,j+1/2} + F^n_{n,i,j+1/2} \right] (v_f)^{n+1}_{i,j+1/2} \Bigg\} \end{aligned} \tag{4.34}$$

$$\begin{aligned} C_2 = \left(\widetilde{\rho'_g v_g} \right)_{i,j+1/2} - \delta t \Bigg\{ & \left[\left(1 - \theta^{n+1}_{f,i,j+1/2} - \theta^{n+1}_{db,i,j+1/2} \right) \alpha^{(n+1)}_{i,j+1/2} \right] \frac{p^{(n+1)}_{i,j+1} - p^{(n+1)}_{i,j}}{\delta z} \\ & - (\rho'_g)^{(n+1)}_{i,j+1/2}\, g - F^n_{gf,i,j+1/2} (v_f)^{n+1}_{i,j+1/2} \Bigg\} \end{aligned} \tag{4.35}$$

where the tilde velocities are defined by

$$\left((\widetilde{\rho'_\ell + \rho'_{db}})u_\ell\right)_{i+1/2,j} = [(\rho'_\ell + \rho'_{db})u_\ell]^n_{i+1/2,j}$$
$$+ \delta t \Bigg\{ Fr^n_{i+1/2,j}(u_f)^n_{i+1/2,j}$$
$$- \frac{< (\rho'_\ell + \rho'_{db})^n u^n_\ell u^n_\ell r >_{i+1/2,j}}{r_{i+1/2}\delta r}$$
$$- \frac{< (\rho'_\ell + \rho'_{db})^n u^n_\ell v^n_\ell >_{i+1/2,j}}{\delta z} \Bigg\} \tag{4.36}$$

$$\left[(\widetilde{\rho'_\ell + \rho'_{db}})v_\ell\right]_{i,j+1/2} = [(\rho'_\ell + \rho'_{db})v_\ell]^n_{i,j+1/2}$$
$$+ \delta t \Bigg\{ (\rho'_\ell + \rho'_{db})^n_{i,j+1/2} g + Fr^n_{i,j+1/2}(v_f)^n_{i,j+1/2}$$
$$- \frac{< (\rho'_\ell + \rho'_{db})^n v^n_\ell u^n_\ell r >_{i,j+1/2}}{r_i \delta r}$$
$$- \frac{< (\rho'_\ell + \rho'_{db})^n v^n_\ell v^n_\ell >_{i,j+1/2}}{\delta z} \Bigg\} \tag{4.37}$$

$$\left(\widetilde{\rho'_g u_g}\right)_{i+1/2,j} = (\rho'_g u_g)^n_{i+1/2,j}$$
$$+ \delta t \left\{ - \frac{< (\rho'_g)^n u^n_g u^n_g r >_{i+1/2,j}}{r_{i+1/2}\delta r} - \frac{< (\rho'_g)^n u^n_g v^n_g >_{i+1/2,j}}{\delta z} \right\} \tag{4.38}$$

$$\left(\widetilde{\rho'_g v_g}\right)_{i,j+1/2} = (\rho'_g v_g)^n_{i,j+1/2}$$
$$+ \delta t \Bigg\{ (\rho'_g)^n_{i,j+1/2} g - \frac{< (\rho'_g)^n v^n_g u^n_g r >_{i,j+1/2}}{r_i \delta r}$$
$$- \frac{< (\rho'_g)^n v^n_g v^n_g >_{i,j+1/2}}{\delta z} \Bigg\} \tag{4.39}$$

Finally, the new (trial) velocities are used to calculate new liquid or gas macroscopic densities by using the "other" continuity equation. For example, for $\alpha_{i,j} < \alpha^*$, we have

$$(\rho'_g)^{(n+1)}_{i,j} = (\rho'_g)^n_{i,j} - \delta t \left[\frac{< (\rho'_g)^{(n+1)} u^{(n+1)}_g r >_{i,j}}{r_i \delta r} + \frac{< (\rho'_g)^{(n+1)} v^{(n+1)}_g >_{i,j}}{\delta z} - J^n_{i,j} \right] \tag{4.40}$$

and from the definition of ρ'_g

$$\alpha_{i,j}^{(n+1)} = \frac{\left(\rho'_g\right)_{i,j}^{(n+1)}}{\left(1 - \theta_{f,i,j+1/2}^{n+1} - \theta_{db,i,j+1/2}^{n+1}\right) \rho_g \left(I_{g,i,j}^n, p_{i,j}^{(n+1)}\right)} \tag{4.41}$$

A new liquid macroscopic density is calculated from its definition, Eq. (3.1).

For $\alpha_{i,j}^n \geq \alpha^*$, the procedure is similar. The calculation of $\left(\rho'_g\right)_{i,j}^{(n+1)}$ is replaced by a calculation of $(\rho'_\ell)_{i,j}^{(n+1)}$ based on the liquid continuity equation as

$$(\rho'_\ell)_{i,j}^{(n+1)} = (\rho'_\ell)_{i,j}^n - \delta t \left[\frac{< (\rho'_\ell)^{(n+1)} u_\ell^{(n+1)} r >_{i,j}}{r_i \delta r} + \frac{< (\rho'_\ell)^{(n+1)} v_\ell^{(n+1)} >_{i,j}}{\delta z} + J_{i,j}^n \right] \tag{4.42}$$

the void fraction is calculated as

$$\alpha_{i,j}^{(n+1)} = 1 - \frac{(\rho'_\ell)_{i,j}^{(n+1)}}{\left(1 - \theta_{f,i,j+1/2}^{n+1} - \theta_{db,i,j+1/2}^{n+1}\right) \rho_\ell \left(I_{\ell,i,j}^n, p_{i,j}^{(n+1)}\right)} \tag{4.43}$$

and a new gas macroscopic density is calculated from Eq. (3.1).

This completes one iteration cycle. The logic of whether to make additional pressure adjustment or to move to the next cell is based on the value of residue D_g or D_ℓ.

The iteration is complete when all cells have $\mid D_\ell \mid$ or $\mid D_g \mid \leq CONV$ simultaneously. When this is achieved, a solution to the mass and momemtum equations for the two fields (liquid and gas) at the energy of the previous time step has been obtained.

4.5 Numerical Formulation for the Liquid/Gas Energy Equations

Although the liquid and gas energy equations are not coupled to the momentum/continuity equations, a significant degree of implicitness is maintained by allowing the coupling between themselves through interfacial heat transfers. This is affected by introducing

$$\widehat{T}_\ell = T_\ell^n + \frac{I_\ell^{n+1} - I_\ell^n}{c_{p\ell}} \tag{4.44}$$

and

$$\widehat{T}_g = T_g^n + \frac{I_g^{n+1} - I_g^n}{c_{pg}} \tag{4.45}$$

and using these quantities to estimate the liquid and gas temperatures at the end of the time step, i.e.,

$$T_\ell^{(n+1)} = \frac{\widehat{T}_\ell + (T_\ell)_{i,j}^n}{2} \tag{4.46}$$

$$T_g^{(n+1)} = \frac{\widehat{T}_g + (T_g)_{i,j}^n}{2} \tag{4.47}$$

The energy equations can then be written in finite-difference form as

$$\begin{aligned}
(\rho'_\ell I_\ell + \rho'_{db} I_{db})_{i,j}^{n+1} &= (\rho'_\ell I_\ell + \rho'_{db} I_{db})_{i,j}^n \\
&- \delta t \Bigg\{ \frac{< [(\rho'_\ell)^{n+1} I_\ell^n + (\rho'_{db})^{n+1} I_{db}^n] u_\ell^{n+1} r >_{i,j}}{r_i \delta r} \\
&+ \frac{< [(\rho'_\ell)^{n+1} I_\ell^n + (\rho'_{db})^{n+1} I_{db}^n] v_\ell^{n+1} >_{i,j}}{\delta z} \\
&+ p_{i,j}^n \left[\frac{(\theta_\ell + \theta_{db})_{i,j}^{n+1} - (\theta_\ell + \theta_{db})_{i,j}^n}{\delta t} + \frac{< (\theta_\ell + \theta_{db})^{n+1} u_\ell^{n+1} r >_{i,j}}{r_i \delta r} \right. \\
&\left. + \frac{< (\theta_\ell + \theta_{db})^{n+1} v_\ell^{n+1} >_{i,j}}{\delta z} \right] + (R_{\ell s})_{i,j}^n \left[\frac{\widehat{T}_\ell + (T_\ell)_{i,j}^n}{2} - (T_s)_{i,j}^n \right] \\
&+ (J h_\ell)_{i,j}^n - (\dot{q}_{f\ell})_{i,j}^n - (\dot{q}_{r,\ell})_{i,j}^n - [F_r I_f]_{i,j}^n \Bigg\}
\end{aligned} \tag{4.48}$$

$$\begin{aligned}
(\rho'_g I_g)_{i,j}^{n+1} &= (\rho'_g I_g)_{i,j}^n \\
&- \delta t \Bigg\{ \frac{< (\rho'_g)^{n+1} I_g^n u_g^{n+1} r >_{i,j}}{r_i \delta r} + \frac{< (\rho'_g)^{n+1} I_g^n v_g^{n+1} >_{i,j}}{\delta z} \\
&+ p_{i,j}^n \left[\frac{\theta_{g,i,j}^{n+1} - \theta_{g,i,j}^n}{\delta t} + \frac{< \theta_g^{n+1} u_g^{n+1} r >_{i,j}}{r_i \delta r} + \frac{< \theta_g^{n+1} v_g^{n+1} >_{i,j}}{\delta z} \right] \\
&+ (R_{gs})_{i,j}^n \left[\frac{\widehat{T}_g + (T_g)_{i,j}^n}{2} - (T_s)_{i,j}^n \right] - (J h_g)_{i,j}^n - (\dot{q}_{fg})_{i,j}^n - (\dot{q}_{r,g})_{i,j}^n \Bigg\}
\end{aligned} \tag{4.49}$$

On this basis, Eq. (4.49) can be solved in closed form to obtain

$$\begin{aligned}
I_{g,i,j}^{n+1} &= \frac{1}{(\rho'_g)_{i,j}^{n+1} + \frac{(R_{gs})_{i,j}^n \delta t}{2 c_{pg}}} \\
&\times \Bigg[(\rho'_g I_g)_{i,j}^n - \delta t \Bigg\{ \frac{< (\rho'_g)^{n+1} I_g^n u_g^{n+1} r >_{i,j}}{r_i \delta r} + \frac{< (\rho'_g)^{n+1} I_g^n v_g^{n+1} >_{i,j}}{\delta z} \\
&+ p_{i,j}^n \left[\frac{\theta_{g,i,j}^{n+1} - \theta_{g,i,j}^n}{\delta t} + \frac{< \theta_g^{n+1} u_g^{n+1} r >_{i,j}}{r_i \delta r} + \frac{< \theta_g^{n+1} v_g^{n+1} >_{i,j}}{\delta z} \right] \\
&+ (R_{gs})_{i,j}^n \left[(T_g)_{i,j}^n - \frac{I_{g,i,j}^n}{2 c_{pg}} - (T_s)_{i,j}^n \right] \\
&- (J h_g)_{i,j}^n - (\dot{q}_{fg})_{i,j}^n - (\dot{q}_{r,g})_{i,j}^n \Bigg\} \Bigg]
\end{aligned} \tag{4.50}$$

while Eq. (4.48) must be solved iteratively so as to allow for thermal equilibration between the debris and the liquid. The form of the equation used is

$$
\begin{aligned}
&(\rho'_\ell I_\ell + \rho'_{db} I_{db})^{n+1}_{i,j} - \frac{(R_{\ell s})^n_{i,j} I^{n+1}_{\ell,i,j}\,\delta t}{2c_{p\ell}} = (\rho'_\ell I_\ell + \rho'_{db} I_{db})^n_{i,j} \\
&- \delta t \Bigg\{ \frac{< [(\rho'_\ell)^{n+1} I^n_\ell + (\rho'_{db})^{n+1} I^n_{db}] u^{n+1}_\ell r >_{i,j}}{r_i \delta r} \\
&\quad + \frac{< [(\rho'_\ell)^{n+1} I^n_\ell + (\rho'_{db})^{n+1} I^n_{db}] v^{n+1}_\ell >_{i,j}}{\delta z} \\
&\quad + p^n_{i,j} \left[\frac{(\theta_\ell + \theta_{db})^{n+1}_{i,j} - (\theta_\ell + \theta_{db})^n_{i,j}}{\delta t} + \frac{< (\theta_\ell + \theta_{db})^{n+1} u^{n+1}_\ell r >_{i,j}}{r_i \delta r} \right. \\
&\quad \left. + \frac{< (\theta_\ell + \theta_{db})^{n+1} v^{n+1}_\ell >_{i,j}}{\delta z} \right] + (R_{\ell s})^n_{i,j} \left[(T_\ell)^n_{i,j} - \frac{I^n_{\ell,i,j}}{2c_{p\ell}} - (T_s)^n_{i,j} \right] \\
&\quad + (Jh_\ell)^n_{i,j} - (\dot{q}_{f\ell})^n_{i,j} - (\dot{q}_{r,\ell})^n_{i,j} - [F_r I_f]^n_{i,j} \Bigg\}
\end{aligned}
\tag{4.51}
$$

and the iteration is performed on the l.h.s. until the (known) r.h.s. is obtained.

Finally, using the predicted values of I_g^{n+1}, I_ℓ^{n+1}, and p^{n+1}, with the equation of state, values for T_g^{n+1} and T_ℓ^{n+1} are obtained. This completes a computational cycle.

4.6 Initial and Boundary Conditions

To begin the solution, initial conditions, the values of all dependent variables throughout the computational mesh are needed. They can be either provided by the user, as part of the input file, or be read from a "restart" file for continuing an ongoing computation. The primary variables are temperatures, pressures, velocities, and volume fractions. Internal energies and densities are computed from the equation of state.

To fully specify the solution, we also need to prescribe values of the dependent variables along all the boundary. As mentioned already, this is accomplished with the help of the fictitious cells illustrated in Figure 4.3. Two types of boundaries are allowed—impermeable, or open-to-flow. The former represents a rigid wall; a free-slip one in particular since the calculation is not intended to resolve viscous boundary layers. The latter can be either an inflow, by specifying the inlet velocities and associated scalar fluxes, or an outflow, by specifying the "external" pressure, or simply stating that the flow exits smoothly ("continuous flux outflow"). Inflows are allowed at the top and left boundaries of the mesh, while outflows, at the bottom and right boundaries. Any number of cells can be combined to form an inlet or outlet, but only up to two distinct inlets/outlets are allowed on each mesh boundary.

Particular shapes of mesh boundaries, or even internal structures, can be synthesized by assigning any number of mesh cells to a solid status. The boundary conditions on these solid cells are enforced in the same manner as those at the flow field boundaries, thus this solid must be at least two cells wide in each direction (to allow for the fictitious cells).

The implementation of these boundary conditions are illustrated in Figures 4.8 through 4.11.

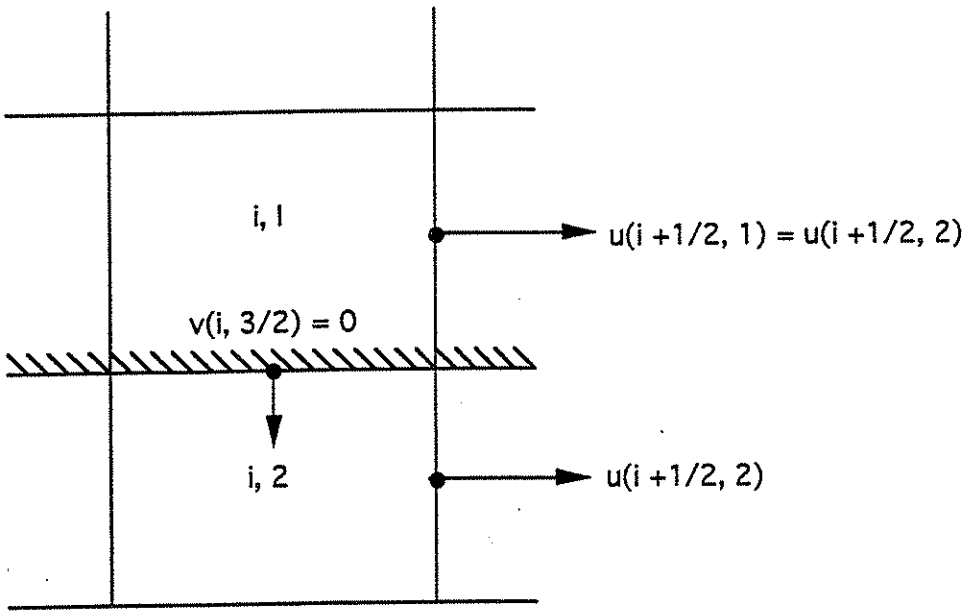

Figure 4.8. Illustration of the free-slip boundary condition specified at a top cell.

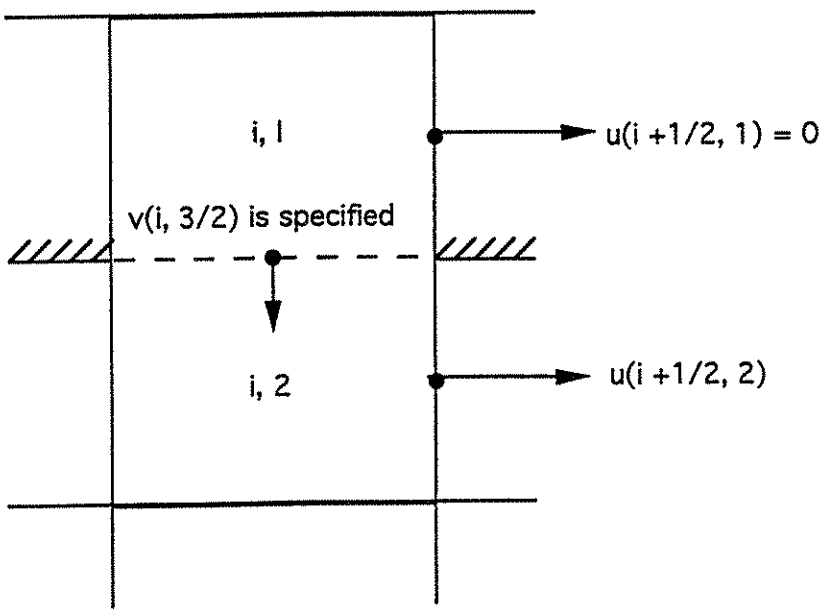

Figure 4.9. Illustration of the specified inflow condition at a top cell.

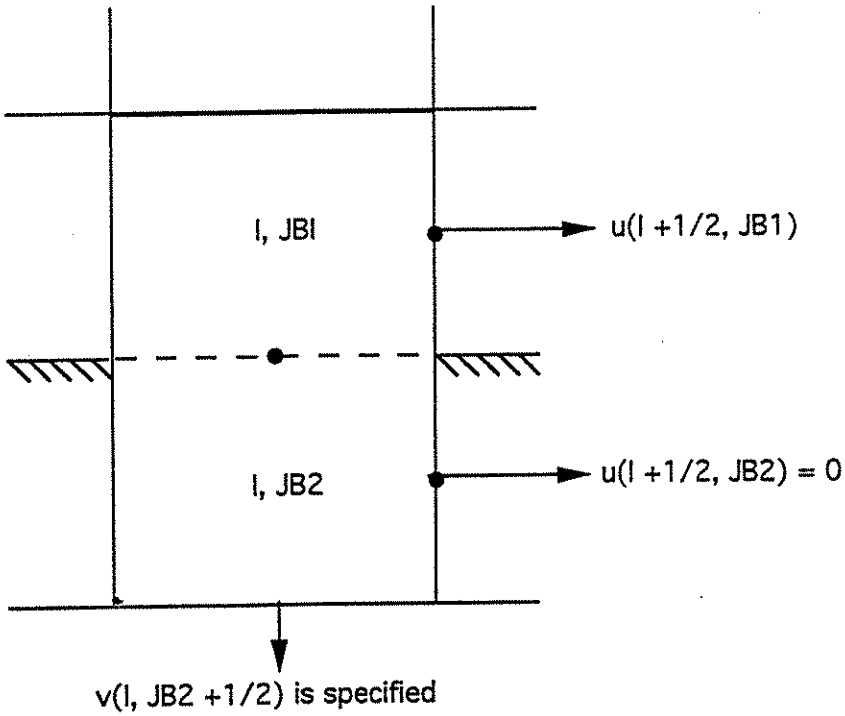

Figure 4.10. Illustration of the specified outflow condition at a bottom cell.

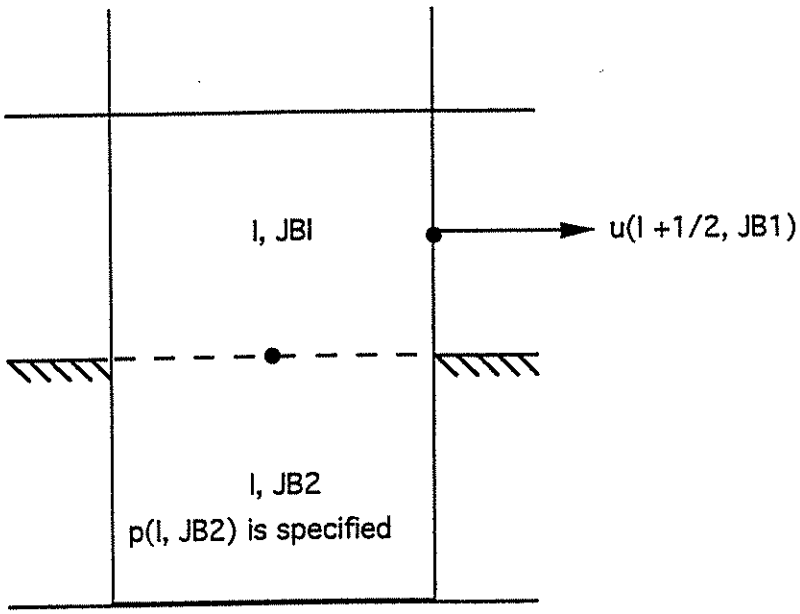

Figure 4.11. Illustration of the specified pressure condition at a bottom cell.

5. PROGRAM STRUCTURE AND CONTROL

5.1 Global Description

The structure of the program and the calling sequence for the various subroutines is shown in Figure 5.1. The calculation begins with the PM-ALPHA main program. The input data is read from input file PM-ALPHA.IN and in the case where the calculation is being continued from the results of a previous calculation, the initial conditions are read from a file named PMALPHA.RST by subroutine RESTART. Subroutine FLIC assigns values to the matrix of flags FL(ij) that is used to distinguish the various type of cells in the computing mesh and around its perimeter. There are five types of cells. Their flags are assigned according to Table 5.1. Subroutine SETUP is called to define various problem constants through subroutine SETC, and to calculate values of internal energies and densities from the equations of state in subroutines CONVERT and CONVTAN.

Table 5.1 Cell Flags

FL (IJ)	Cell Types
1	Fluid cell
2	Solid cell with free-slip boundaries
4	Continuous outflow boundary cell
5	Specified flux inflow cell
6	Specified boundary pressure cell

Control is then transferred to subroutine PROG for the rest of the calculation. The saturation state that corresponds to each cell pressure is calculated and transport properties of each phase are evaluated from the pressure and specific internal energies. Subroutine BDRY sets the boundary conditions around the mesh perimeter and the interior obstacles. Data dump options are checked at this point.

Subroutines TILDEP, EPCOOL, DPEXP, VELEPP and ICONVP are then executed to obtain time level $(n+1)$ values for the macroscopic density of fuel and debris, fuel velocities and fuel internal energy. Specifically, the subroutine EPCOOL is first executed to generate the new

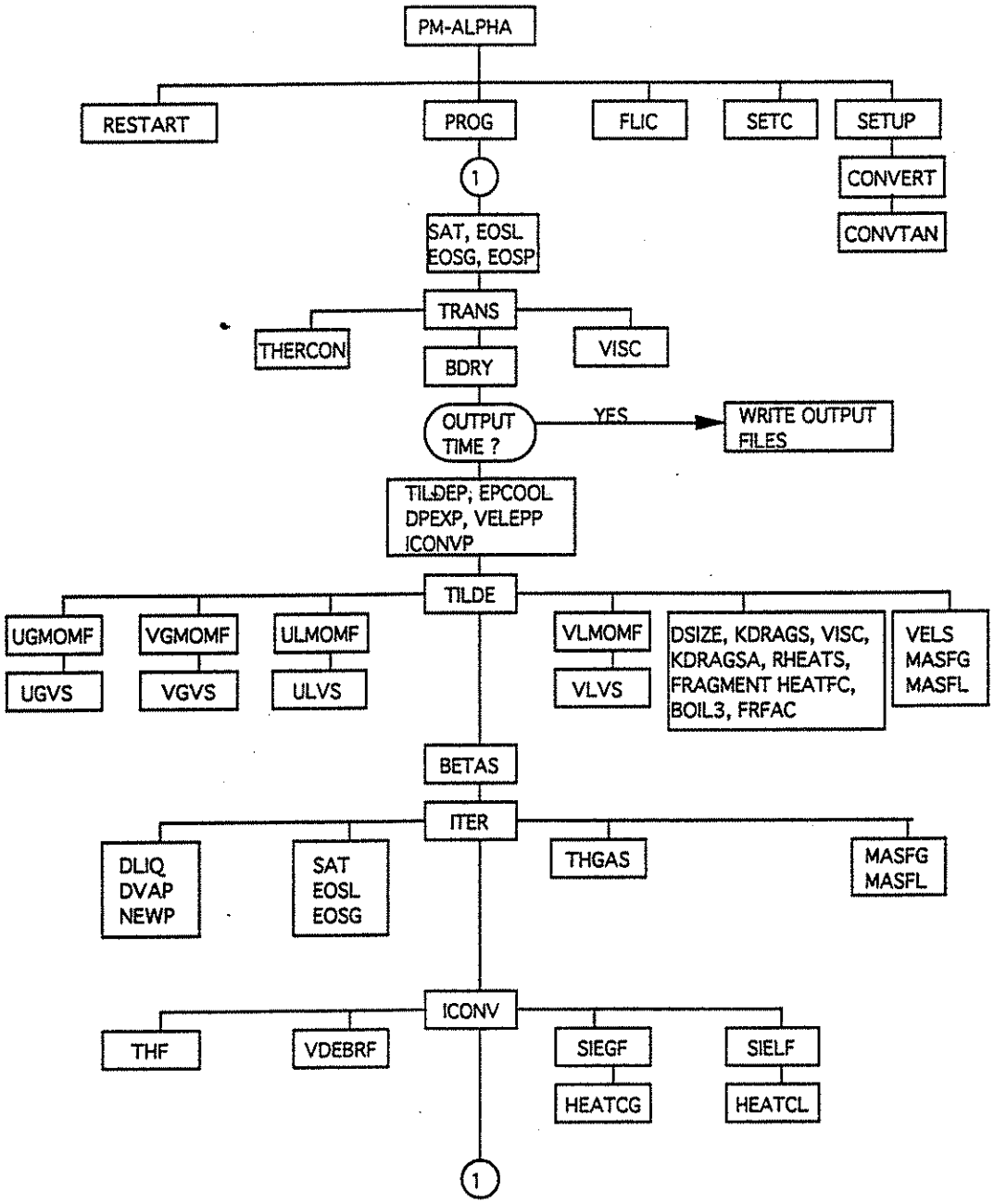

Figure 5.1. The PM-ALPHA program and subroutine calling sequence.

macroscopic densities of fuel and debris, ${\rho'_{f\,i,j}}^{n+1}$ and ${\rho'_{db\,i,j}}^{n+1}$. The subroutines VELEPP and TILDEP are then executed to generate the new velocities for the fuel, $\mathbf{u}^{n+1}_{f,i,j}$. The fuel internal energy and fuel length scale, $I^{n+1}_{f,i,j}$ and $D^{n+1}_{f,i,j}$, are then updated in subroutines ICONVP and DPEXP.

Subroutine TILDE then initiates the time advance sequence for liquid and gas by computing the tilde values of momentum flux and going on to estimate values of the new velocities, mass flux, and exchange rates for mass, momentum and energy. Subroutine BETAS then calculates the convergence criteria from Eq. (4.18) and the values of $\frac{dD_l}{dp}$ and $\frac{dD_g}{dp}$ from Eqs. (4.22) and (4.23). Subroutine ITER adjusts the pressure field until the convergence criterion is met simultaneously in all cells. The time level $(n+1)$ values are thus determined for the liquid and gas velocities, macroscopic densities, pressure and void fractions. Time level $(n+1)$ values of the specific internal energies are determined in subroutine ICONV. Time level $(n+1)$ values of the temperatures and microscopic densities are then computed from the equations of state. This completes the computational cycle, and control is returned to the control box 1.

5.2 Description of Input Files

In addition to the main program, PMALPHA.F, a number of additional files are needed for the running of the code. The basic files are PMALPHA.IN, COM.INC and STEAM.TBL1. The file COM.INC contains all the common variables of the code. STEAM.TBL1 contains property data for water and steam generated from numerical interpolation of a standard table (Harr et al., 1984). The initial conditions, boundary conditions and values of various program parameters are set in PMALPHA.IN. If the "restart" option is chosen, the file PMALPHA.RST is required. If the zonal method version of the radiation model is used, the exchange factors must also be provided as input files. They are EXCH.DATA, EXSIDE.DATA and EXTOP.DATA.

In general, the file STEAM.TBL1 should remain unchanged unless the user wants to use an alternate steam table. The data in EXCH.DATA, EXSIDE.DATA and EXTOP.DATA correspond to the exchange factors $g_{ij}g_{i_1j_1}$, $g_{ij}s_{j_1}$ and $g_{ij}t_{i_1}$ respectively. They should be calculated prior to the computation for the selected geometry and grid size using the procedure as outlined in Appendix B.

The "parameter" statement in COM.INC defines the number of cells in the two directions, IB2 and JB2. It also contains the name and dimension of all variables used in the calculation. The file COM.INC needs to be present during the compilation of the main program PMALPHA.F. Whenever the geometry is changed, the code has to be recompiled. It should be noted that even for a two-dimensional calculation, PM-ALPHA treats all variables as a one-dimensional array.

The input file, PMALPHA.IN, is to a wide extent self-explanatory. For clarity, input parameters are grouped into different sections identified with section title. Physical descriptions of the entries and the associated input format are also provided at the same line and the line above. For completeness, all entries are explained in the rest of this section. A sample input file is provided in Appendix C, and we use the number identifying each group as the key in the explanations that follow. Quantities are in c.g.s. units.

1. The user specifies the title of the run (line 5), which will appear as header on the main output.

2. The coordinate system and the cell size are defined. Specification of integer 0 or 1 selects Cartesian or cylindrical coordinate system respectively. Cell size is given in terms of horizontal (radial) and vertical (axial) dimensions for the Cartesian (cylindrical) coordinate system and must obey the format shown above the line of entry. The origin of the coordinates is the upper left corner of the actual numerical grid.

3. The inlets and outlets to the flow field are defined. As discussed earlier, the whole flow field is surrounded by a "layer" of cells, which are not part of the numerical scheme but are used to specify boundary conditions. For each boundary, the user can specify up to two openings for inlet (at the top and left wall and must have flag of either 2 or 3) or outlet (at the bottom and right wall and must have flag of either 4, 5 or 6). In each group, flags for the opening are defined first, followed by the coordinates of the inlets (outlets): if only one inlet (outlet) per boundary is specified, the smaller coordinate of the inlet (outlet) is given first, followed by the larger one; the remaining two values are also set to be equal to the larger coordinate of the opening. If two openings are assigned, the last two values are set to be the smaller and larger coordinate of the second opening. The identification of flags with cell types is given in Table 5.1.

4. The boundary conditions for the cells that define the rest of the boundaries (rigid walls), and any internal obstacles, are given. The integer 0 must be specified to stand for free slip at the wall. Each wall (top, left, bottom and right) is defined separately. For each obstacle left and right, top and bottom coordinates of the obstacle are given.

5. The initial conditions are specified uniformly for the whole flow field and are limited to those of a stationary fluid (all velocities zero). The order is: the two velocity components, pressure, void fraction, coolant volume fraction, coolant temperature and fuel temperature. In addition, the acceleration of gravity is specified and lower/upper bounds of the internal energies of the water and steam and the steam temperature are given. The need for the specification of bounds for internal energies arises from the fact that in PM-ALPHA, the

main parameter is not the temperature, rather the internal energy. At this point, the code will search, within the specified bounds, for internal energies for water and steam which are consistent with the prescribed temperatures. The parameter ERSIE defined in the same line is the maximum percentage error accepted in this search.

6. The user inputs are designed in anticipation that for many practical premixing calculations, the geometry of interest is a pool of water with a free surface. The user can specify a gap of two-phase mixture over the pool of water (JGAP), the value of void fraction to be assigned to this gap (THGAP), and any superheat of the steam in this gap (DTGSAT). The parameter JGAP represents the number of rows, including the fictitious boundary layer at the top, that constitute the gap. The conditions specified for the steam gap in this section override the initial conditions in the region. Finally, TINTER is a time parameter which controls the inlet conditions of the top left opening as specified in the next group.

7. The inlet and outlet conditions are specified. For each inlet opening, coolant velocity, particle velocity, pressure, void fraction, coolant volume fraction, coolant temperature, particle temperature, and bounds for the internal energies of the water and steam and the steam temperature are given. The first two groups of input are for the top wall left inlet. The conditions specified in the first group are applied from time zero to time TINTER (specified above), while the second group applies from time TINTER to the end of the calculation. The two input conditions allow some flexibility in modelling discontinuous inlet condition (for example, an inlet pour of fuel over a finite time interval). The third group of input specified inlet conditions on the second top opening (if any), and the next two are for the two inlets on the left boundary. The next four groups are for the outlets on the right and bottom boundaries, depending on the flag assigned to each one of them. In each group, the same set of variables as those described above for inlet openings are specified. Variables which are not required by the assigned boundary conditions will be ignored by the code.

8. The output specifications and time step are listed. The ITD parameter is used to define whether this a new run or a continuation (restart) one, and whether a restart file (PMALPHA.RST) is to be written or not. The possible options set by ITD are shown in Table 5.2. The parameter NSDMP represents the frequency (number of time steps) between successive dumps to the restart file. The NWDMP parameter is a counter to define restart file dumps, and the value specified here is the time for the first dump. The next group of parameters are for time step control of the program. The usage of these parameters is summarized in Table 5.3.

Table 5.2 Options Set by Parameter ITD	
ITD	Options
0	Do not read or write PMALPHA.RST
1	Write but do not read PMALPHA.RST
2	Read but do not write PMALPHA.RST
3	Read and write PMALPHA.RST

Table 5.3 Time Control Parameters in PM-ALPHA	
Parameters	Purpose
TIME	Starting time of the calculation
TSTOP	Stopping time of the calculation
DT	Time step
TPR	Time interval to write data on output files

9. Constants and material properties for gas, liquid, and fuel are given. Gas properties are given first, followed by liquid and fuel properties.

10. In the next four groups of inputs, parameters for four physical models utilized in the code are specified. The first group is for the fuel heat conduction model. If the value of IHCM is set equal to zero the model is not used, if it is set equal to 1 it is used. In the latter case, ISMIJTR defines the number of cells in which the detailed temperature history is recorded as output. The IJ counter for those cells and the name of the associated output file are specified right after. This model should not be used if fuel fragmentation and/or breakup are allowed in the calculation.

The next group of parameters are for the phase change model. DELTS is the degree of subcooling/superheating of the steam/water before heat transfer enhancement is turned on. RHEATGMX and RHEATLMX stand for $\delta t/\tau_g$ and $\delta t/\tau_\ell$ where τ_g and τ_ℓ are time constants defined in Eqs. (3.61) and (3.62) respectively. In the calculation of the bounding boiling/condensation rate by Eq. (3.63), the characteristic time, τ_e, is assumed to be proportional to the computational time step. XPHTC and XPHTEV are the proportionality constants set for condensation and boiling respectively.

The parameters for the fragmentation model are set in the next group. The model is turned on by setting MFRAG to be 1. COEFL and COEFG are the correlation constants for the dimensionless breakup time (β_i in Eqs. (3.65)) for the liquid and gas phase respectively. The user is allowed to set minimum relative velocity for liquid and gas phase at which fragmentation is turned on. These velocities are VMINL and VMING. The drag coefficient used in the definition of Bond number is DRGCOEF. To simulate the effect of thermal fragmentation, the user can set a multiplicative factor XFRAG. XDMSODT is a constant fragmentation rate which the user can specify as another option. The actual fragmentation rate used in the code is the sum of XDMSODT and XFRAG times the value predicted by Eq. (3.81). DMSODTMX is an upper bound allowing for the fragmentation rate. TMSTART is a delay time over which the fuel can achieve the fragmentation rate as predicted by the constitutive law. It is used to prevent major discontinuities in the computation, and it is normally set at a small enough value to not distort the model. The fragmentation, after its initiation, can be continued at some minimum rate even when the relative velocities start to decrease. This minimum rate is given by a fraction of the maximum fragmentation rate computed previously in the same computational cell. XFM is that fraction. Finally, the fragmentation of fuel is expected to stop when the fuel particle becomes solidified. DTF is the liquid fraction of the fuel particle below which the fragmentation is turned off. The breakup mechanism, as described in section 3, is assumed to be active only when the void fraction is greater than THBR. BETABR is the breakup parameter, β_b, defined in Eq. (3.79). Note that the backup model can be turned off by setting THBR to be negative.

The next group of parameters are for the radiation model. When IRAD is set to be 1, the radiation model based on the zonal method is used. Otherwise, the simplified model is used. In the simplified model, the radiation emitted by the fuel is absorbed only by the water within the same computational cell. In the droplet flow regime, only a fraction of the radiation is absorbed. FRAD is that fraction (E_d in Eq. (3.50)). The remaining energy is returned back to the fuel. AWGIN is the steam absorption coefficient needed by the zonal model. It must be pre-calculated with the analysis presented in Appendix B.

11. This group of parameters is for control of the numerical iteration. EPSG and EPSL correspond to the convergence parameters ϵ_g and ϵ_ℓ introduced in Section 4. If the pressure iteration (in subroutine ITER) leads to two consecutive pressure predictions with a difference of less than DPRESMN, the code will also assume convergence.

12. The parameter, IJEX, is the IJ counter of one cell next to an opening at which the exit of masses is calculated in subroutine EXHSTY. The pairs (IP1, JP1) and (IP2, JP2) define two cells in which the subroutine INHSTY records detailed time step data from the calculation. On the next line, DTHSTY defines the step between successive calls of the subroutines INHSTY and EXHSTY. These special outputs may be needed for diagnostic purposes.

5.3 Description of Output Files

The main output is written to the file DATR at every time step defined by the TPR parameter. For every cell, values of all variables are written in the following order: icounter, jcounter, flag, radial gas velocity, radial liquid velocity, radial melt velocity, "free," evaporation rate, drag coefficient between gas and liquid, coolant volume fraction, axial gas velocity, axial liquid velocity, axial melt velocity, drag coefficient between gas and melt, drag coefficient between liquid and melt, density of gas, void fraction, gas temperature, liquid temperature, fuel temperature, saturation temperature, saturation pressure, fuel particle size, heat transfer rate from liquid to interface, internal energy of gas, liquid and fuel, heat flux from fuel to gas, heat flux from fuel to liquid, pressure. The variable "free" gives the user some flexibility in writing a selected variable into the DATR file at the assigned position This output file can then be manipulated to the desired form depending on the type of visualization software utilized.

In addition, single-parameter dedicated files are written by the code for a more coherent depiction of the results. Files DTH, DEPS, DUL, DUP, DUG, DVL, DVP, DVG, DTL, DTP, DTG contain the output for every cell in the grid for the void fraction, the coolant volume fraction, radial velocities for the liquid, particles, and gas, axial velocities for the liquid, particles and gas, temperature of liquid, particles and gas, respectively.

6. SAMPLE PROBLEM

The sample problem is that of a pour of 1500 °C zirconium oxide particles, 2.9 mm in diameter, entering the numerical grid at 4.1 m/s. The particles travel through a region containing steam only which is 39 cm long, then plunge into saturated water at atmospheric conditions. The liquid pool depth is 81 cm. The calculation is carried out in a cylindrical coordinate system. The diameter of the liquid pool is 60 cm and the diameter of the particle cloud is 24 cm. Inlet particle volume fraction is 2.0%. The particle inflow stops after 0.3 s and the calculation is carried on until 0.7 s after the initial pour. There is an outflow opening, kept at atmospheric pressure, at the uppermost right boundary of the numerical grid, 6 cm in height. Cell size is 3.0 cm in both radial and axial directions. These conditions are typical for the experimental runs in the MAGICO-2000 facility. The actual input file is given in Appendix D.

To execute the run, the source code is first compiled within the same directory that also contains the file COM.INC, which contains the specification of the number of cells of the numerical grid. In a workstation with a FORTRAN-77 compiler, for example, the following command is executed to create an executable file PMALPHA.X from a source code PMALPHA.F

```
F77 PMALPHA.F -o PMALPHA.X
```

The execution itself is then started by the command line:

```
PMALPHA.X < PMALPHA.IN > OUT
```

so that the input is read from file PMALPHA.IN and standard output is redirected to the file OUT: the latter contains the current calculation time so that one can check the progress of the calculation.

Utilizing available graphic software, typical output data generated by PM-ALPHA are shown as in two-dimensional contour plots in Figures 6.1 through 6.14. In these figures, the evolution of the premixing process in time is illustrated by two-dimensional contour lines of constant void fraction (the "lighter" lines), superposed with contour lines of constant fuel volume fraction (the "darker" lines).

These figures show the initial fuel penetration into water, the resulting "swelling" of the water level, and the subsequent slowing down and accumulation of fuel at the front. The momentum transfer from the fuel to the water causes the latter to move and subsequently to vaporize and generate a voided region in the pool. At 0.3 sec, the influx of fuel from the top opening stops. The fuel in the mixing region, however, continues to cause boiling and maintain the voided region. The fuel velocity data (not included here) show that the fuel is temporary suspended (at $\sim$ 0.3 - 0.4 sec) by the strong vapor fluxes flowing upward. The fuel finally reaches the bottom of the pool at about 0.7 sec. More detailed discussions on the physics of premixing have been presented elsewhere (see for example, Theofanous, et.al. 1995)

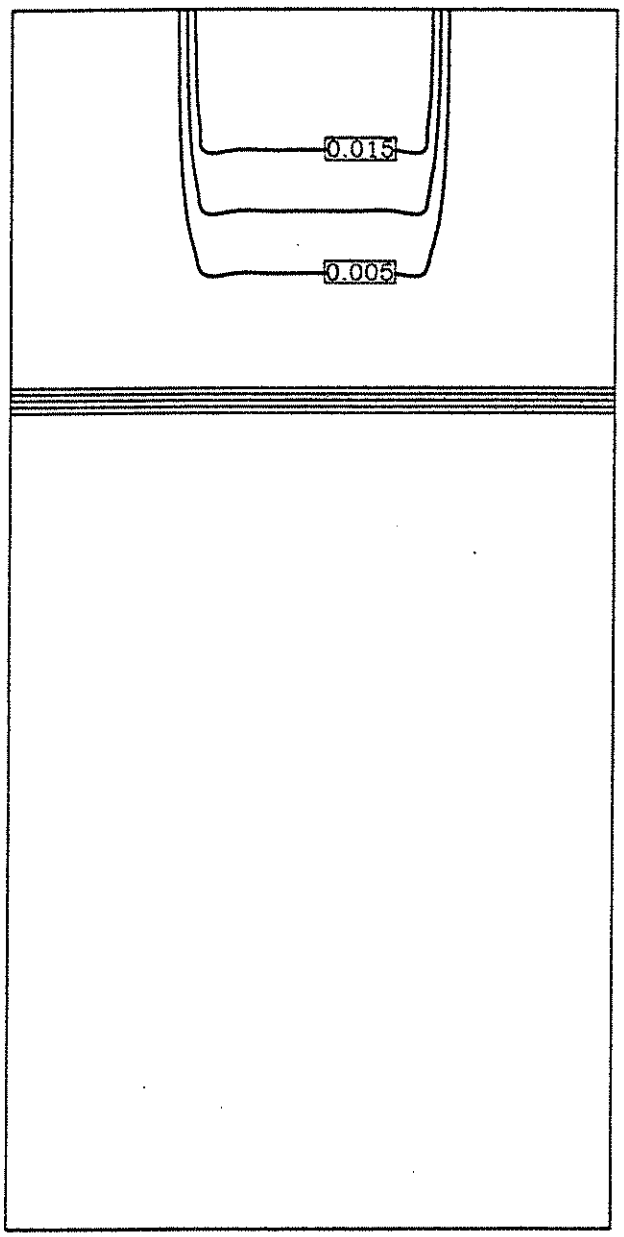

Figure 6.1. Contour plots of fuel volume fraction (marked darker lines) and void fraction (lighter lines) at time = 0.05 s. The void fraction contours begin (on the liquid side) with 0.9 and are in increments of 0.2.

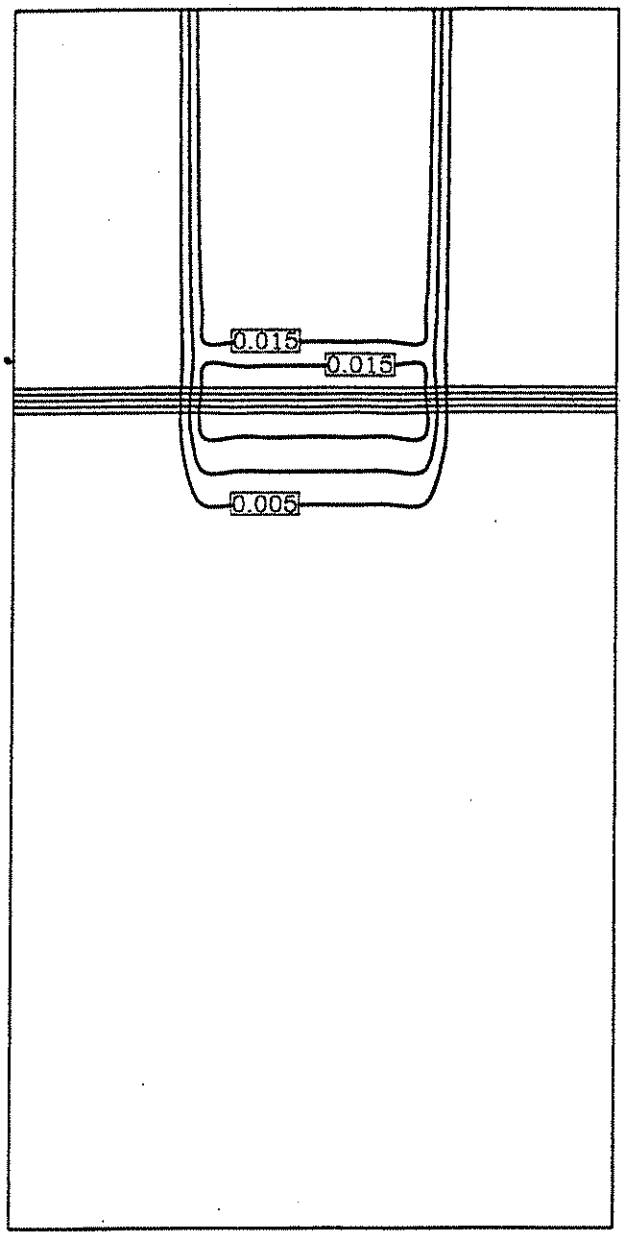

Figure 6.2. Contour plots of fuel volume fraction (marked darker lines) and void fraction (lighter lines) at time = 0.1 s. The void fraction contours begin (on the liquid side) with 0.9 and are in increments of 0.2.

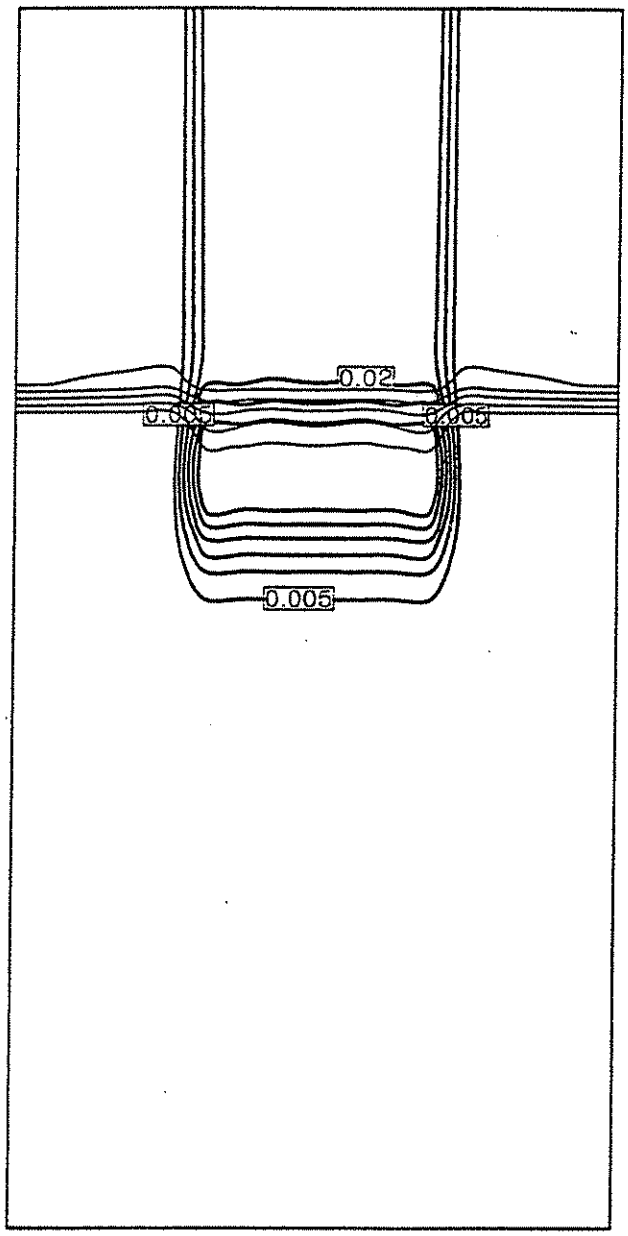

Figure 6.3. Contour plots of fuel volume fraction (marked darker lines) and void fraction (lighter lines) at time = 0.15 s. The void fraction contours begin (on the liquid side) with 0.9 and are in increments of 0.2.

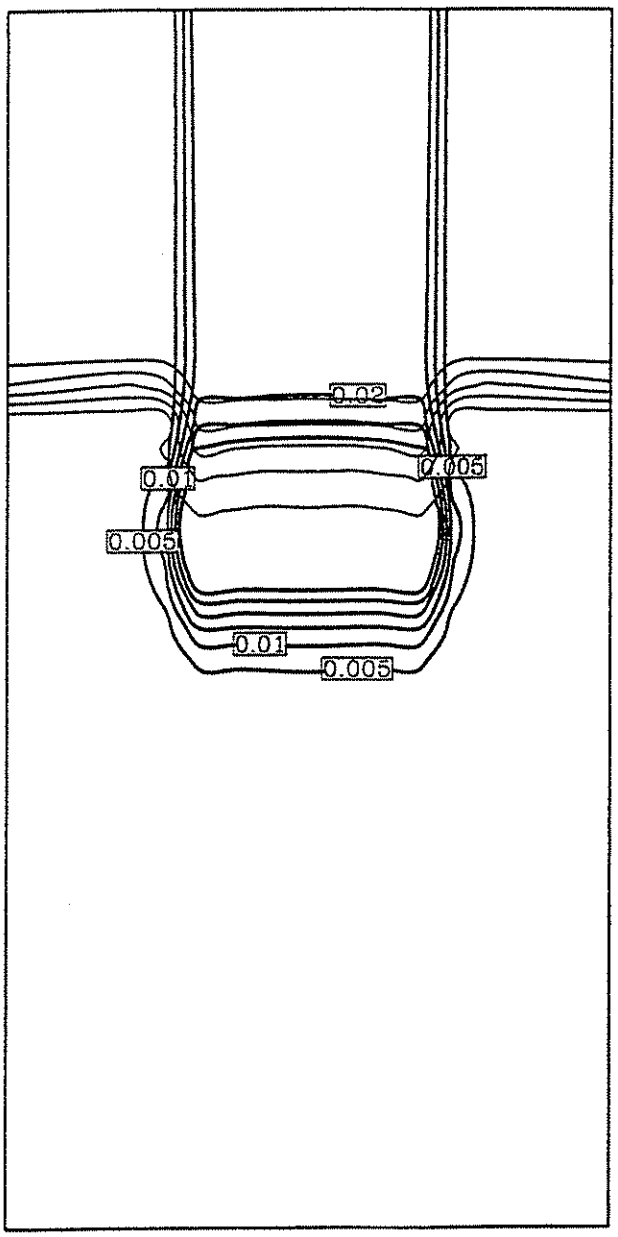

Figure 6.4. Contour plots of fuel volume fraction (marked darker lines) and void fraction (lighter lines) at time = 0.2 s. The void fraction contours begin (on the liquid side) with 0.9 and are in increments of 0.2.

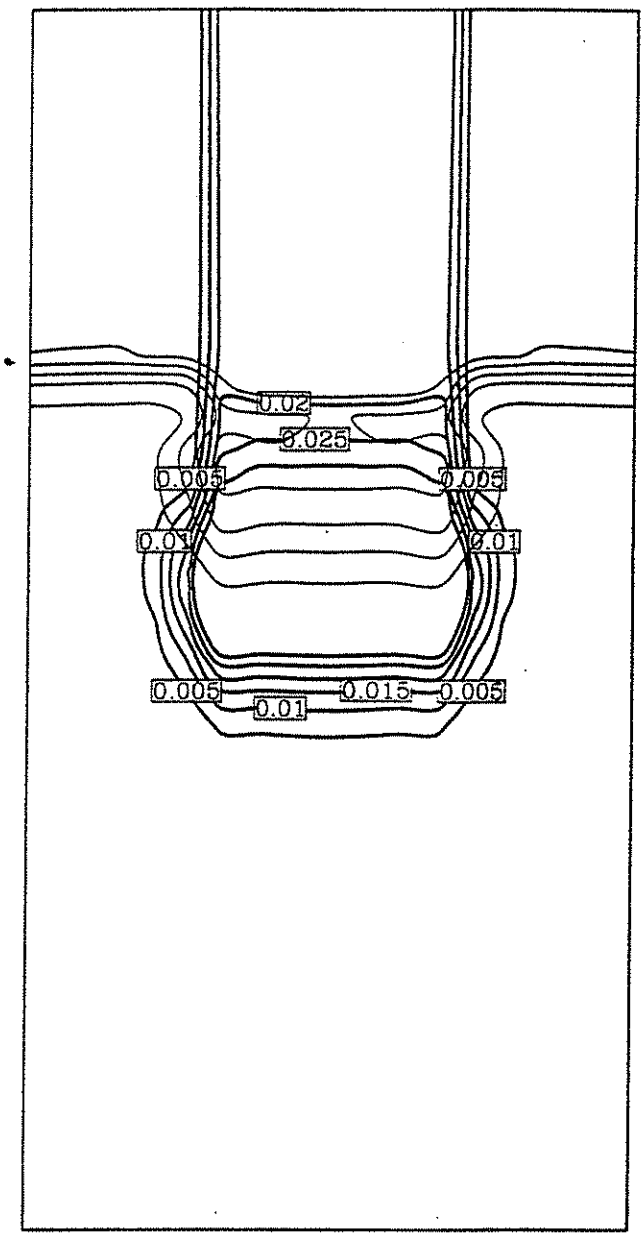

Figure 6.5. Contour plots of fuel volume fraction (marked darker lines) and void fraction (lighter lines) at time = 0.25 s. The void fraction contours begin (on the liquid side) with 0.9 and are in increments of 0.2.

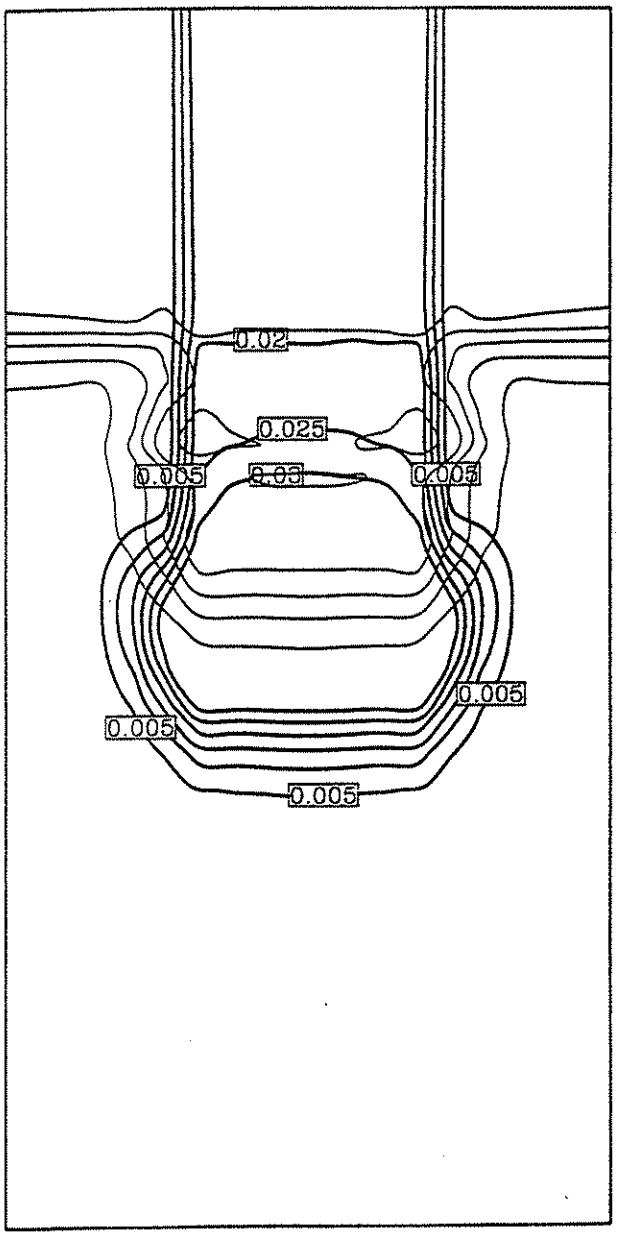

Figure 6.6. Contour plots of fuel volume fraction (marked darker lines) and void fraction (lighter lines) at time = 0.3 s. The void fraction contours begin (on the liquid side) with 0.9 and are in increments of 0.2.

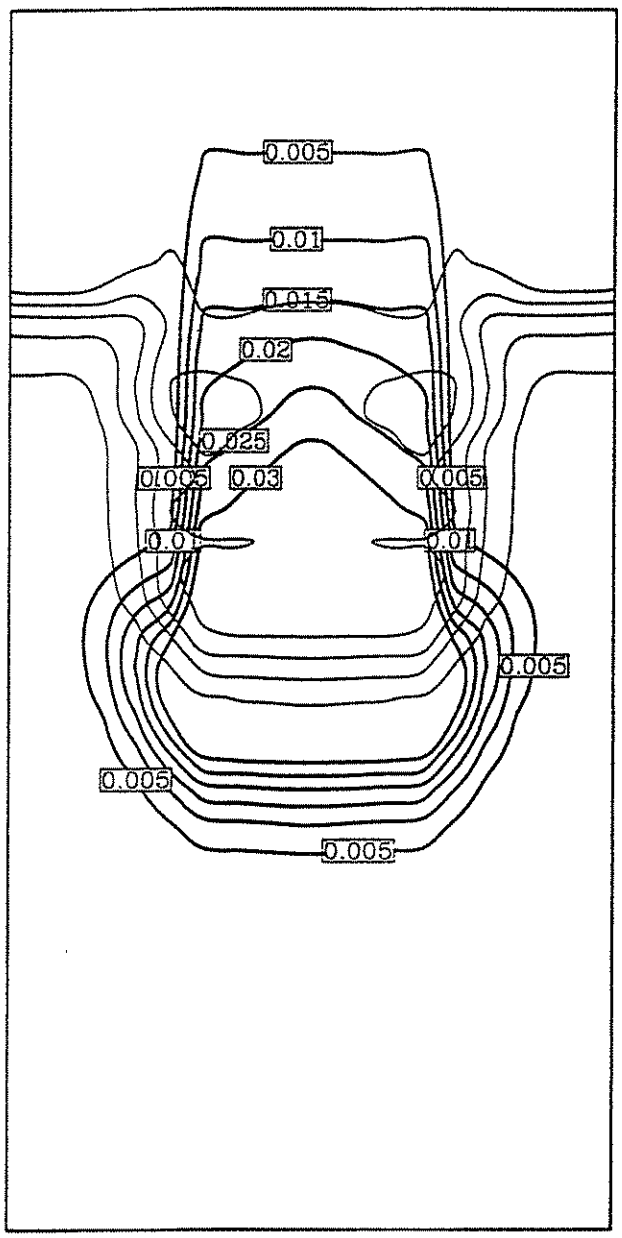

Figure 6.7. Contour plots of fuel volume fraction (marked darker lines) and void fraction (lighter lines) at time = 0.35 s. The void fraction contours begin (on the liquid side) with 0.9 and are in increments of 0.2.

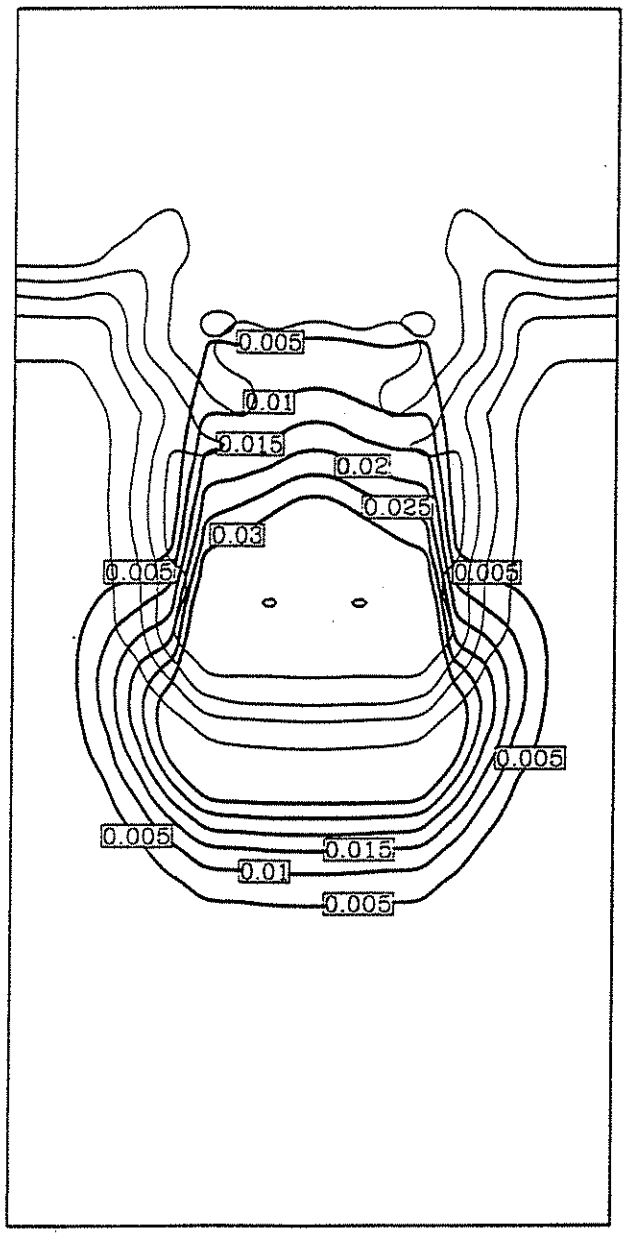

Figure 6.8 Contour plots of fuel volume fraction (marked darker lines) and void fraction (lighter lines) at time = 0.4 s. The void fraction contours begin (on the liquid side) with 0.9 and are in increments of 0.2.

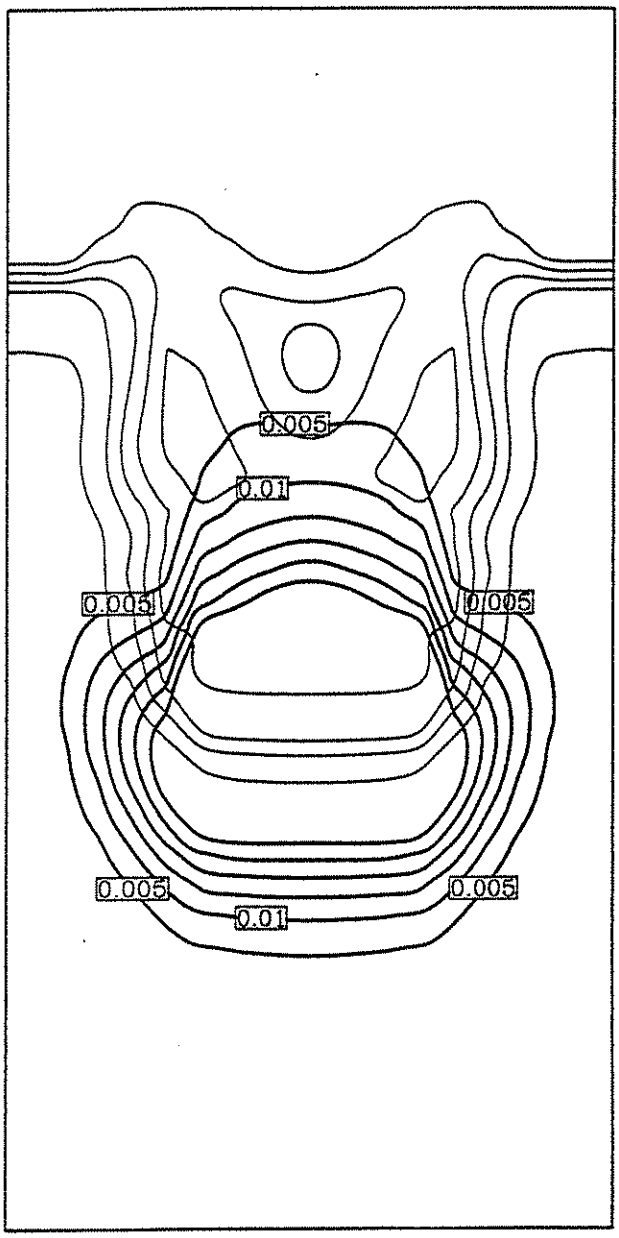

Figure 6.9. Contour plots of fuel volume fraction (marked darker lines) and void fraction (lighter lines) at time = 0.45 s. The void fraction contours begin (on the liquid side) with 0.9 and are in increments of 0.2.

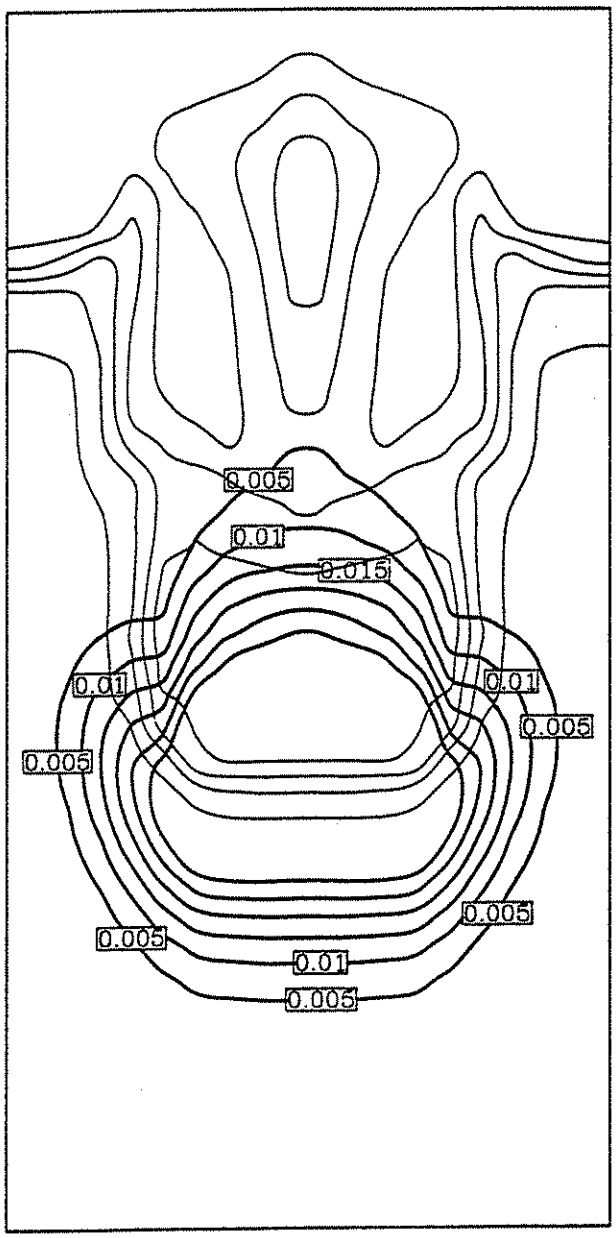

Figure 6.10. Contour plots of fuel volume fraction (marked darker lines) and void fraction (lighter lines) at time = 0.5 s. The void fraction contours begin (on the liquid side) with 0.9 and are in increments of 0.2.

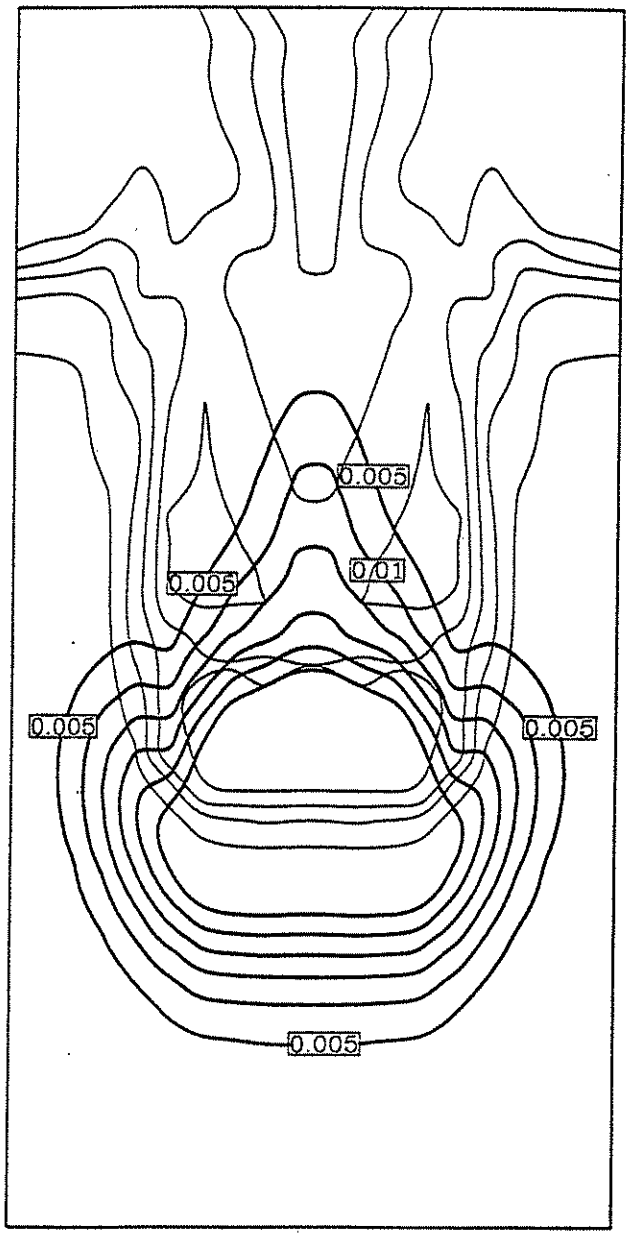

Figure 6.11. Contour plots of fuel volume fraction (marked darker lines) and void fraction (lighter lines) at time = 0.55 s. The void fraction contours begin (on the liquid side) with 0.9 and are in increments of 0.2.

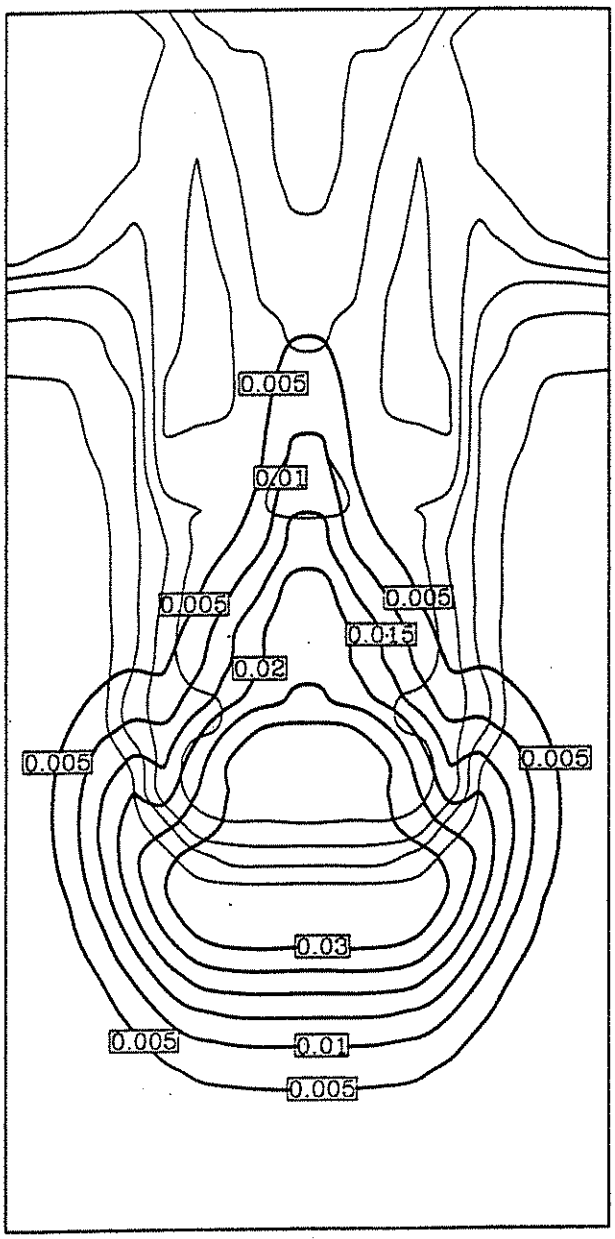

Figure 6.12. Contour plots of fuel volume fraction (marked darker lines) and void fraction (lighter lines) at time = 0.6 s. The void fraction contours begin (on the liquid side) with 0.9 and are in increments of 0.2.

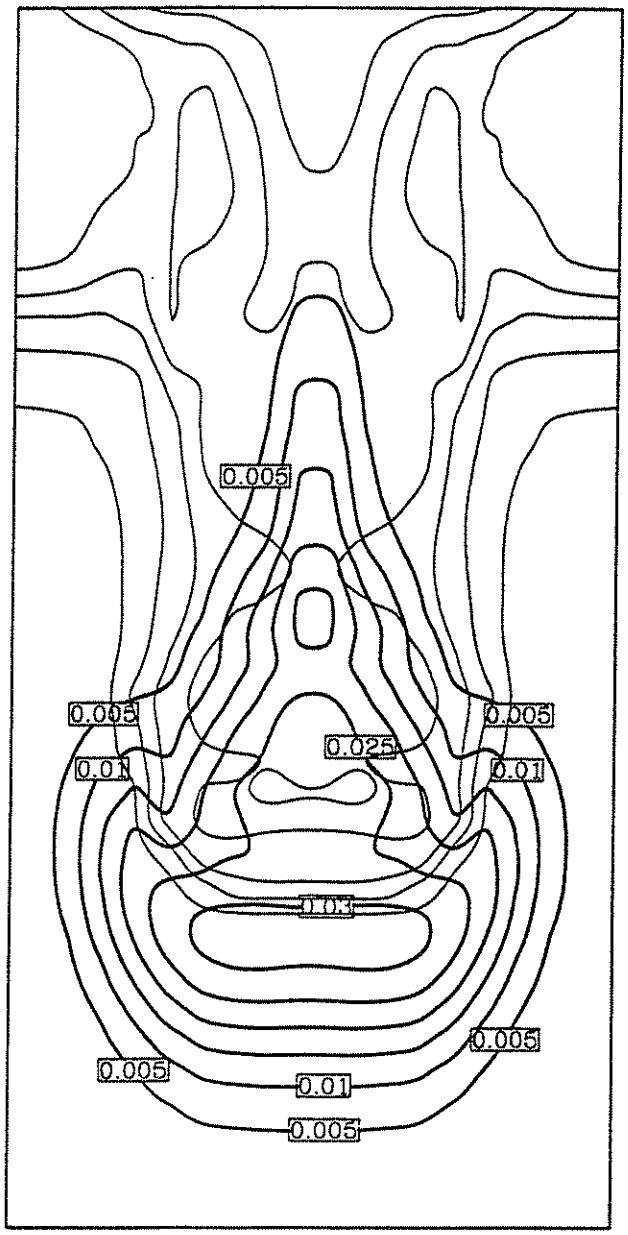

Figure 6.13. Contour plots of fuel volume fraction (marked darker lines) and void fraction (lighter lines) at time = 0.65 s. The void fraction contours begin (on the liquid side) with 0.9 and are in increments of 0.2.

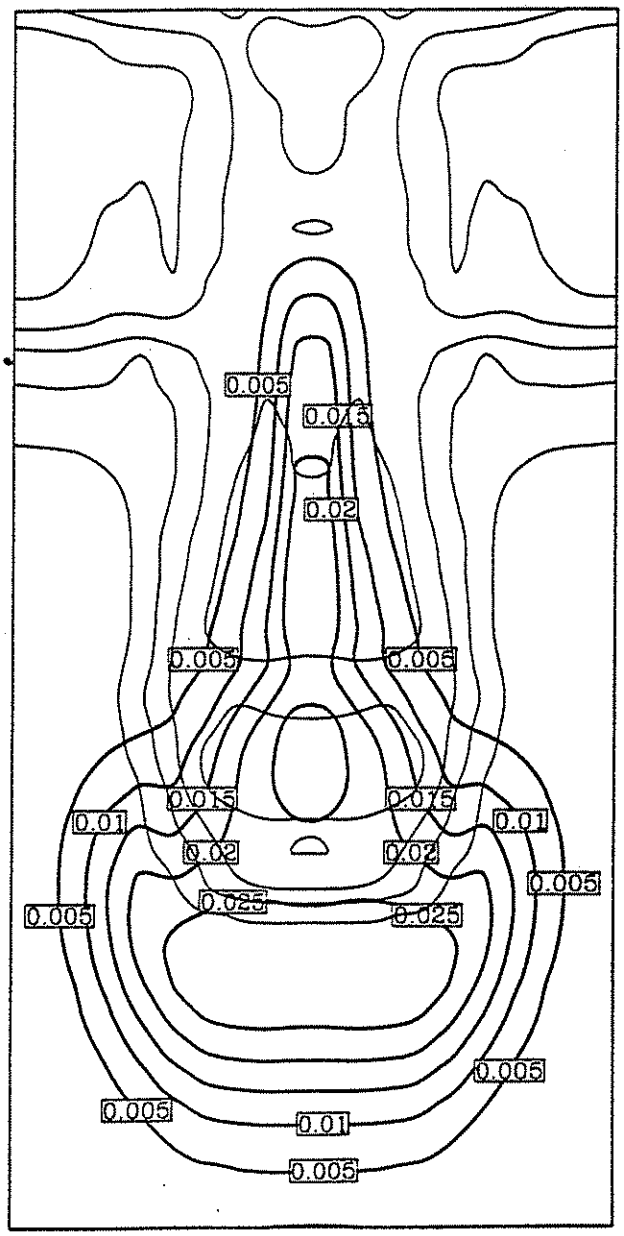

Figure 6.14. Contour plots of fuel volume fraction (marked darker lines) and void fraction (lighter lines) at time = 0.7 s. The void fraction contours begin (on the liquid side) with 0.9 and are in increments of 0.2.

7. REFERENCES

1. Amsden, A. A. and F. H. Harlow (1970), "The SMAC Method: A Numerical Technique for Calculating Incompressable Flows," Los Alamos Scientific Laboratory Report LA-4370.

2. Bird, R. B., W. E. Stewart and E. N. Lightfoot (1960), *Transport Phenomena*, Wiley, New York.

3. Bürger, M. S.H. Cho, E.v. Berg and A. Schatz (1993), "Breakup of Melt Jets as Pre-Condition for Premixing: Modeling and Experimental Verification," Proceedings, CSNI Specialists Meeting on Fuel-Coolant Interactions, Santa Barbara, CA, January 5-8, NUREG/CP-0127, March 1994.

4. Edwards, D. K. (1976), "Molecular Gas band Radiation," Advances in Heat Transfer, **12**, 115–193.

5. Fletcher D. F. and A. Thyagaraja (1991), "The CHYMES Coarse Mixing Model," Progress in Nuclear Engineering, **26**, 31–61.

6. Haar, L., J.S. Gallagher and G.S. Kell (1984), *NBS/NRC Steam Tables*, Hemisphere Publishing Corp.

7. Harlow, F.H. and A.A. Amsden (1971), J. Computational Physics, **8**, 197.

8. Hottel, H.C. and A.F. Sarofilm (1967), *Radiative Transfer*, McGraw Hill Book Co. New York.

9. Incropera, F.P. and D.P. DeWitt (1981), Fundamentals of Heat Transfer, John Wiley and Sons.

10. Ishii, M. (1975), "Thermo-Fluid Dynamic Theory of Two-Phase Flow," Eyrolles.

11. Ishii, M. and N. Zuber (1979), "Drag Coefficient and Relative Velocity in Bubbly, Droplet or Particulate Flow," AIChE Journal **25**, 843.

12. Liu, C. and T.G. Theofanous (1994), "Film Boiling on Spheres in Single- and Two-Phase Flows," DOE/ER/12933-3, Final Report, December 1994.

13. Patel, P. D. and T. G. Theofanous (1981), "Hydrodynamic Fragmentation of Drops," Journal of Fluid Mechanics**103**, 207–223.

14. Rashid, Y.R., T.G. Theofanous and H. Foadian (1995), "Failure Assessment of Reactor Vessel Support Structure Subjected to Ex-Vessel Steam Explosion Loads," 1995 ASME/JSME Pressure Vessel and Piping Conference, Honolulu, Hawaii, July 23-27, 1995. *Trans. of the ASME, Jl. of Pressure Vessel Technology* (submitted).

15. Rivard, W. C., O. A. Farmer and T. D. Butler (1974), "A Computer Program for Multi-component Chemically Reactive Flows at All Speeds," Los Alamos Scientific Laboratory Report LA-5812.

16. Rivard, W.C. and M.D. Torrey (1977) "K-FIX: A Computer Program for Transient, Two-Dimensional, Two-Fluid Flow," LA-NUREG-6623.

17. Rohsenow, W.M. and J.P. Hartnett (1973), Handbook of Heat Transfer, McGraw Hill Book Co., New York.

18. Siegel, R. and J. R. Howell (1992), *Thermal Radiation Heat Transfer*, 3rd. Ed. Hemisphere Publishing Corp.

19. Sissom, L. E. and D. R. Pitts (1972), *Elements of Transport Phenomena*, McGraw Hill, New York.

20. Theofanous, T. G., W.W. Yuen, S. Angelini and X. Chen (1995), "The Study of Steam Explosions in Nuclear Systems," DOE/ID-10489, January 1995.

21. Theofanous, T. G., C. Liu, S. Additon, S. Angelini, O. Kymäläinen and T. Salmassi (1994), "In-Vessel Coolability and Retention of a Core Melt," DOE/ID-10460, November 1994 (peer review version).

22. Theofanous, T. G. and W. W. Yuen (1994), "The Probability of Alpha-Mode Containment Failure Updated," Proceeding of the CSNI Specialists Meeting on Fuel-Coolant Interactions, NUREG/CP-0127, March 1994, 330–342.

23. Wallis, G. F. (1989), "Inertial Coupling in Two-Phase Flow: Macroscopic Properties of Suspensions in an Inviscid Fluid," Multiphase Sci. Technol5, 239–261.

24. Yuen, W. W. (1990), "Development of a Network Analogy and Evaluation of Mean Beam Lengths for Multi-dimensional Absorbing/Isotropically Scattering Media," J. of Heat Transfer **112** 408–413.

25. Yuen, W. W., X. Chen and T. G. Theofanous (1994), "On the Fundamental Microinteractions that Support the Propagation of Steam Explosions," Nuclear Engineering and Design **146**, 133–146.

26. Yuen W. W. and A. Ma (1992), "Evaluation of Total Emittance of an Isothermal Nongray Absorbing, Scattering Gas-Particle Mixture Based on the Concept of Absorption Mean Beam Length," ASME J. Heat Transfer **114**, 653–658

APPENDIX A

EFFECTIVE STEAM ABSORPTION IN AN ENCLOSURE

Since the absorption coefficient of steam depends strongly on wavelength, an exact treatment of the radiative absorption by steam is too complicated mathematically and beyond the scope of PM-ALPHA. A effective "average" absorption coefficient is thus required. Physcially, the steam absorption of radiation emitted by fuel depends on steam temperature, pressure, fuel temperature, the surrounding geometry and reflectivity of the boundary. The objective of this appendix is to develop an approximate value for the absorption coefficient which can account for most of the relevant physics.

In premixing, the effect of steam absorption is important only during the early stage when the fuel is "falling" through the voided region above the water surface and only for the special case that the flow domain is enclosed (as in the FARO experiments). After the fuel penetrates into water, the absorption by water dominates and the accuracy of the steam absorption coefficient is unimportant. The current development is thus focused on a typical "falling" fuel geometry as shown in Figure A1. The steam is assumed to be at a uniform temperature T_g and presure p. The fuel and the wall are at temperature T_f and T_w respectively. In general, the wall temperature is expected to be small in comparison with the fuel temperature, and the radiation emitted by the fuel is the only important energy term in the estimate of steam absorption.

For the absorption coefficient of steam, we use the narrow-band fixed-line-spacing model (Edwards, 1976), which has been established to be an effective engineering approximation for the spectral absorption behavior for most real gases. Specifically, the absorption coefficient (suppressing the subscript λ for simplicity) is given by

$$a = \frac{\rho C^2 sinh(\pi B^2 p_e/2)}{cosh(\pi B^2 p_e/2) - cos(2\pi\nu^*/d)} \qquad (A1)$$

where ν^* is the wavenumber measured from the center of the band, $C^2(\nu, T)$, $B^2(\nu, T)$, d and p_e are specified in terms of isothermal gas correlation parameters as

$$C^2 = (C_1/C_3)e^{-\nu^*/C_3} \qquad (A2)$$

$$B^2 = C_2^2/(4C_1C_3) \qquad (A3)$$

$$d = d_0 C_3(T_0), \quad T_0 = 100K \qquad (A4)$$

$$p_e = [(p_B + bp_A)/p_0]^n, \quad p_0 = 1\ atm \qquad (A5)$$

with p_A being the partial pressure of the absorbing gas and p_B the partial pressure of the N_2 broadening gas. The gas correlation parameters, C_1, C_2, C_3, b and n are defined for the four absorption bands for steam in standard references (e.g. Edwards 1976). By setting $d_0 = 30\ cm^{-1}$, the above model was shown to be effective in calculating the total emittance for common gases such as CO_2 and H_2O (Yuen and Ma, 1992).

For a layer of steam of thickness L, temperature T_g and pressure p, the absorptance of radiation emitted by a surface at a temperature T_f is given by

$$\alpha_g(T_f, T_g, pL) = \frac{1}{\sigma T_f^4} \sum_{i=1}^{4} \int_{ith\ band} e_{\omega,b}(T_f) \left[1 - e^{-a_{\omega,g} L}\right] d\omega \qquad (A6)$$

Four separate integrals are needed to be evaluated over the four separate absorption bands. An effective "average" absorption coefficient for the gas layer is defined by

$$a_g = -log\left[1 - \alpha_g(T_f, T_g, pL)\right] \qquad (A7)$$

For a three-dimensional enclosure as shown in Figure A1, equation (A7) can be directly utilized if the surrounding wall is black. Specifically, a mean beam length, L_{mb}, can be defined for the steam volume by (Hottel and Sarofim, 1967)

$$L_{mb} = 3.6 \frac{V_g}{A_w + A_f} \qquad (A8)$$

where V_g is the volume of steam, A_w and A_f are areas of the surrounding wall (including the water surface) and the surface area of the radiating fuel column respectively. The effective average absorption coefficient of the gas volume is then given by

$$a_g = -log\left[1 - \alpha_g(T_f, T_g, pL_{mb})\right] \qquad (A7)$$

If the surrounding wall is reflecting (with a reflectivity $1 - \epsilon_w$), the heat absorption by steam can be calculated by a radiation network analysis (Yuen, 1990). An "exact" analysis, however, would require a multiple zone analysis which is too extensive and beyond the scope of the current application. A three-node network representation is sufficient to capture the effect to the first order. Specifically, the network representation for the geometrical configuration of Figure B.1, accounting for the effect of both fuel and wall emissivity, is shown in Figure B2. For simplicity, the water surface is assumed to have the same emissivity as the surrounding wall. Since the surface area of water is expected to be small in comparison to the surrounding surface

area, this assumption is not expected to lead to significant error. The relevant resistance elements are

$$gs_f = A_f \alpha_g(T_f, T_g, pL_{mb}) \tag{A8}$$

$$s_f s_w = A_f.[1 - \alpha_g(T_f, T_g, pL_{mb})] \tag{A9}$$

$$gs_w = A_w \alpha_g(T_f, T_g, pL_{mb}) \tag{A10}$$

$$R_{i,w} = \frac{1 - \epsilon_w}{A_w \epsilon_w} \tag{A11}$$

$$R_{i,f} = \frac{1 - \epsilon_f}{A_f \epsilon_f} \tag{A12}$$

The emission from the surrounding wall and steam are assumed to be small in comparison to the emission from the fuel (i.e., $T_w = T_g = 0$). Solution to the network analysis yields the following expression for the net absorption by the steam

$$Q_g = q_{o,f} gs_f + q_{o,w} gs_w \tag{A13}$$

with $q_{o,w}$ and $q_{o,f}$ being the radiosity (emission plus reflection) of the fuel surface and surrounding wall (and water surface) respectively. They are given by

$$q_{o,w} = \frac{\epsilon_f (1 - \epsilon_w) s_f s_w A_f e_b(T_f)}{D} \tag{A14}$$

$$q_{o,f} = \frac{\epsilon_f \left[(s_f s_w + gs_w)(1 - \epsilon_w) + A_w \epsilon_w \right] A_f e_b(T_f)}{D} \tag{A15}$$

with

$$\begin{aligned} D =& s_f s_w \left[(gs_f + gs_w)(1 - \epsilon_w)(1 - \epsilon_f) + A_f \epsilon_f (1 - \epsilon_w) + A_w \epsilon_w (1 - \epsilon_f) \right] \\ &+ \left[gs_f (1 - \epsilon_f) + A_f \epsilon_f \right] \left[gs_w (1 - \epsilon_w) + A_w \epsilon_w \right] \end{aligned} \tag{A16}$$

Based on equations (A13) thru (A16), the effective average absorption coefficient for the steam volume accounting for the effect of surface reflectivity can now be written as

$$a_g = -log \left[1 - \frac{Q_g}{A_f \epsilon_f e_b(T_f)} \right] \tag{A17}$$

The numerical algorithm for the evaluation of the effective average absorption coefficient is not included in this manual. This calculation should be performed prior to the running of PM-ALPHA to generate an input value for the effective absorption coefficient for steam.

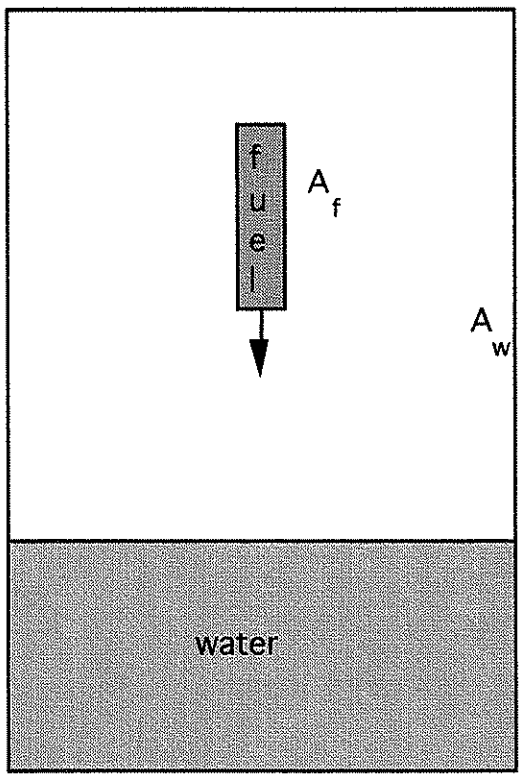

Figure A1. Geometric configuration of fuel, steam and water used in the evaluation of the effective average absorption coefficient of steam.

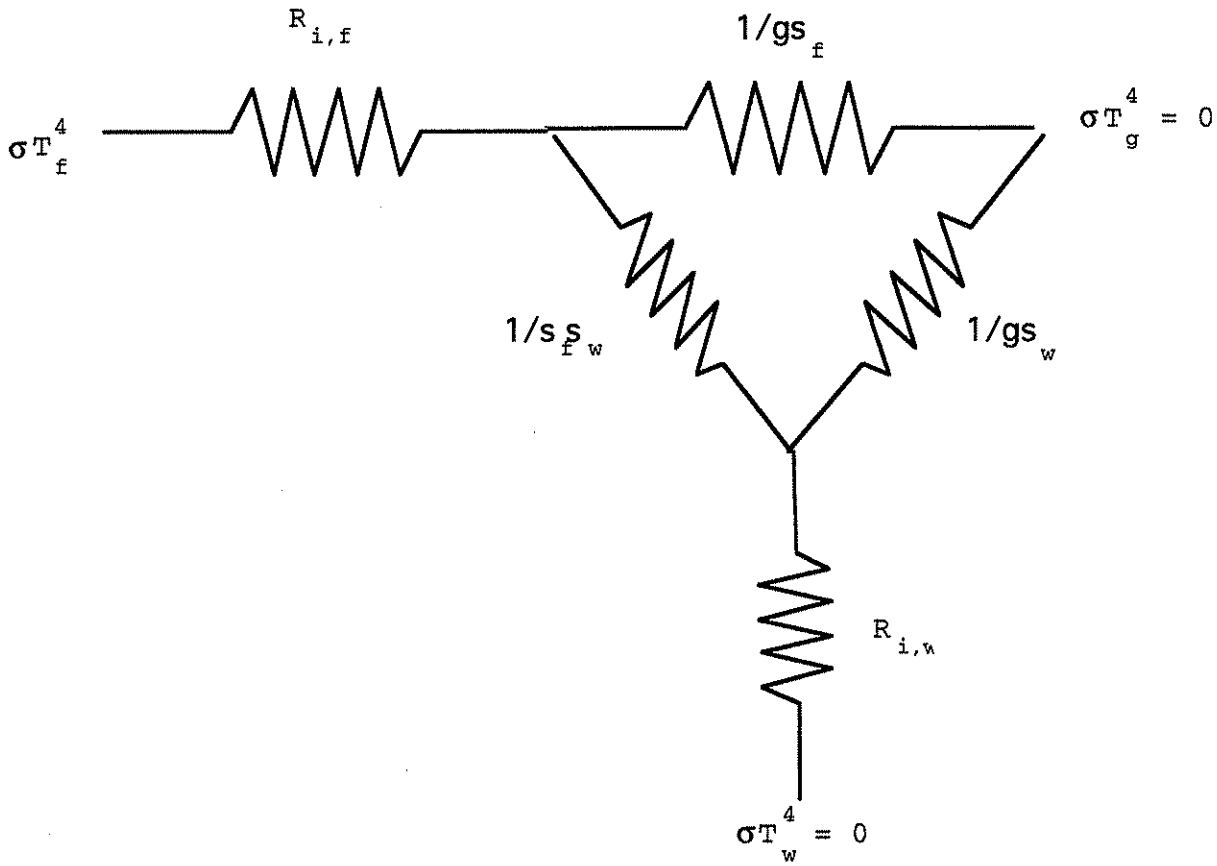

Figure A2. Network representation of the radiative transfer between fuel, water and steam with geometry as shown in Figure A1.

APPENDIX B

EXCHANGE FACTORS FOR RADIATIVE HEAT TRANSFER

B.1 Introduction

The various terms for radiation heat transfer, $\dot{q}_{a,\ell}(\vec{r})$, $\dot{q}_{a,g}(\vec{r})$, $\dot{q}_{a,\ell}(\vec{r})$, q_{ex} and the exchange factor $F(\vec{r},\vec{r}')$ appeared in the main text are evaluated in this Appendix. Specifically, detailed expressions are developed for cylindrical elements. Corresponding expressions for rectangular elements (which is simpler) can be readily generated with similar procedure.

The numerical algorithm for the evaluation of exchange factors is not provided with this mannual. The analysis and the associated equations provided in this Appendix can be readily programmed to generate the required exchange factors which can then be read in to PM-ALPHA as input files.

B.2 Overview of Relevant Physics and the Mathematical Approach

The zonal method (Hottel and Sarofim, 1967) is used as the basis for the evaluation of the varous radiatiave terms. Two extensions are required, however, to deal with the non-uniform material distribution and the discrete nature of the emitter (i.e. the fuel particles) in the present application. The first extension is relevant to the formulation of the exchange factors, and is presented in section B.3, together with an introduction to the method in its original form. The second extension is relevant to the formulation of the self-absorption within a cell, and it is given in section B.4. The above two results are then put together in section B.5, to obtain the actual formula for radiative fluxes required by PM-ALPHA. Finally, the details of the numerical evaluation of these formulas are presented in section B.6.

B.3 Formulation of the Zonal Method in Inhomogenous, Non-isothermal Media

The first important concept in the zonal method is the exchange factor between volume elements which, for the current application, are cylindrical ring elements of height dz and radial width dr. Physically, if the volumetric radiative emission leaving volume V_{ij} is $\dot{q}_{ex,ij}$, the energy absorbed by volume V_{i1j1} due to this emission is

$$\dot{Q}_{ij,i1j1} = \dot{q}_{ex,ij} g_{ij} g_{i_1 j_1} \qquad (B1)$$

Mathematically, the exchange factor is written formally as

$$g_{ij} g_{i_1 j_1} = k_{ij} k_{i_1 j_1} \Delta r^2 \Delta z^2 F_{gg}(k_{a,ij,i_1 j_1} \Delta z, \frac{\Delta r}{\Delta z}) \qquad (B2)$$

where

$$F_{gg}(k_{a,ij,i_1j_1}\Delta z, \frac{\Delta r}{\Delta z}) = \frac{1}{k_{ij}k_{i1j1}\Delta r^2 \Delta z^2}\int_{V_{ij}}\int_{V_{i_1j_1}} \frac{e^{-\tau}dV_{ij}dV_{i_1j_1}}{\pi r^2} \qquad (B3)$$

and τ being the optical thickness between the differential volume element dV_{ij} and $dV_{i_1j_1}$ given by

$$\tau = \int_{\vec{r}_{ij}}^{\vec{r}_{i_1j_1}} k ds \qquad (B4)$$

and

$$s = |\vec{r} - \vec{r}_{ij}| \qquad (B5)$$

The integration is performed along a straight line extending from $\vec{r}_{ij}$ to $\vec{r}_{i_1j_1}$.

The evaluation of equation (B3) for a homogenous isothermal medium (i.e. k = constant) is presented in section B.6. The integration is non-trivial because of the presence of singularity in equation (B3) when the volume elements V_{ij} and $V_{i_1j_1}$ are not disjoint. Results of section B.6 can be applied approximately to an inhomogeneous non-isothermal medium by letting $k = k_{a,ij,i_1j_1}$ with k_{a,ij,i_1j_1} defined to be the "line" average absorption coefficient for all "lines of sight" connecting all possible pairs of differential elements dV_{ij} and $dV_{i_1j_1}$. The absorption coefficient k_{ij} in the definition of $g_{ij}g_{i1j1}$ is taken to be the "local" average absorption coefficient over the volume V_{ij}. Note that $k_{ij} \neq k_{a,ij,ij}$ in the evaluation of the "self" exchange factor $g_{ij}g_{ij}$.

For a given volume fractions for water, steam, fuel and debris. The "local" average absorption coefficient is calculated based on the volumetric contribution of the different components. For simplicity, the absorption coefficient for debris is assumed to be identical to that of water in the current treatment. The "local" average absorption coefficient is

$$k_{ij} = a_f + (\theta_\ell + \theta_{db})a_\ell + \theta_g a_g \qquad (B6)$$

where a_f is evaluated by Eq. (3.44) and a_g is calculated based on the method presented in Appendix A.

Based on the volume index notation of code, the volume element V_{2j} is a circular disk of radius Δr. The "local" average absorption coefficient is identical to the "line" average absorption coefficient and one obtains

$$k_{a,2j,2j} = k_{2j} \qquad (B7)$$

The volume element V_{ij} with $i > 2$ is a circular ring between $(i-1)\Delta r$ and $(i-2)\Delta r$. Since the line of sight between differential volume elements in V_{ij} must also go through volume elements $V_{i'j}$ with $i' \leq i$. The "line" average absorption coefficient is thus given by

$$k_{a,ij,ij} = \frac{\sum_{i'=2}^{i} V_{i'j}k_{i'j}}{\sum_{i'=2}^{i} V_{i'j}} \qquad (B8)$$

For two disjoint elements V_{ij} and $V_{i_1 j_1}$, the volumes intersected by all lines of sight between the two volume elements need to be first identified. Without loss of generality, one can assume that $i < i_1$. The "maximum i" intersected by a line drawn between the two volume elements with a horizontal plane at j' is given by

$$i_{max}(j') = int\left[(j'-j)\left(\frac{i_1 - i}{j_1 - j}\right) + i\right] \qquad (B9)$$

where the symbol "int[ ]' stands for the integral value of the enclosed parameter. The "minimum i", on the other hand, can be written as

$$i_{min}(j') = max\begin{cases} 2 \\ int\left[-(j'-j)(\frac{i_1+i-3}{j_1-j}) + i\right] \end{cases} \qquad (B10)$$

Note that in the notation of the code, the first "fluid" element has the index i = 2. The "line" average absorption coefficient is now written as

$$k_{a,ij,i_1 j_1} = \frac{\sum_{j'=j_{min}}^{j_{max}} \sum_{i'=i_{min}(j')}^{i_{max}(j')} V_{i'j'} k_{i'j'}}{\sum_{j'=j_{min}}^{j_{max}} \sum_{i'=i_{min}(j')}^{i_{max}(j')} V_{i'j'}} \qquad (B11)$$

with $j_{min} = min(j, j_1)$ and $j_{max} = max(j, j_1)$ respectively.

B.4 Evaluation of Self Absorption by Volume Elements

To complete the mathematical description of radiative exchange and to calculate the appropriate energy source term for PM-ALPHA, the radiative emission from each computational cell ($\dot{q}_{ex,ij}$ in Eq. (B1)) must be determined. Physically, the net emission and self absorption of a cell depend on the physical properties of the fuel (temperature and emissivity) and its geometric parameters (diameter and volume fraction and packing arrangement). Since PM-ALPHA does not predict the packing arrangement of fuel particles within a computational cell, the estimate of these two parameters can only be done approximately. There are two limiting approaches.

B.4.1 Disperse Particle Approach

In this approach, the fuel particles are assumed to be sufficiently dispersed such that there is no "self absorption" unless the total particle surface area exceeds the surface area of the volume element. Specifically, the total radiating surface area of the fuel particle with diameter $D_f(ij)$ in a computational cell is given by

$$A_f(ij) = \frac{6}{D_f(ij)}\theta_f(ij)V(ij) \qquad (B12)$$

The total rate of energy emission by the particles is

$$\dot{Q}_e(ij) = A_f(ij)\epsilon_f \sigma T_f^4(ij) \tag{B13}$$

The actual surface area which can be seen by the medium outside of the consider volume is the surface area of the cylindrical element which is

$$A_m(ij) = 2\pi(2i-3)\Delta r(\Delta r + \Delta z) \tag{B14}$$

In this approach, the difference between $A_f(ij)$ and $A_m(ij)$ determines the self absorption of the emitted energy. Specifically, the energy re-absorbed by the fuel particles is

$$\dot{Q}_{a,f}(ij,ij) = \begin{cases} 0 & A_f(ij) < A_m(ij) \\ \dot{Q}_e(ij)\frac{1}{2-\epsilon_f}\left[1 - \frac{A_m(ij)}{A_f(ij)}\right] e^{-k_{\ell g,ij}L_{ij}} & A_f(ij) > A_m(ij) \end{cases} \tag{B15}$$

where the factor $\frac{1}{2-\epsilon_f}$ is introduced to account approximately for the effect of surface emissivity and $k_{\ell g,ij}$ is the local average absorption coefficient of water and steam given by

$$k_{\ell g,ij} = \theta_\ell a_\ell + \phi_g a_g \tag{B16}$$

The mean beam length, L_{ij}, is the characteristic length of radiative absorption. It can be expressed as

$$L_{ij} = \frac{4V(ij)}{A_f(ij) + A_m(ij)} \tag{B17}$$

with $V(ij)$ being the volume of the computational cell which is

$$V(ij) = 2\pi(2i-3)\Delta r^2 \Delta z \tag{B18}$$

Using the concept of mean beam length and assuming that the self absorption by the steam/water mixture is distributed to the two components in accordance to their contribution to $k_{\ell g,ij}$, the self absorptions by water and steam are given by

$$\dot{Q}_{a,\ell}(ij,ij) = \dot{Q}_e(ij)[1 - e^{-k_{\ell g,ij}L_{ij}}]\frac{\theta_\ell a_\ell}{k_{\ell g,ij}} \tag{B19}$$

and

$$\dot{Q}_{a,g}(ij,ij) = \dot{Q}_e(ij)[1 - e^{-k_{\ell g,ij}L_{ij}}]\frac{\theta_g a_g}{k_{\ell g,ij}} \tag{B20}$$

The energy exiting from the volume becomes

$$\dot{q}_{ex,ij} = \frac{1}{V_{ij}}\left[\dot{Q}_e(ij) - \dot{Q}_{a,f}(ij,ij) - \dot{Q}_{a,\ell}(ij,ij) - \dot{Q}_{a,g}(ij,ij)\right] \tag{B21}$$

B.4.2 Packed Particle Approach

In this limit, the fuel particles are assumed to be tightly packed so that it becomes an effective sphere with an effective diameter

$$D_{eff} = \left[\frac{6}{\pi} V(ij)\theta_f(ij)\right]^{\frac{1}{3}} \tag{B22}$$

and an effective radiating area

$$A_{eff} = \pi D_{eff}^2 \tag{B23}$$

The self absorptions by particles, water and steam are thus given by

$$\dot{Q}_{a,f}(ij,ij) = \dot{Q}_e \left(1 - \frac{A_{eff}}{A_f(ij)}\right) \tag{B24}$$

$$\dot{Q}_\ell(ij,ij) = \dot{Q}_e \frac{A_{eff}}{A_f(ij)} \left[1 - e^{-k_{\ell g,ij} L_{ij,eff}}\right] \frac{\theta_\ell a_\ell}{k_{\ell g,ij}} \tag{B25}$$

$$\dot{Q}_g(ij,ij) = \dot{Q}_e \frac{A_{eff}}{A_f(ij)} \left[1 - e^{-k_{\ell g,ij} L_{ij,eff}}\right] \frac{\theta_g a_g}{k_{\ell g,ij}} \tag{B26}$$

where $L_{ij,eff}$ is the mean beam length based on $A_f(ij)$ and A_{eff} which is

$$L_{ij,eff} = \frac{4V(ij)}{A_{eff} + A_m(ij)} \tag{B27}$$

The exiting energy, $\dot{q}_{ex,ij}$, is again given by equation (B21).

B.4.3 Final expression for $\dot{q}_{ex,ij}$, $\dot{q}_{r,\ell}$, $\dot{q}_{r,g}$ and $\dot{q}_{r,f}$

The approach which yields the lower self absorption by the fuel particles, $\dot{Q}_{a,f}(ij,ij)$, is selected as the accepted approximation. The basis of this selection is to maximize the absorption of the emitted radiation by water and steam. The volumetric self absorption for the three species are then expressed as

$$\dot{q}_{a,f}(ij) = \frac{\dot{Q}_{a,f}(ij,ij)}{V(ij)} \tag{B28}$$

$$\dot{q}_{a,\ell}(ij) = \frac{\dot{Q}_{a,\ell}(ij,ij)}{V(ij)} \tag{B29}$$

$$\dot{q}_{a,g}(ij) = \frac{\dot{Q}_{a,g}(ij,ij)}{V(ij)} \tag{B30}$$

and $\dot{q}_{ex}(ij)$ is again given by Eq. (B.21).

B.5 Evaluation of Radiative Flux Terms

After the expression of $\dot{q}_{ex,ij}(ij)$ is obtained, the radiative absorption by the three components in cell i_1j_1 can be written as

$$\dot{Q}_f(ij, i_1j_1) = \frac{\dot{q}_{ex,ij}C(ij)}{4k_{ij}V(ij) - g_{ij}g_{ij}} g_{ij}g_{i_1j_1} \frac{a_f(i_1j_1)}{k_{i_1j_1}} \tag{B31}$$

$$\dot{Q}_\ell(ij, i_1j_1) = \frac{\dot{q}_{ex,ij}C(ij)}{4k_{ij}V(ij) - g_{ij}g_{ij}} g_{ij}g_{i_1j_1} \frac{\theta_\ell(i_1j_1)a_\ell}{k_{i_1j_1}} \tag{B32}$$

$$\dot{Q}_g(ij, i_1j_1) = \frac{\dot{q}_{ex,ij}C(ij)}{4k_{ij}V(ij) - g_{ij}g_{ij}} g_{ij}g_{i_1j_1} \frac{\theta_g(i_1j_1)a_g}{k_{i_1j_1}} \tag{B33}$$

Because of the finite size of the computational volume and the approximate usage of exchange factor in inhomogeneous medium, a normalization factor $C(ij)$ is introduce to ensure energy conservation. Specifically, it is given by

$$C(ij) = \frac{4k_{ij}V(ij) - g_{ij}g_{ij}}{\sum_{i_1j_1} g_{ij}g_{i_1j_1} + \sum_k g_{ij}s_k + \sum_k g_{ij}t_k + \sum_k g_{ij}b_k} \tag{B34}$$

where $g_{ij}s_k$, $g_{ij}t_k$ and $g_{ij}b_k$ are exchange factors between $V(ij)$ and area elements $A(k)$ at the side, top and bottom surface respectively. Evaluation of these factors are also presented in section B.6.

The integrals appeared in Eqs. (3.45) thru (3.47) in the main text, for a given computational cell (ij), become

$$\left[\int_{\mathbf{r}'\neq\mathbf{r}} \dot{q}_{ex}(\mathbf{r}')F(\mathbf{r},\mathbf{r}')a_\ell(\mathbf{r})dV'\right]_{ij} = \sum_{i_1j_1\neq ij} \dot{Q}_\ell(i_1j_1, ij) \tag{B35}$$

$$\left[\int_{\mathbf{r}'\neq\mathbf{r}} \dot{q}_{ex}(\mathbf{r}')F(\mathbf{r},\mathbf{r}')a_g(\mathbf{r})dV'\right]_{ij} = \sum_{i_1j_1\neq ij} \dot{Q}_g(i_1j_1, ij) \tag{B36}$$

$$\left[\int_{\mathbf{r}'\neq\mathbf{r}} \dot{q}_{ex}(\mathbf{r}')F(\mathbf{r},\mathbf{r}')a_f(\mathbf{r})dV'\right]_{ij} = \sum_{i_1j_1\neq ij} \dot{Q}_f(i_1j_1, ij) \tag{B37}$$

B.6 Evaluation of Exchange Factors

In this section, the detail mathematics for the evaluation of $g_{ij}g_{i_1j_1}$, $g_{ij}s_k$, $g_{ij}t_k$ and $g_{ij}b_k$ are described. These evaluations are non-trivial because of the appearance of singularity in the integrand for joint volumes and volume/surface.

B.6.1 Evaulation of $g_{ij}g_{i_1j_1}$

Without loss of generality, it is only necessary to evaluate $g_{i2}g_{i_1j_1}$ with $i_1 > i$, all other factors can be obtained by reciprocity (i.e. $g_ig_j = g_jg_i$). Consider the geometry as shown in Figure B1, the expression for dV_{i2}, equation (B3) becomes

$$g_{i2}g_{i_1j_1} = 2\pi \int_{(i-2)\Delta r}^{(i-1)\Delta r} \int_0^{\Delta z} \int_{V_{i_1j_1}} \frac{k_{i2}k_{i_1j_1}e^{-\tau}r_{i2}dr_{i2}dz_{i2}dV_{i_1j_1}}{\pi r^2} \qquad (B38)$$

To avoid the apparent singularity at r = 0, the volume element $dV_{i_1j_1}$ can be written as

$$dV_{i_1j_1} = drdA_{p,i_1j_1} \qquad (B39)$$

where dA_{p,i_1j_1} is the "projected" area of the integration volume element $dV_{i_1j_1}$ in the line of sight extending from $\vec{r}_{ij}$ to $\vec{r}_{i_1j_1}$. In term of the solid angle, equation (B39) can be written as

$$dV_{i_1j_1} = r^2drd\Omega = r^2sin\phi drd\phi d\theta \qquad (B40)$$

and equation (B38) becomes

$$g_{i2}g_{i_1j_1} = 2\int_{(i-2)\Delta r}^{(i-1)\Delta r} \int_0^{\Delta z} \int_0^{2\pi} \int_{\phi_{min}(\theta)}^{\phi_{max}(\theta)} \int_{L_{min}(\phi,\theta)}^{L_{max}(\phi,\theta)} k_{ij}k_{i_1j_1}e^{-\tau}r_{i2}drsin\phi d\phi d\theta dz_{i2}dr_{i2} \qquad (B41)$$

with $L_{min}(\phi,\theta)$ and $L_{max}(\phi,\theta)$ as shown in Figure B1. For a given θ, $\phi_{min}(\theta)$ and $\phi_{max}(\theta)$ are the minimum and maximum polar angle subtended by the volume $V(i_1j_1)$.

Assuming that k_{ij} and $k_{i_1j_1}$ are constant within the two volume elements, equation (B41) can be rewritten in the following normalized form

$$\frac{g_{i2}g_{i_1j_1}}{k_{ij}k_{i_1j_1}\Delta r^2\Delta z} = 2\int_{(i-2)}^{(i-1)} \int_0^1 \int_0^{2\pi} \int_{\phi_{min}(\theta)}^{\phi_{max}(\theta)} \int_{L_{min}(\phi,\theta)}^{L_{max}(\phi,\theta)} e^{-\tau}\eta_r drsin\phi d\phi d\theta d\eta_z d\eta_r \qquad (B42)$$

where η_r and η_z are dimensionless variables given by

$$\eta_r = \frac{r_{i2}}{\Delta r} \qquad (B43)$$

and

$$\eta_z = \frac{z_{i2}}{\Delta z} \qquad (B44)$$

In the evaluation of the integral, the absorption coefficient along the different lines of sight between the two volumes will be considered as constant, the optical thickness τ can be written as

$$\tau = k_ar \qquad (B45)$$

equation (B42) can be integrated once to yield

$$\frac{g_{i2}g_{i_1j_1}}{k_{i2}k_{i_1j_1}\Delta r^2\Delta z^2} = F_{gg}(i2, i_1j_1, k_a\Delta z, \frac{\Delta r}{\Delta z}) \tag{B46}$$

with

$$F_{gg}(i2, i_1j_1, k_a\Delta z, \frac{\Delta r}{\Delta z}) = \frac{2}{k_a\Delta z}\times \tag{B47}$$
$$\int_{(i-2)}^{(i-1)}\int_0^1\int_0^{2\pi}\int_{\phi_{min}(\theta)}^{\phi_{max}(\theta)}\left[e^{-k_aL_{min}(\phi,\theta)} - e^{-k_aL_{max}(\phi,\theta)}\right]\eta_r sin\phi d\phi d\theta d\eta_z d\eta_r$$

For totally disjoint volumes with $i_1 > i$ and $j_1 > j$, the integral in ϕ at a fixed θ can be written as four components as follow

$$G_1(ij, i_1j_1, \eta_r, \eta_z, \theta) = \int_{\phi_{min}(\theta)}^{\phi_{max}(\theta)}\left[e^{-k_aL_{min}(\phi,\theta)} - e^{-k_aL_{max}(\phi,\theta)}\right] sin\phi d\phi \tag{B48}$$
$$= F_1\left((i_1-2)\Delta r, j_1, \eta_r, \eta_z, \theta\right) - F_1\left((i_1-1)\Delta r, j_1, \eta_r, \eta_z, \theta\right)$$
$$+ F_2\left(i_1, (j_1-2)\Delta z, \eta_r, \eta_z, \theta\right) - F_2\left(i_1, (j_1-1)\Delta z, \eta_r, \eta_z, \theta\right)$$

with

$$F_1(R, j_1, \eta_r, \eta_z, \theta) = \left[\int_{z=(j_1-2)\Delta z}^{z=(j_1-1)\Delta z} e^{-k_aL(\phi)} sin(\phi)d\phi\right]_{r=R} \tag{B49}$$

and

$$F_2(i_1, Z, \eta_r, \eta_z, \theta) = \left[\int_{r=(i_1-2)\Delta r}^{r=(i_1-1)\Delta r} e^{-k_aL(\phi)} sin(\phi)d\phi\right]_{z=Z} \tag{B50}$$

The limits of integration for equation (B49) and (B50) are shown in Figures B2a and B2b. Based on these limits, equations (B49) becomes

$$F_1(R, j_1, \eta_r, \eta_z, \theta) = \int_{\phi_{min}}^{\phi_{max}} e^{-k_a\frac{S(\theta)}{sin\phi}} sin(\phi)d\phi \tag{B51}$$

with

$$S(\theta) = (R^2 - \eta_r^2\Delta r^2 sin^2\theta)^{\frac{1}{2}} - \eta_r\Delta r cos\theta \tag{B52}$$

$$\phi_{min} = tan^{-1}\frac{S(\theta)}{(j_1 - 1 - \eta_z)\Delta z} \tag{B53}$$

$$\phi_{max} = tan^{-1}\frac{S(\theta)}{(j_1 - 2 - \eta_z)\Delta z} \tag{B54}$$

For the case of $i_1 = i + 1$, $R = (i_1 - 2)\Delta r$ and $\eta_r = 1$, the evaluation of equation (B51) requires special consideration. Specifically,

$$F_1\left((i_1 - 2)\Delta r, j_1, 1, \eta_z, \theta\right) = \begin{cases} 2 & \theta \leq \frac{\pi}{2}, j_1 - 2 < \eta_z < j_1 - 1 \\ 1 & \theta \leq \frac{\pi}{2}, \eta_z = j_1 - 2 or j_1 - 1 \\ \int_{\phi_{min}}^{\phi_{max}} e^{-k_a \frac{S(\theta)}{sin\phi}} sin(\phi) d\phi & otherwise \end{cases} \tag{B55}$$

Equation (B50) is

$$F_2(i_1, Z, \eta_r, \eta_z, \theta) = \begin{cases} 0 & Z = \eta_z \\ \int_{\phi_{min}}^{\phi_{max}} e^{-k_a \frac{Z - \eta_z \Delta z}{cos\phi}} sin(\phi) d\phi & Z \neq \eta_z \end{cases} \tag{B56}$$

with

$$\phi_{min} = tan^{-1} \frac{S_{min}(\theta)}{Z - \eta_z \Delta z} \tag{B57}$$

$$\phi_{max} = tan^{-1} \frac{S_{max}(\theta)}{Z - \eta_z \Delta z} \tag{B58}$$

and

$$S_{min}(\theta) = \Delta r \left[(i_1 - 2)^2 - \eta_r^2 sin^2\theta\right]^{\frac{1}{2}} - \eta_r \Delta r cos\theta \tag{B59}$$

$$S_{max}(\theta) = \Delta r \left[(i_1 - 1)^2 - \eta_r^2 sin^2\theta\right]^{\frac{1}{2}} - \eta_r \Delta r cos\theta \tag{B60}$$

Equation (B47) becomes

$$F_{gg}\left(i2, i_1 j_1, k_a \Delta z, \frac{\Delta r}{\Delta z}\right) = \frac{2}{k_a \Delta z} \int_{(i-2)}^{(i-1)} \int_0^1 \int_0^{2\pi} G_1(i2, i_1 j_1, \eta_r, \eta_z, \theta) d\theta d\eta_z d\eta_r \tag{B61}$$

For the remaining elements with $i_1 = i$, Equation (B47) is first evaluated for cases for $V(i'2)$ and $V(i'j_1)$ with $j_1 \geq 2$. $V(i'2)$ is a circular disk of radius $(i-1)\Delta r$, thickness Δz and $V(i'j_1)$ is a circular disk of radius $(i-1)\Delta r$, thickness $(j_1 - 1)\Delta z$. The base of both volumes is at the plane z = 0. $L_{min}(\phi, \theta)$ is zero in these cases. To evaluate the required integral as in Eq. (B47), one must first evaluate

$$H_{gg}(i'2, i'j_1, k_a \Delta z, \frac{\Delta r}{\Delta z}) = \frac{2}{k_a \Delta z} \times \tag{B62}$$

$$\int_0^{i-1} \int_0^1 \int_0^{2\pi} \int_{\phi_{min}(\theta)}^{\phi_{max}(\theta)} [1 - e^{-k_a L_{max}(\phi,\theta)}] \eta_r sin\phi d\phi d\theta d\eta_z d\eta_r$$

The geometry for the required integration in θ and ϕ is shown in Figure B3. For a fixed θ,

$$L_{max}(\phi, \theta) = \begin{cases} \frac{\Delta z(j_1 - 1 - \eta_z)}{cos(\phi)} & 0 \leq \phi \leq \phi_1(\theta) \\ \frac{S(\theta)}{sin(\phi)} & \phi_1(\theta) \leq \phi \leq \phi_2(\theta) \\ \frac{-\Delta z \eta_z}{cos(\phi)} & \phi_2(\theta) \leq \phi \leq \pi \end{cases} \tag{B63}$$

with

$$\phi_1(\theta) = tan^{-1}\frac{S(\theta)}{\Delta z(j_1 - 1 - \eta_z)} \tag{B64}$$

$$\phi_2(\theta) = \pi - tan^{-1}\frac{S(\theta)}{\Delta z \eta_z} \tag{B65}$$

and

$$S(\theta) = \Delta r\left(\left[(i_1 - 1)^2 - \eta_r^2 sin^2\theta\right]^{\frac{1}{2}} - \eta_r sin\theta\right) \tag{B66}$$

The integration in ϕ becomes

$$G_2(i'2, i_1'j_1, \eta_r, \eta_z, \theta) = 2 + \int_0^{\pi} e^{-k_a L_{max}(\phi,\theta)} sin\phi d\phi \tag{B67}$$

and Eq. (B62) becomes

$$H_{gg}\left(i'2, i_1'j_1, k_a\Delta z, \frac{\Delta r}{\Delta z}\right) = \frac{2}{k_a\Delta z}\int_0^{(i-1)}\int_0^1\int_0^{2\pi} G_2(i'2, i_1'j_1, \eta_r, \eta_z, \theta) d\theta d\eta_z d\eta_r \tag{B68}$$

For $i = i_1 = 2$, the normalized exchange factor for $j_1 = 2$ is

$$F_{gg}\left(22, 22, k_a\Delta z, \frac{\Delta r}{\Delta z}\right) = H_{gg}\left(2'2, 2'2, k_a\Delta z, \frac{\Delta r}{\Delta z}\right) \tag{B69}$$

For $j_1 > 2$, $F_{gg}(22, 2j_1, k_a\Delta z, \frac{\Delta r}{\Delta z})$ is calculated recursively by

$$F_{gg}\left(22, 2j_1, k_a\Delta z, \frac{\Delta r}{\Delta z}\right) = H_{gg}\left(2'2, 2'j_1, k_a\Delta z, \frac{\Delta r}{\Delta z}\right) - \sum_{m=2}^{j_1-1} F_{gg}\left(22, 2m, k_a\Delta z, \frac{\Delta r}{\Delta z}\right) \tag{B70}$$

The exchange factors for $j_1 = 2$ and $i_1 = i$ can then be generated by the recursive relations

$$F_{gg}\left(i2, i2, k_a\Delta z, \frac{\Delta r}{\Delta z}\right) = H_{gg}\left(i'2, i'2, k_a\Delta z, \frac{\Delta r}{\Delta z}\right) \tag{B71}$$
$$- \sum_{m=2}^{i-1}\sum_{n=2}^{i} F_{gg}\left(m2, n2, k_a\Delta z, \frac{\Delta r}{\Delta z}\right) - \sum_{n=2}^{i-1} F_{gg}\left(i2, n2, k_a\Delta z, \frac{\Delta r}{\Delta z}\right)$$

The exchange factor for $i_1 = i \neq 2$ and $j_1 > 2$ is given by

$$F_{gg}\left(i2, ij, k_a\Delta z, \frac{\Delta r}{\Delta z}\right) = H_{gg}\left(i'2, i'j, k_a\Delta z, \frac{\Delta r}{\Delta z}\right) \tag{B72}$$
$$- \sum_{m=2}^{i-1}\sum_{n=2}^{i}\sum_{p=2}^{j} F_{gg}\left(m2, np, k_a\Delta z, \frac{\Delta r}{\Delta z}\right) - \sum_{n=2}^{i-1}\sum_{p=2}^{j} F_{gg}\left(i2, np, k_a\Delta z, \frac{\Delta r}{\Delta z}\right)$$
$$- \sum_{p=2}^{j-1} F_{gg}\left(i2, ip, k_a\Delta z, \frac{\Delta r}{\Delta z}\right)$$

B.6.2 Evaulation of $g_{ij}s_{j_1}$

$g_{ij}s_{j_1}$ is the exchange factor between $V(ij)$ and $A(j_1)$ where $A(j_1)$ is a circular ring between $z = (j_1 - 2)\Delta z$ and $z = (j_1 - 1)\Delta z$ at the boundary of the computational domain ($r = R_o$). Again, it is sufficient to consider only $g_{i2}s_{j_1}$ For the geometry as shown in Figure B4, it is given by

$$g_{i2}s_{j_1} = 2\pi \int_{(i-2)\Delta r}^{(i-1)\Delta r} \int_0^{\Delta z} \int_{A_{j_1}} \frac{k_{i2}e^{-\tau}r_{i2}cos\theta_{i2,k}dr_{i2}dz_{i2}dA_{j_1}}{\pi r^2} \qquad (B73)$$

Following the same normalization procedure as in the previous section, Eq. (B73) can be rewritten as

$$g_{i2}s_{j_1} = 2\int_{(i-2)\Delta r}^{(i-1)\Delta r} \int_0^{\Delta z} \int_0^{2\pi} \int_{\phi_{min}(\theta)}^{\phi_{max}(\theta)} k_{ij}e^{-\tau}r_{i2}drsin\phi d\phi d\theta dz_{i2}dr_{i2} \qquad (B74)$$

$$\frac{g_{i2}s_{j_1}}{k_{i2}\Delta r^2\Delta z} = F_{gs}\left(i2, j_1, k_a\Delta z, \frac{\Delta r}{\Delta z}\right) \qquad (B75)$$

with

$$F_{gs}\left(i2, j_1, k_a\Delta z, \frac{\Delta r}{\Delta z}\right) = \frac{2}{k_a\Delta z}\times \qquad (B76)$$

$$\int_{(i-2)}^{(i-1)} \int_0^1 \int_0^{2\pi} \int_{\phi_{min}(\theta)}^{\phi_{max}(\theta)} e^{-k_aL_{j_1}(\phi,\theta)}\eta_r sin\phi d\phi d\theta d\eta_z d\eta_r$$

$$= \frac{2}{k_a\Delta z}\int_{(i-2)}^{(i-1)} \int_0^1 \int_0^{2\pi} F_1(R_o, j_1, \eta_r, \eta_z, \theta)\eta_r d\theta d\eta_z d\eta_r$$

where $F_1(R_o, j_1, \eta_r, \eta_z, \theta)$ is as defined by Eq. (B49)

B.6.3 Evaulation of $g_{ij}t_{i1j1}$ and $g_{ij}b_i1j1$

For both integrals, it suffices to consider the exchange between $V(i2)$ and $A(i_1j_1)$ where $A(i_1j_1)$ is a circular strip with $(i_1 - 2)\Delta r \leq r \leq (i_1 - 1)\Delta r$ and $z = j_1\Delta z$. For the geometry as shown in Figure B5, the required integral is similar to that for the exchange factor $g_{ij}s_{j_1}$. Following similar development, the exchange factor is reduced to

$$\frac{g_{i2}t_{i_1j_1}}{k_{i2}\Delta r^2\Delta z} = F_{gt}\left(i2, i_1j_1, k_a\Delta z, \frac{\Delta r}{\Delta z}\right) \qquad (B77)$$

with

$$F_{gt}\left(i2, i_1j_1, k_a\Delta z, \frac{\Delta r}{\Delta z}\right) = \frac{2}{k_a\Delta z}\times \qquad (B78)$$

$$\int_{(i-2)}^{(i-1)} \int_0^1 \int_0^{2\pi} \int_{\phi_{min}(\theta)}^{\phi_{max}(\theta)} e^{-k_aL_{i_1j_1}(\phi,\theta)}\eta_r sin\phi d\phi d\theta d\eta_z d\eta_r$$

$$= \frac{2}{k_a\Delta z}\int_{(i-2)}^{(i-1)} \int_0^1 \int_0^{2\pi} F_2((i_1, j_1\Delta z, \eta_r, \eta_z, \theta)\eta_r d\theta d\eta_z d\eta_r$$

where $F_2(i_1, j_1 \Delta z, \eta_r, \eta_z, \theta)$ is as defined by Eq. (B50). Note that it suffices to consider only cases with $i_1 \geq i$ since, by reciprocity,

$$g_{i2} t_{i_1 j_1} = g_{i_1 2} t_{i j_1} \tag{B79}$$

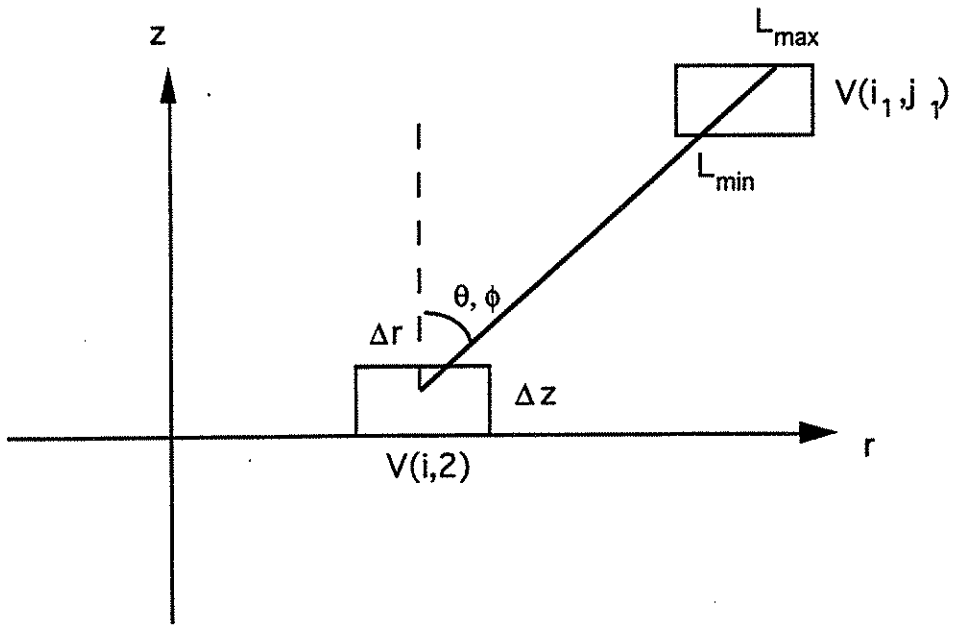

Figure B1. Geometry for the evaluation of the exchange factor $g_{ij} g_{i1j1}$.

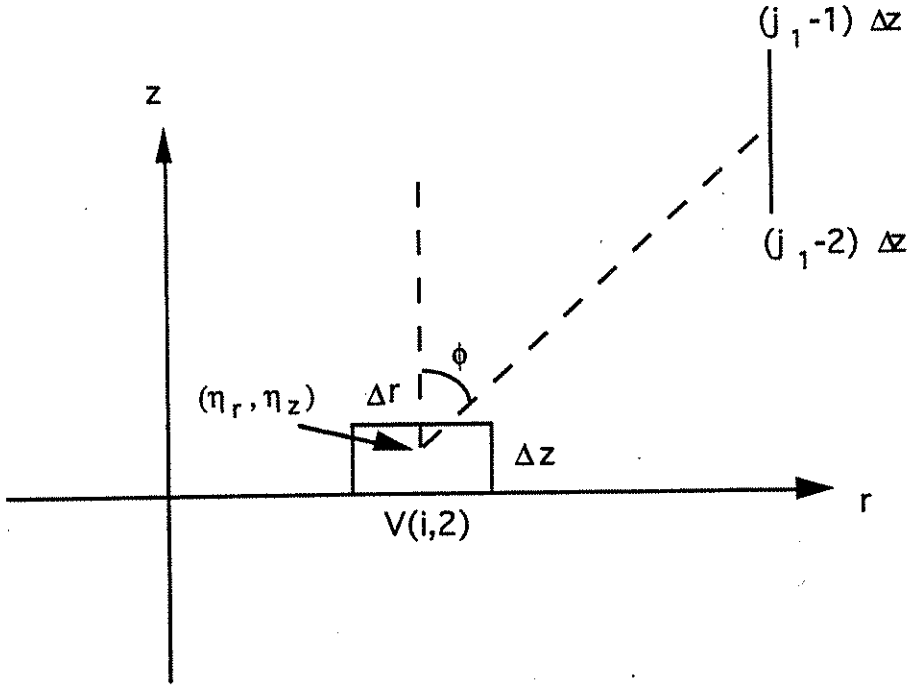

Figure B2a. Illustration of the limit of integration in Eq. (B49).

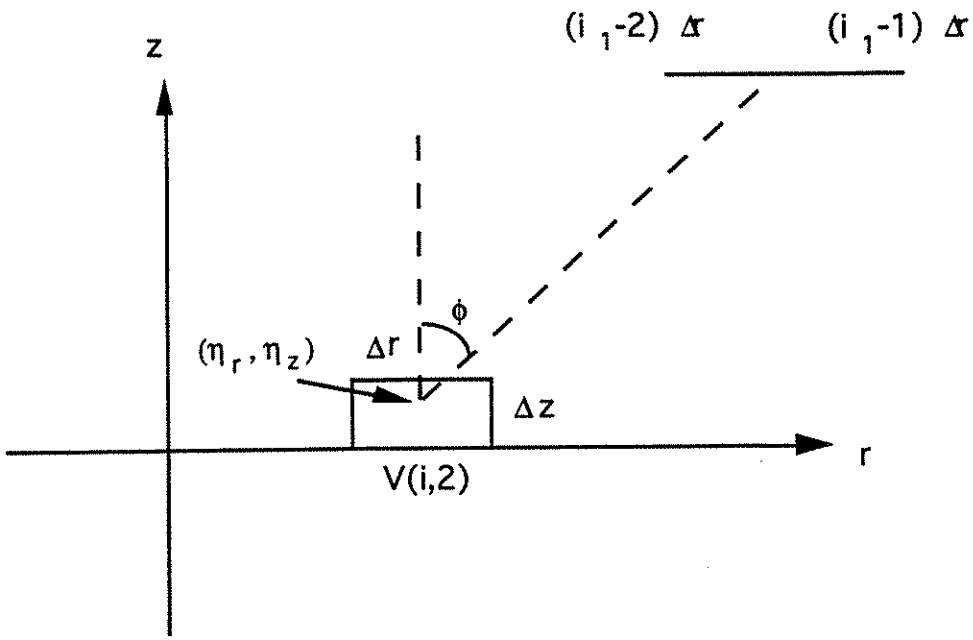

Figure B2b. Illustration of the limit of integration in Eq. (B50).

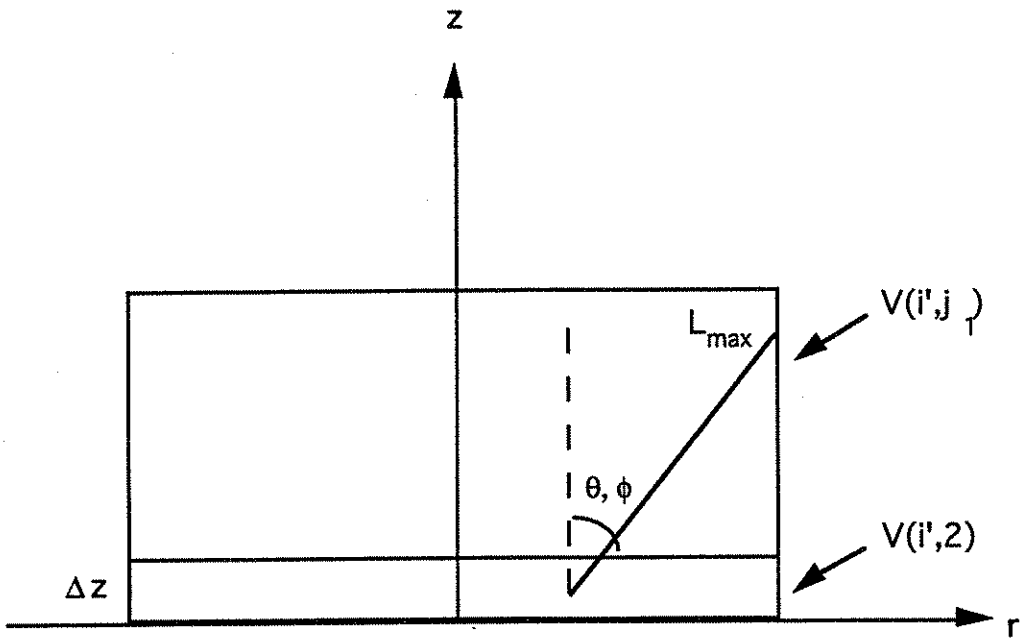

Figure B3. Geometry for the evaluation of the function $H_{gg}\left(i'2, i'j_1, k_a\Delta z, \frac{\Delta r}{\Delta z}\right)$.

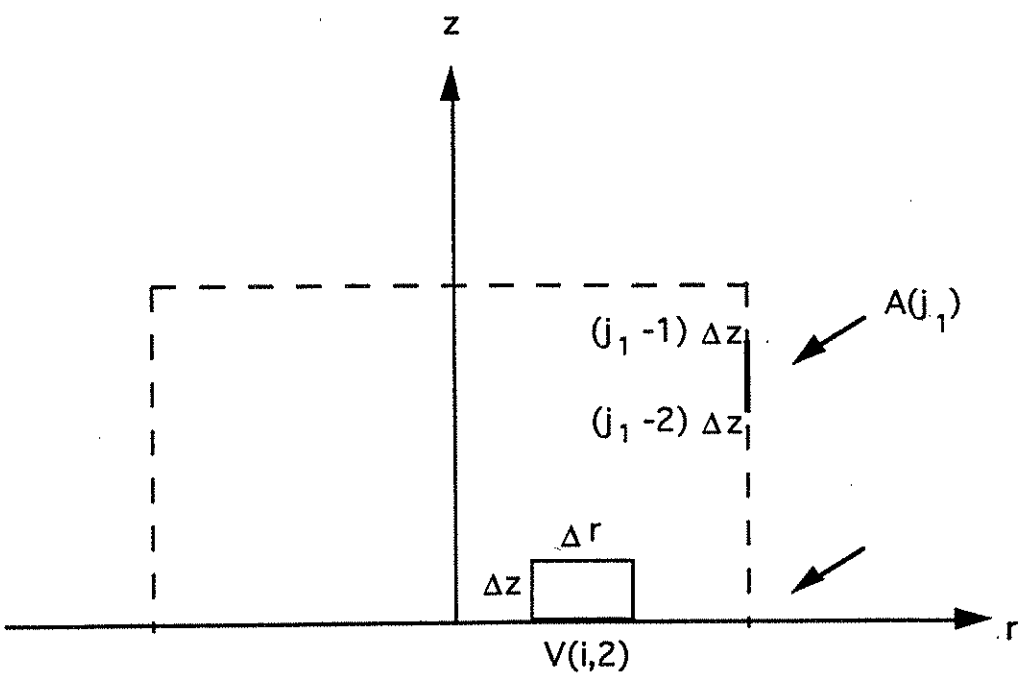

Figure B4. Geometry for the evaluation of the exchange factor $g_{ij}s_{j1}$.

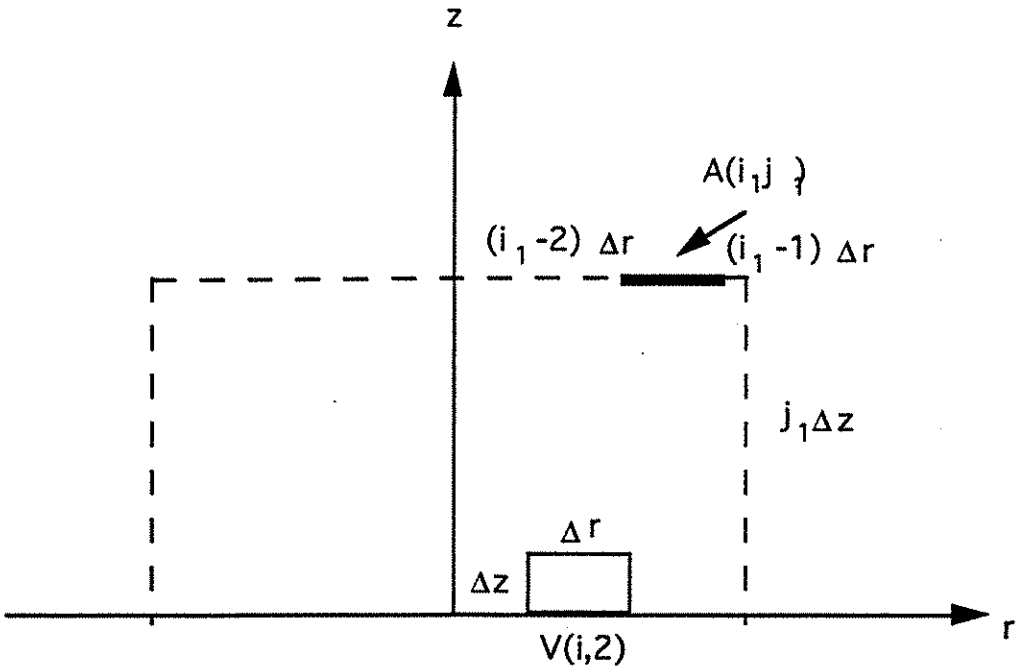

Figure B5. Geometry for the evaluation of the exchange factor $g_{ij}t_{i1j1}$.

APPENDIX C

A HEAT CONDUCTION MODEL FOR FUEL PARTICLES

The purpose of this model is to simulate the effect of fuel thermal properties on the solidification process. Since the thermal conductivity of some "fuel" materials which are of interest to the reactor safety community can be quite low, the amount of solidified fuel predicted by the default option of PM-ALPHA, which assumes a uniform fuel temperature within the particle, can understimate the solidification of the fuel particle.

The heat transfer model within the fuel interior has no effect formally on the set of conservation equations used by PM-ALPHA. In the constitutive laws on fuel/coolant heat transfer presented in section (3.2.2.1) and (3.2.2.2), T_f must now be interpreted as the fuel surface temperature. The internal energy of fuel, I_f, is related only to the "average" temperature $T_{f,av}$. At a given time step, $I_{f,i,j}^{n+1}$ and $T_{f,av,i,j}^{n+1}$ are generated from the numerical solution to the field equations. The objective of this model is to determine the updated surface temperature $T_{f,i,j}^{n+1}$ so that the appropriate heat transfer for the next computational step can be calculated.

Assuming a spherical fuel particle of diameter D_f, a three-node model, as shown in Figure C.1, is utilized. Numerical experiments show that this simplified model is quite reliable for premixing applications since the fuel particle diameter is expected to be in the order of centimeters. Based on standard conduction heat transfer equation, the finite-difference energy balance for the two interior nodes (identified as nodes a and b in Figure C.1) can be written as

$$\rho_f V_a \frac{I_{f,a}^{n+1} - I_{f,a}^{n}}{\delta t} = k_{f,a} A_a \frac{T_{f,b}^{n} - T_{f,a}}{\delta r} \qquad (C.1)$$

$$\rho_f V_b \frac{I_{f,b}^{n+1} - I_{f,b}^{n}}{\delta t} = k_{f,b} A_b \frac{T_{f,c}^{n} - T_{f,b}}{\delta r} - k_{f,a} A_a \frac{T_{f,b}^{n} - T_{f,a}}{\delta r} \qquad (C.2)$$

The overall energy balance on the fuel particle provides the third equation, which (suppressing the subscript indices (i,j)) is

$$V_a \frac{I_{f,a}^{n+1} - I_{f,a}^{n}}{\delta t} + V_b \frac{I_{f,b}^{n+1} - I_{f,b}^{n}}{\delta t} + V_c \frac{I_{f,c}^{n+1} - I_{f,c}^{n}}{\delta t} = V_f \frac{I_f^{n+1} - I_f^{n}}{\delta t} \qquad (C.3)$$

In the above equations, V_a, V_b and V_c are the volumes of the three nodal elements. A_a, A_b and A_c are the corresponding areas of the interfaces between nodes. The "average" thermal

conductivities are denoted by k_a, k_b and k_c, for the region of the three nodes respectively. These conductivities are volumetric averages which take into account the difference between liquid and solid thermal conductivity of the fuel.

Eqs. (C.1), (C.2) and (C.3) are applied to each computational node for a given value of I_f^{n+1} to obtain internal energies of the three nodes, $I_{f,a}^{n+1}$, $I_{f,b}^{n+1}$ and $I_{f,c}^{n+1}$. They are then inverted to yield the new nodal temperatures, $T_{f,a}^{n+1}$, $T_{f,b}^{n+1}$ and $T_{f,c}^{n+1}$, and the corresponding liquid fractions (if appropriate).

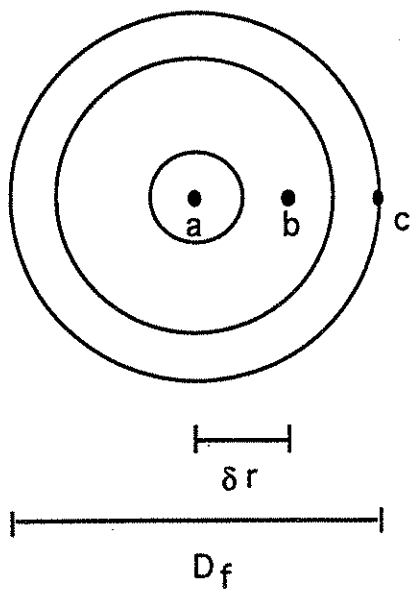

Figure C.1: Nodal system used in the conduction heat transfer model for the interior of a fuel particle.

APPENDIX D

SAMPLE PROBLEM INPUT DATA SET

```
==========================================================================
PMALPHA INPUT FILE

1. cccccccccccccccccccccccccccccccccccccccccccccccccccccccccccc
PMALPHA testing
2. ======================================================================
 Coordinate system type and grid size

 i xx.xxx xx.xxx
 1  2.000  2.500  system type (0 Cartesian; 1 cylindrical);
                   dr ; dz (cm) (1x,i1,2(1x,f6.3))
3.a ======================================================================
 Top and left wall inlets

 i i
 5 2  Flags for top wall left/right and
 2 2   left wall top/bottom inlets(2(1x,i1)),/)
       2 - solid free slip
       4 - continuous outflow
       5 - continuous inflow
       6 - constant pressure

 xxx.xxx xxx.xxx xxx.xxx xxx.xxx
   0.000  10.000  10.000  10.000   coordinates (cm) for inlets along
                                    the top wall (4(1x,f7.3))

 xxx.xxx xxx.xxx xxx.xxx xxx.xxx
   0.000   0.000   0.000   0.000   coordinates (cm) for inlets along
                                    the left wall (4(1x,f7.3))
3.b ======================================================================
Bottom and right wall outlets

 i i
 2 2  Flags for bottom wall left/right and left wall
 6 2   top/bottom outlets;  flag numbers as above (2(2(1x,i1)),/)

 xxx.xxx xxx.xxx xxx.xxx xxx.xxx
   0.000   0.000   0.000   0.000   coordinates (cm) for outlets along
                                    the bottom wall (4(1x,f6.3))

 xxx.xxx xxx.xxx xxx.xxx xxx.xxx
   0.000   2.500   2.500   2.500   coordinates (cm) for outlets along
                                    the right wall (4(1x,f6.3))
4. ======================================================================
Wall boundary conditions and interior obstacles

 i i i i
 0 0 0 0  Flags for top, left, bottom, and right wall boundary
          conditions, (0: free slip)  (4(1x,i1))
 ii
  0 Number of obstacles (1x,i2)

    B.C.; left;  right ; top; bottom coordinates (cm) of obstacle
    B.C. of obstacle: 0 free slip , 1 no slip
    left; right: left and right (radial) coordinates of the obstacle
    top; bottom: top and bottom (axial) coordinates of the obstacle
    (1x,4(1x,f7.3))
 i xxx.xxx xxx.xxx xxx.xxx xxx.xxx
```

```
5. ==================================================================================

Initial conditions

 xxx.xxx xxx.xxx
   0.000   0.000   initial u (r) ; v (z) velocity (cm/s) (2(lx,7.3))
 xx.xxxxxe_xx
  0.10132e+07      pressure (dyne/cm2) (lx,el2.5)
 x.xxxx x.xxxx
 0.0002 0.9999     steam void fraction ; coolant volume fraction
                                        2(lx,f6.4)
 xxxx.x xxxx.x
  373.0  373.0     coolant ; particle temperature (K) (2(lx,f6.1))
 xxx.x
 981.0             acceleration of gravity (cm/s2) (lx,f5.1)
  x.xxxxe_xx  x.xxxxe_xx  x.xxxxe_xx  x.xxxxe_xx  x.xxxxe_xx x.xxxxe_xx
  0.8000e+09  0.1500e+11  0.1000e+11  0.3000e+11  0.1000e-02 0.5750e+03
  sielolo     sielohi     siegolo     siegohi     ersie      tgo
                                        (all erg/g, tgo is K)
6. ==================================================================================
User inputs:
 size of steam gap (jgap), void fraction in steam gap(thgap), initial steam
 superheat (dtgsat), time for second set of initial conditions (tinter)

 iii x.xxxxe_xx xx.xxxxe_xx x.xxxxe_xx
   7 0.9999e+00 -0.1000e+01 0.1000e+02  jgap, thgap, dtgsat, tinter

7. ==================================================================================
Inlet and outlet conditions

 Top wall left inlet
 xxx.xxx xxx.xxx
   0.000   0.000            coolant u (r) ; v (z) velocity (cm/s) (2(lx,f7.3))
 xx.xxxxxe_xx xx.xxxxxe_xx
  0.00000e+00  0.07200e+03  particle u (r) ; v (z) velocity (cm/s) (2(lx,el2.5))
 xx.xxxxxe_xx
  0.10132e+07      pressure (dyne/cm2) (lx,el2.5)
 x.xxxx x.xxxx
 0.9999 0.9750     steam void fraction ; coolant volume fraction
                                          2(lx,f6.4)
 xxxx.x xxxx.x
  373.0 1023.0     coolant ; particle temperature (K) (2(lx,f6.1))
  x.xxxxe_xx  x.xxxxe_xx  x.xxxxe_xx  x.xxxxe_xx  x.xxxxe_xx
  0.2000e+10  0.1200e+11  0.1000e+11  0.3000e+11  0.3730e+03
  sieloloinl  sielohiinl  siegoloinl  siegohiinl  tginl (all erg/g, tginl is K)

 Top wall left inlet interrupt
 xxx.xxx xxx.xxx
   0.000   0.000            coolant u (r) ; v (z) velocity (cm/s) (2(lx,f7.3))
 xx.xxxxxe_xx xx.xxxxxe_xx
  0.00000e+00  0.10000e+01  particle u (r) ; v (z) velocity (cm/s) (2(lx,el2.5))
 xx.xxxxxe_xx
  0.10132e+07      pressure (dyne/cm2) (lx,el2.5)
 x.xxxx x.xxxx
 0.9999 0.9999     steam void fraction ; coolant volume fraction
                                          2(lx,f6.4)
 xxxx.x xxxx.x
  373.0  373.0     coolant ; particle temperature (K) (2(lx,f6.1))
  x.xxxxe_xx  x.xxxxe_xx  x.xxxxe_xx  x.xxxxe_xx  x.xxxxe_xx
  0.2000e+10  0.1200e+11  0.1000e+11  0.3000e+11  0.3730e+03
  sieloloinl2 sielohiinl2 siegoloinl2 siegohiinl2 tginl2 (all erg/g, tginl2 is K
```

```
Top wall right inlet
xxx.xxx xxx.xxx
  0.000   0.000   coolant u (r) ; v (z) velocity (cm/s) (2(1x,7.3))
xx.xxxxxe_xx xx.xxxxxe_xx
 0.00000e+00  0.00000e+04  particle u (r) ; v (z) velocity (cm/s) (2(1x,el2.5))
xx.xxxxxe_xx
 0.00000e+00      pressure (dyne/cm2) (1x,el2.5)
x.xxxx x.xxxx
0.0000 0.0000     steam void fraction ; coolant volume fraction
                                        2(1x,f6.4)
xxxx.x xxxx.x
   0.0    0.0     coolant ; particle temperature (K) (2(1x,f6.1))
 x.xxxxe_xx  x.xxxxe_xx  x.xxxxe_xx  x.xxxxe_xx  x.xxxxe_xx
 0.2000e+10  0.1200e+11  0.1000e+11  0.3000e+11  0.3730e+03
 sieloloinr  sielohiinr  siegoloinr  siegohiinr  tginr (all erg/g, tginr is K)

Left wall top inlet
xxx.xxx xxx.xxx
  0.000   0.000   coolant u (r) ; v (z) velocity (cm/s) (2(1x,7.3))
  0.000   0.000   particle u (r) ; v (z) velocity (cm/s) (2(1x,7.3))
xx.xxxxxe_xx
 0.00000e+00      pressure (dyne/cm2) (1x,el2.5)
x.xxxx x.xxxx
0.0000 0.0000     steam void fraction ; coolant volume fraction
                                        2(1x,f6.4)
xxxx.x xxxx.x
   0.0    0.0     coolant ; particle temperature (K) (2(1x,f6.1))
 x.xxxxe_xx  x.xxxxe_xx  x.xxxxe_xx  x.xxxxe_xx  x.xxxxe_xx
 0.2000e+10  0.1200e+11  0.1000e+11  0.3000e+11  0.3730e+03
 sieloloinb  sielohiinb  siegoloinb  siegohiinb  tginb (all erg/g, tginb is K)

Left wall bottom inlet
xxx.xxx xxx.xxx
  0.000   0.000   coolant u (r) ; v (z) velocity (cm/s) (2(1x,7.3))
  0.000   0.000   particle u (r) ; v (z) velocity (cm/s) (2(1x,7.3))
xx.xxxxxe_xx
 0.00000e+00      pressure (dyne/cm2) (1x,el2.5)
x.xxxx x.xxxx
0.0000 0.0000     steam void fraction ; coolant volume fraction
                                        2(1x,f6.4)
xxxx.x xxxx.x
   0.0    0.0     coolant ; particle temperature (K) (2(1x,f6.1))
 x.xxxxe_xx  x.xxxxe_xx  x.xxxxe_xx  x.xxxxe_xx  x.xxxxe_xx
 0.2000e+10  0.1200e+11  0.1000e+11  0.3000e+11  0.3730e+03
 sieloloint  sielohiint  siegoloint  siegohiint  tgint (all erg/g, tgint is K)

Bottom wall left outlet
xxx.xxx xxx.xxx
  0.000   0.000   coolant u (r) ; v (z) velocity (cm/s) (2(1x,7.3))
  0.000   0.000   particle u (r) ; v (z) velocity (cm/s) (2(1x,7.3))
xx.xxxxxe_xx
 0.00000e+00      pressure (dyne/cm2) (1x,el2.5)
x.xxxx x.xxxx
0.0000 0.0000     steam void fraction ; coolant volume fraction
                                        2(1x,f6.4)
xxxx.x xxxx.x
   0.0    0.0     coolant ; particle temperature (K) (2(1x,f6.1))
 x.xxxxe_xx  x.xxxxe_xx  x.xxxxe_xx  x.xxxxe_xx  x.xxxxe_xx
 0.2000e+10  0.1200e+11  0.1000e+11  0.3000e+11  0.3730e+03
 sielolootl  sielohiotl  siegolootl  siegohiotl  tgotl (all erg/g, tgotl is K)
```

```
Bottom wall right outlet
xxx.xxx xxx.xxx
  0.000   0.000    coolant u (r) ; v (z) velocity (cm/s) (2(1x,7.3))
  0.000   0.000    particle u (r) ; v (z) velocity (cm/s) (2(1x,7.3))
xx.xxxxxe_xx
 0.00000e+00       pressure (dyne/cm2) (1x,e12.5)
x.xxxx x.xxxx
0.0000 0.0000      steam void fraction ; coolant volume fraction
                                          2(1x,f6.4)

xxxx.x xxxx.x
   0.0    0.0      coolant ; particle temperature (K) (2(1x,f6.1))
 x.xxxxe_xx  x.xxxxe_xx  x.xxxxe_xx  x.xxxxe_xx  x.xxxxe_xx
 0.2000e+10  0.1200e+11  0.1000e+11  0.3000e+11  0.3730e+03
 sielolootr  sielohiotr  siegolootr  siegohiotr  tgotr (all erg/g, tgotr is K)

Right wall top outlet
xxx.xxx xxx.xxx
  0.000   0.000    coolant u (r) ; v (z) velocity (cm/s) (2(1x,7.3))
  0.000   0.000    particle u (r) ; v (z) velocity (cm/s) (2(1x,7.3))
xx.xxxxxe_xx
 0.10132e+07       pressure (dyne/cm2) (1x,e12.5)
x.xxxx x.xxxx
0.9999 0.9990      steam void fraction ; coolant volume fraction
                                          2(1x,f6.4)

xxxx.x xxxx.x
 373.0  373.0      coolant ; particle temperature (K) (2(1x,f6.1))
 x.xxxxe_xx  x.xxxxe_xx  x.xxxxe_xx  x.xxxxe_xx  x.xxxxe_xx
 0.2000e+10  0.1200e+11  0.1000e+11  0.3000e+11  0.3730e+03
 sielolootb  sielohiotb  siegolootb  siegohiotb  tgotb (all erg/g, tgotb is K)

Right wall bottom outlet
xxx.xxx xxx.xxx
  0.000   0.000    coolant u (r) ; v (z) velocity (cm/s) (2(1x,7.3))
  0.000   0.000    particle u (r) ; v (z) velocity (cm/s) (2(1x,7.3))
xx.xxxxxe_xx
 0.00000e+00       pressure (dyne/cm2) (1x,e12.5)
x.xxxx x.xxxx
0.0000 0.0000      steam void fraction ; coolant volume fraction
                                          2(1x,f6.4)

xxxx.x xxxx.x
   0.0    0.0      coolant ; particle temperature (K) (2(1x,f6.1))
 x.xxxxe_xx  x.xxxxe_xx  x.xxxxe_xx  x.xxxxe_xx  x.xxxxe_xx
 0.2000e+10  0.1200e+11  0.1000e+11  0.3000e+11  0.3730e+03
 sieloloott  sielohiott  siegoloott  siegohiott  tgott (all erg/g, tgott is K)
```

8. ==========

```
Output parameters and time step

 iiiii iiiii iiiii
     1  2000     0 itd,nsdmp,nwdmp

 xx.xxxxe_xx xx.xxxxe_xx xx.xxxxe_xx xx.xxxxe_xx
  0.0000e-00  0.1000e+01  0.5000e-04  0.5000e-01  time;tstop;dt;tpr
```

9. ==========

```
 Constants for the gas, liquid, and particles

  gas properties
 xx.xxxxxe_xx
```

```
 0.11200e+08 cvgo       specific heat of gas at constant volume (erg/(K g))
 0.46200e+07 xcrg       characteristic gas constant of gas  (erg/(K g))
 0.13300e+01 xcpvg      ratio of specific heats for gas
 0.25067e+11 siegref    internal energy of gas at reference temperature (erg/g)
 0.25000e+04 xkg        thermal conductivity of gas (erg/(K cm s))
 0.12000e-03 xmug       coefficient of viscosity of gas (dyne s/cm2)

 liquid/coolant properties [conl()]
xx.xxxxxe_xx
 0.42000e+08 cplref     specific heat of liquid at constant pressure (erg/K g))
 0.30000e-02 xmul       coefficient of viscosity of liquid (dyne s/cm2)
 0.68100e+05 xklref     thermal conductivity of liquid (erg/(K cm s))
 0.41906e+10 sielref    internal energy of liquid at reference (erg/g)
 0.22570e+11 xlheat     latent heat of vaporization of coolant (erg/g)
 0.95840e+00 rlref      density of liquid at ref. temp. and pres. (g/cm3)
 0.72000e+02 xsurtenl   surface tension of steam-water at ref. temp (dyne/cm)
 0.12289e+06 cso        speed of sound of liquid at ref. cond. (cm/s)

  fuel properties
xx.xxxxe_xx         MATERIAL: steel
 0.5440e+09         siepfref (erg/g), internal energy at reference cond.
 0.5440e+07         cpfref (erg/K g), specific heat at reference cond.
 0.7900e+01         rpfref (g/cm3), fuel density at reference cond.
 0.1473e+04         tpmelt (K),  melting temperare of fuel
 0.6000e+09         enpmelt (erg/g),  heat of fusion of fuel
 0.6530e+10         siespm (erg/g), internal energy of solid fuel at melt.
 0.7200e+02         xsurtenf (dyne/cm),   surface tension of fuel/water
 0.7500e+00         empf, emissivity of fuel
 0.5672e-04         xsigma (erg/(K4 cm2 s)), Stefan-Boltzmann Const.
 0.9115e+06         thconps (erg/s cm K) thermal conductivity for solid fuel
 0.1959e+06         thconpl (erg/s cm K) thermal conductivity for liquid fuel
 0.1500e-00         dpfint (cm), initial particle diameter

10. ==================================================================
 Heat conduction model control parameters

   0            ihcm - flag particle heat conduction
   0            number of tracing cells, ismijtr
 164            cell number!these two lines to stay even of conduction model
 trace-164      output file name!is not used. If ismijtr>1, add lines accordingl

 phase change parameters
 xx.xxxxxe_xx
  0.10000e+01   delts, maximum (minimum) superheat (subcooling)
  0.10000e+01   rheatgmx, heat transfer enhancement factor for steam
  0.10000e+01   rheatlmx, heat transfer enhancement factor for water
  0.10000e+02   xphtev, factor used in estimate bound for boiling rate
  0.10000e+02   xphtc, factor used in estimate bound for condensation rate

 fragmentation model parameter
 iii
   0          mfrag          model flag
 xx.xxxxxe_xx
  0.15000e+02 coefl          fragmentation coefficient for liquid
  0.15000e+02 coefg          fragmentation coefficient for gas
  0.25000e+01 vminl          minimum velocity to start liquid fragmentation (cm/
  0.25000e+01 vming          minimum velocity to start gas fragmentation (cm/s)
  2.50000e+00 drgcoef        drag coefficient
  0.10000e+01 xfrag          enhancement factor
  0.00000e+03 xdmsodt        minimum rate per particle
```

```
 0.40000e+04 dmsodtmx        maximum rate per particle
 0.50000e-04 tmstart         delay time for fragmentation
 0.00000e-00 xfm             xfm*dmdtmx is the minimum fragmentation rate
 0.80000e+03 dtf             liquid fraction to turn off fragmentation
-0.00500e+00 thbr            void fraction above which to turn off breakup
 0.00000e+00 betabr          breakup paramaeter

 radiation model parameter
iii
  0            irad    irad .ne. 1, use old radiation model
 0.12300e+01   awgin   absorption coefficient for steam
 0.30000e+00   frad    fraction of radient energy absorbed by liquid drops

11. ==================================================================
 Numerical solution parameters
xx.xxxxxe_xx
 0.10000e-05  epsg
 0.10000e-05  epsl
 0.10000e+01  dpresmn limit for abs(p1-p2) to decide ignoring further iteration

12. ==================================================================
History and diagnostics

iii iii iii iii iii
 23   2   2   2  10 ijex,ip1,jp1,ip2,jp2 (6(1x,i3))

xx.xxxxe_xx
 0.1000e-04 dthsty (1x,e11.4)
```

APPENDIX E

SAMPLE PROBLEM OUTPUT DATA SET

For the purpose of description and comparison, Tables E.1 thru E.4 show the contents of the files DTH, DEPS, DVL and DTP at two different times in the calculation.

In each of the specified time, the cycle counts, time and time step of the calculation are first printed, followed by a line identifying the name of the variables. Each line of the data contains the J counter, followed by the variables from I = 2 to I = IB1, with IB1 = IB2 − 1. For example, in Table E.1, the first data line contains J(=41) and TH(I, 41) with $2 \leq I \leq$ IB1.

Table E.1a. Numerical Data for Void Fraction (DTH) at Time 0.3 s

cycle- 6000 time- .30000000 dt- .00005000

********* th *********

41	.0003	.0003	.0003	.0003	.0003	.0003	.0003	.0003	.0003	.0003
40	.0003	.0003	.0003	.0003	.0004	.0004	.0004	.0004	.0004	.0004
39	.0003	.0003	.0003	.0003	.0003	.0003	.0003	.0003	.0003	.0003
38	.0003	.0003	.0002	.0002	.0003	.0003	.0003	.0003	.0003	.0002
37	.0002	.0002	.0002	.0002	.0002	.0002	.0002	.0002	.0002	.0002
36	.0002	.0002	.0002	.0002	.0002	.0002	.0002	.0002	.0002	.0002
35	.0002	.0002	.0002	.0002	.0002	.0002	.0002	.0002	.0002	.0002
34	.0002	.0002	.0002	.0002	.0002	.0002	.0002	.0002	.0002	.0002
33	.0002	.0002	.0002	.0002	.0002	.0002	.0002	.0002	.0002	.0002
32	.0002	.0002	.0002	.0002	.0002	.0002	.0002	.0002	.0002	.0002
31	.0002	.0002	.0002	.0002	.0002	.0002	.0002	.0002	.0002	.0002
30	.0002	.0002	.0002	.0002	.0002	.0002	.0002	.0002	.0002	.0002
29	.0002	.0002	.0002	.0002	.0002	.0002	.0002	.0002	.0002	.0002
28	.0002	.0002	.0002	.0002	.0002	.0002	.0002	.0002	.0002	.0002
27	.0002	.0002	.0002	.0002	.0002	.0002	.0002	.0002	.0002	.0002
26	.0003	.0003	.0003	.0002	.0002	.0002	.0002	.0002	.0002	.0002
25	.0004	.0004	.0003	.0003	.0003	.0002	.0003	.0003	.0003	.0003
24	.0034	.0028	.0023	.0015	.0003	.0003	.0003	.0003	.0003	.0004
23	.0316	.0279	.0255	.0178	.0023	.0004	.0003	.0003	.0004	.0004
22	.1679	.1583	.1562	.1299	.0236	.0024	.0004	.0003	.0003	.0004
21	.4632	.4501	.4589	.4259	.1299	.0187	.0019	.0004	.0003	.0003
20	.7016	.6983	.7032	.7031	.3243	.0711	.0088	.0009	.0003	.0003
19	.7858	.7889	.7908	.8013	.5105	.1490	.0232	.0023	.0004	.0003
18	.7322	.7340	.7341	.7322	.4697	.1783	.0352	.0039	.0004	.0003
17	.6834	.6903	.7193	.7839	.5002	.2175	.0458	.0050	.0005	.0003
16	.8846	.8998	.9186	.9550	.8524	.3435	.0567	.0050	.0004	.0002
15	.8386	.8588	.8774	.9190	.7023	.2392	.0333	.0025	.0002	.0002
14	.7183	.7227	.7628	.7433	.4779	.1672	.1003	.1005	.1089	.1148
13	.7313	.7182	.7565	.8020	.5206	.3955	.3679	.3657	.3678	.3711
12	.9868	.9958	1.0000	.9978	.8460	.9091	.8956	.8807	.8669	.8525
11	1.0000	.9999	.9999	.9999	.9884	.9993	1.0000	1.0000	1.0000	.9999
10	.9999	.9999	.9999	.9999	.9998	.9999	.9999	.9999	.9999	.9999
9	.9999	.9999	.9999	.9999	.9999	.9999	.9999	.9999	.9999	.9999
8	.9999	.9999	.9999	.9999	.9999	.9999	.9999	.9999	.9999	.9999
7	.9999	.9999	.9999	.9999	.9999	.9999	.9999	.9999	.9999	.9999
6	.9999	.9999	.9999	.9999	.9999	.9999	.9999	.9999	.9999	.9999
5	.9999	.9999	.9999	.9999	.9999	.9999	.9999	.9999	.9999	.9999
4	.9999	.9999	.9999	.9999	.9999	.9999	.9999	.9999	.9999	.9999
3	.9999	.9999	.9999	.9999	.9999	.9999	.9999	.9999	.9999	.9999
2	.9999	.9999	.9999	.9999	.9999	.9999	.9999	.9999	.9999	.9999

Table E.1b. Numerical Data for Void Fraction (DTH) at Time 0.6 s

cycle= 12000 time= .60000000 dt= .00005000

********* th *********

41	.0003	.0003	.0003	.0003	.0003	.0003	.0003	.0003	.0003	.0003
40	.0003	.0003	.0003	.0003	.0004	.0004	.0004	.0004	.0004	.0004
39	.0003	.0003	.0003	.0003	.0003	.0003	.0003	.0003	.0003	.0003
38	.0003	.0003	.0003	.0003	.0003	.0003	.0003	.0003	.0003	.0003
37	.0002	.0002	.0002	.0002	.0002	.0002	.0002	.0002	.0002	.0002
36	.0002	.0002	.0002	.0002	.0002	.0002	.0002	.0002	.0002	.0002
35	.0002	.0002	.0002	.0002	.0002	.0002	.0002	.0002	.0002	.0002
34	.0002	.0002	.0002	.0002	.0002	.0002	.0002	.0002	.0002	.0002
33	.0003	.0003	.0002	.0002	.0002	.0002	.0002	.0002	.0002	.0002
32	.0007	.0007	.0005	.0003	.0002	.0002	.0002	.0002	.0002	.0002
31	.0089	.0091	.0074	.0032	.0004	.0002	.0002	.0002	.0002	.0002
30	.0811	.0832	.0738	.0407	.0051	.0004	.0002	.0002	.0002	.0002
29	.4293	.4335	.4015	.2424	.0461	.0029	.0003	.0002	.0002	.0002
28	.6982	.6911	.6916	.6625	.2394	.0228	.0010	.0003	.0002	.0002
27	.7828	.7905	.7953	.7384	.6296	.0772	.0026	.0003	.0002	.0002
26	.7786	.7875	.7887	.7584	.6286	.1230	.0072	.0004	.0003	.0002
25	.7122	.7220	.7132	.6812	.5818	.3838	.0112	.0005	.0003	.0003
24	.7655	.7364	.7251	.6547	.5799	.4318	.0174	.0009	.0003	.0003
23	.8605	.8488	.8643	.8031	.6120	.3003	.0206	.0012	.0003	.0003
22	.8761	.8814	.9004	.8617	.6010	.2377	.0279	.0017	.0004	.0004
21	.8481	.8645	.8778	.8387	.5443	.2511	.0378	.0027	.0005	.0004
20	.8086	.8183	.8317	.7943	.4942	.2485	.0402	.0039	.0006	.0004
19	.7515	.7539	.7727	.7390	.4838	.2471	.0448	.0060	.0007	.0003
18	.6837	.7061	.7250	.6964	.5753	.2588	.0613	.0108	.0012	.0003
17	.6627	.7285	.7429	.7385	.7785	.2723	.0944	.0196	.0023	.0008
16	.6946	.7922	.8293	.8504	.8919	.2827	.1413	.0317	.0065	.0040
15	.7165	.8196	.8978	.9213	.9113	.2902	.1861	.0510	.0239	.0197
14	.7148	.8089	.9204	.9438	.9006	.3196	.2308	.0995	.0740	.0671
13	.7045	.7779	.9217	.9481	.8695	.4117	.2753	.1816	.1597	.1525
12	.6808	.7354	.9138	.9499	.8348	.4961	.3181	.2797	.2638	.2687
11	.6374	.6860	.8983	.9538	.8071	.5730	.4811	.4260	.4298	.4810
10	.5806	.6432	.8708	.9555	.7919	.6345	.6587	.7886	.8679	.9364
9	.5290	.6116	.8312	.9512	.7815	.6764	.8036	.9590	1.0000	1.0000
8	.4816	.5880	.7854	.9370	.7703	.7805	.9232	1.0000	.9999	.9999
7	.4257	.5766	.7381	.9098	.7676	.9062	.9755	.9998	.9999	.9999
6	.3781	.5830	.6924	.8708	.7830	.9313	.9795	.9998	.9999	.9999
5	.3461	.5832	.6449	.8235	.8217	.9446	.9838	.9999	.9999	.9999
4	.3374	.5427	.5780	.7560	.8751	.9523	.9891	.9999	.9999	.9999
3	.3260	.4696	.4850	.6259	.9017	.9562	.9953	.9999	.9999	.9999
2	.3306	.4051	.4214	.4556	.7320	.9034	.9974	.9999	.9999	.9999

Table E.2a. Numerical Data for Coolant Volume Fraction (DEPS) at Rime 0.3 s

cycle= 6000 time= .30000000 dt= .00005000

********* eps *********

41	.9994	.9994	.9994	.9994	.9994	.9994	.9994	.9994	.9994	.9994
40	.9999	.9999	.9999	.9999	.9999	.9999	.9999	.9999	.9999	.9999
39	.9999	.9999	.9999	.9999	.9999	.9999	.9999	.9999	.9999	.9999
38	.9999	.9999	.9999	.9999	.9999	.9999	.9999	.9999	.9999	.9999
37	.9999	.9999	.9999	.9999	.9999	.9999	.9999	.9999	.9999	.9999
36	.9999	.9999	.9999	.9999	.9999	.9999	.9999	.9999	.9999	.9999
35	.9999	.9999	.9999	.9999	.9999	.9999	.9999	.9999	.9999	.9999
34	.9999	.9999	.9999	.9999	.9999	.9999	.9999	.9999	.9999	.9999
33	.9999	.9999	.9999	.9999	.9999	.9999	.9999	.9999	.9999	.9999
32	.9999	.9999	.9999	.9999	.9999	.9999	.9999	.9999	.9999	.9999
31	.9998	.9998	.9998	.9998	.9999	.9999	.9999	.9999	.9999	.9999
30	.9996	.9996	.9997	.9997	.9998	.9999	.9999	.9999	.9999	.9999
29	.9991	.9991	.9992	.9992	.9997	.9999	.9999	.9999	.9999	.9999
28	.9976	.9977	.9979	.9980	.9992	.9998	.9999	.9999	.9999	.9999
27	.9943	.9946	.9948	.9952	.9980	.9994	.9998	.9999	.9999	.9999
26	.9879	.9883	.9886	.9892	.9952	.9986	.9997	.9999	.9999	.9999
25	.9772	.9777	.9780	.9788	.9897	.9968	.9993	.9998	.9999	.9999
24	.9634	.9637	.9638	.9646	.9812	.9936	.9985	.9997	.9999	.9999
23	.9511	.9509	.9506	.9518	.9718	.9893	.9973	.9995	.9999	.9999
22	.9462	.9455	.9452	.9477	.9665	.9857	.9959	.9992	.9998	.9999
21	.9491	.9485	.9485	.9537	.9693	.9852	.9953	.9990	.9998	.9999
20	.9539	.9539	.9545	.9621	.9783	.9887	.9960	.9990	.9998	.9999
19	.9590	.9596	.9609	.9687	.9883	.9938	.9975	.9993	.9998	.9998
18	.9647	.9656	.9670	.9727	.9952	.9976	.9989	.9996	.9998	.9998
17	.9697	.9703	.9715	.9751	.9988	.9993	.9996	.9997	.9997	.9997
16	.9741	.9745	.9752	.9769	.9998	.9998	.9997	.9997	.9997	.9997
15	.9760	.9761	.9765	.9771	.9997	.9998	.9998	.9998	.9998	.9998
14	.9770	.9768	.9772	.9774	.9999	.9999	.9999	.9999	.9999	.9999
13	.9794	.9791	.9794	.9798	.9999	.9999	.9999	.9999	.9999	.9999
12	.9819	.9818	.9819	.9823	.9999	1.0000	1.0000	1.0000	1.0000	1.0000
11	.9827	.9827	.9827	.9827	1.0000	1.0000	1.0000	1.0000	1.0000	1.0000
10	.9825	.9825	.9825	.9825	1.0000	1.0000	1.0000	1.0000	1.0000	1.0000
9	.9822	.9822	.9823	.9823	1.0000	1.0000	1.0000	1.0000	1.0000	1.0000
8	.9820	.9820	.9820	.9820	1.0000	1.0000	1.0000	1.0000	1.0000	1.0000
7	.9818	.9818	.9818	.9818	1.0000	1.0000	1.0000	1.0000	1.0000	1.0000
6	.9815	.9815	.9815	.9815	1.0000	1.0000	1.0000	1.0000	1.0000	1.0000
5	.9812	.9812	.9812	.9812	1.0000	1.0000	1.0000	1.0000	1.0000	1.0000
4	.9809	.9809	.9809	.9810	1.0000	1.0000	1.0000	1.0000	1.0000	1.0000
3	.9806	.9806	.9806	.9806	1.0000	1.0000	1.0000	1.0000	1.0000	1.0000
2	.9803	.9803	.9803	.9803	1.0000	1.0000	1.0000	1.0000	1.0000	1.0000

Table E.2b Numerical Data for Coolant Volume Fraction (DEPS) at Time 0.6 s

cycle= 12000 time= .60000000 dt= .00005000

********* eps *********

41	.9984	.9984	.9984	.9985	.9986	.9987	.9987	.9987	.9987	.9987
40	.9995	.9995	.9995	.9996	.9997	.9998	.9999	.9999	.9999	.9999
39	.9989	.9990	.9990	.9991	.9994	.9997	.9998	.9999	.9999	.9999
38	.9979	.9980	.9981	.9983	.9989	.9994	.9997	.9998	.9999	.9999
37	.9962	.9963	.9965	.9969	.9978	.9988	.9995	.9998	.9999	.9999
36	.9934	.9935	.9938	.9944	.9960	.9978	.9990	.9996	.9998	.9999
35	.9892	.9892	.9896	.9905	.9932	.9961	.9982	.9994	.9998	.9999
34	.9835	.9835	.9839	.9852	.9890	.9934	.9969	.9989	.9997	.9999
33	.9767	.9766	.9770	.9787	.9836	.9898	.9950	.9981	.9994	.9998
32	.9700	.9697	.9701	.9720	.9778	.9854	.9924	.9970	.9991	.9998
31	.9650	.9647	.9649	.9670	.9727	.9809	.9895	.9956	.9987	.9997
30	.9637	.9635	.9637	.9657	.9702	.9775	.9868	.9942	.9982	.9996
29	.9663	.9662	.9666	.9686	.9714	.9760	.9849	.9930	.9977	.9994
28	.9679	.9679	.9691	.9729	.9762	.9770	.9844	.9924	.9974	.9993
27	.9673	.9678	.9700	.9750	.9820	.9799	.9855	.9926	.9974	.9993
26	.9657	.9663	.9699	.9771	.9856	.9840	.9879	.9935	.9976	.9993
25	.9688	.9699	.9745	.9814	.9891	.9887	.9909	.9949	.9981	.9994
24	.9746	.9772	.9819	.9878	.9927	.9923	.9939	.9965	.9986	.9995
23	.9761	.9802	.9850	.9908	.9953	.9951	.9964	.9978	.9990	.9996
22	.9752	.9808	.9859	.9926	.9971	.9973	.9981	.9988	.9994	.9997
21	.9768	.9837	.9892	.9947	.9985	.9987	.9991	.9993	.9996	.9997
20	.9800	.9875	.9925	.9965	.9993	.9994	.9996	.9996	.9997	.9998
19	.9837	.9916	.9954	.9980	.9997	.9997	.9998	.9998	.9998	.9998
18	.9854	.9937	.9971	.9989	.9999	.9998	.9999	.9999	.9999	.9999
17	.9877	.9949	.9979	.9993	.9999	.9999	.9999	.9999	.9999	.9999
16	.9896	.9958	.9984	.9995	.9999	1.0000	1.0000	1.0000	1.0000	1.0000
15	.9912	.9964	.9987	.9996	1.0000	1.0000	1.0000	1.0000	1.0000	1.0000
14	.9927	.9968	.9989	.9997	1.0000	1.0000	1.0000	1.0000	1.0000	1.0000
13	.9943	.9972	.9990	.9997	1.0000	1.0000	1.0000	1.0000	1.0000	1.0000
12	.9961	.9976	.9991	.9997	1.0000	1.0000	1.0000	1.0000	1.0000	1.0000
11	.9977	.9981	.9992	.9998	1.0000	1.0000	1.0000	1.0000	1.0000	1.0000
10	.9987	.9986	.9993	.9998	1.0000	1.0000	1.0000	1.0000	1.0000	1.0000
9	.9992	.9990	.9994	.9998	1.0000	1.0000	1.0000	1.0000	1.0000	1.0000
8	.9994	.9994	.9996	.9998	1.0000	1.0000	1.0000	1.0000	1.0000	1.0000
7	.9995	.9996	.9996	.9998	1.0000	1.0000	1.0000	1.0000	1.0000	1.0000
6	.9996	.9997	.9997	.9998	1.0000	1.0000	1.0000	1.0000	1.0000	1.0000
5	.9995	.9996	.9996	.9997	1.0000	1.0000	1.0000	1.0000	1.0000	1.0000
4	.9994	.9994	.9995	.9996	1.0000	1.0000	1.0000	1.0000	1.0000	1.0000
3	.9993	.9993	.9993	.9994	1.0000	1.0000	1.0000	1.0000	1.0000	1.0000
2	.9988	.9987	.9987	.9987	.9999	1.0000	1.0000	1.0000	1.0000	1.0000

Table E.3a. Numerical Data for Liquid Velocity (DVL) at Time 0.3 s

cycle= 6000 time= .30000000 dt= .00005000

********* vl *********

41	.0	.0	.0	.0	.0	.0	.0	.0	.0	.0
40	.0	.0	.0	.0	.0	.0	.0	.0	.0	.0
39	.1	.0	.0	.0	.0	.0	.0	.0	.0	-.1
38	.1	.1	.1	.1	.0	.0	.0	.0	-.1	-.1
37	.2	.2	.1	.1	.0	.0	.0	-.1	-.1	-.1
36	.3	.2	.2	.2	.1	.0	-.1	-.1	-.1	-.2
35	.4	.4	.3	.2	.1	.0	-.1	-.1	-.2	-.2
34	.6	.5	.5	.3	.2	.1	-.1	-.2	-.3	-.3
33	.9	.8	.7	.5	.3	.1	-.1	-.3	-.4	-.4
32	1.4	1.2	1.0	.8	.4	.1	-.1	-.4	-.5	-.6
31	2.1	1.9	1.6	1.2	.7	.2	-.2	-.5	-.8	-.9
30	3.0	2.8	2.4	1.7	1.0	.3	-.3	-.8	-1.1	-1.3
29	4.5	4.1	3.5	2.6	1.5	.5	-.4	-1.1	-1.6	-1.8
28	6.5	6.1	5.1	3.9	2.2	.7	-.6	-1.6	-2.2	-2.5
27	9.3	8.7	7.5	5.6	3.1	.8	-1.0	-2.2	-3.1	-3.5
26	13.2	12.5	10.8	8.3	4.3	.9	-1.6	-3.3	-4.3	-4.8
25	18.3	17.5	15.4	12.0	5.8	.8	-2.6	-4.8	-6.1	-6.7
24	25.4	24.5	21.9	17.6	7.8	.3	-4.2	-6.9	-8.4	-9.1
23	35.3	34.4	31.2	25.8	10.5	-.7	-6.8	-9.9	-11.5	-12.1
22	48.4	47.3	43.9	37.2	14.2	-2.3	-10.4	-13.8	-15.2	-15.8
21	60.1	58.9	55.6	47.9	17.1	-4.7	-15.0	-18.6	-19.7	-20.1
20	23.2	21.5	21.2	18.8	8.8	-9.5	-20.5	-24.0	-24.6	-24.7
19	-36.6	-36.0	-31.3	-29.8	-4.5	-15.5	-25.9	-29.3	-29.5	-29.3
18	-6.7	-5.9	-6.9	-17.8	-18.8	-22.2	-31.0	-34.1	-34.0	-33.6
17	-9.1	-8.7	-7.6	-23.4	-32.2	-29.6	-35.8	-38.3	-38.0	-37.5
16	47.2	52.2	79.3	72.6	-10.2	-32.2	-39.6	-41.7	-41.4	-41.0
15	34.1	45.9	61.1	70.1	-44.3	-44.2	-44.9	-44.9	-44.6	-43.9
14	-72.2	-67.1	-54.7	-41.6	-90.8	-60.0	-50.4	-47.3	-47.7	-46.2
13	-93.7	-94.8	-100.2	-87.8	-101.0	-63.0	-50.7	-47.4	-50.0	-47.3
12	14.9	23.9	33.0	29.7	-62.0	-29.8	-25.0	-25.6	-32.9	-27.4
11	.0	.0	.0	.5	-18.5	-.3	11.8	10.1	5.9	11.4
10	.0	.1	.1	.1	-1.1	.0	.0	.0	.0	.0
9	.0	.1	.1	.1	.0	.0	.0	.0	.0	.0
8	.1	.1	.1	.1	.0	.0	.0	.0	.0	.0
7	.1	.1	.1	.1	.0	.0	.0	.0	.0	.0
6	.1	.1	.1	.1	.0	.0	.0	.0	.0	.0
5	.1	.1	.1	.1	.0	.0	.0	.0	.0	.0
4	.1	.1	.1	.1	.0	.0	.0	.0	.0	.0
3	.1	.1	.1	.1	.0	.0	.0	.0	.0	.0
2	.1	.1	.1	.1	.0	.0	.0	.0	.0	.0

Table E.3b.Numerical Data for Liquid Velocity (DVL) at Time 0.6 s

cycle= 12000 time= .60000000 dt= .00005000

********* vl *********

41	.0	.0	.0	.0	.0	.0	.0	.0	.0	.0
40	.4	.4	.4	.3	.2	.0	-.1	-.1	-.2	-.2
39	.9	.9	.8	.6	.3	.1	-.1	-.3	-.4	-.4
38	1.5	1.4	1.3	1.0	.6	.1	-.2	-.4	-.6	-.6
37	2.2	2.1	1.9	1.5	.8	.2	-.3	-.6	-.9	-1.0
36	3.1	2.9	2.6	2.1	1.2	.3	-.5	-.9	-1.2	-1.3
35	4.0	3.9	3.6	2.9	1.6	.3	-.7	-1.4	-1.7	-1.9
34	5.1	5.1	4.7	3.9	2.2	.4	-1.0	-1.9	-2.4	-2.5
33	6.4	6.4	6.1	5.3	3.0	.5	-1.5	-2.6	-3.2	-3.4
32	7.7	8.0	7.8	6.9	3.9	.6	-2.0	-3.5	-4.1	-4.3
31	9.3	9.6	9.6	8.7	5.1	.9	-2.5	-4.4	-5.2	-5.4
30	11.1	11.1	11.2	10.5	6.4	1.4	-2.7	-5.2	-6.2	-6.4
29	12.9	12.5	11.4	9.5	6.8	2.2	-2.7	-5.8	-7.0	-7.2
28	-41.6	-41.6	-37.8	-23.2	2.6	3.5	-2.0	-5.9	-7.4	-7.8
27	-50.7	-46.9	-38.7	-24.0	-5.3	5.8	-.1	-5.2	-7.3	-7.7
26	-48.2	-45.9	-42.0	-38.3	-18.5	7.6	2.3	-3.9	-6.4	-7.0
25	-87.5	-86.6	-88.3	-82.1	-47.8	3.6	4.2	-2.0	-4.9	-5.5
24	-129.3	-128.9	-132.8	-122.7	-66.7	-.9	6.5	.5	-2.6	-3.3
23	-149.8	-146.0	-143.3	-131.9	-71.2	-3.8	8.7	3.3	.3	-.4
22	-140.1	-132.2	-125.7	-107.3	-67.7	-7.2	9.8	6.2	3.8	3.3
21	-177.4	-163.5	-151.2	-132.4	-81.3	-13.8	8.8	8.9	7.8	7.7
20	-231.5	-221.0	-210.3	-183.3	-102.2	-21.5	7.3	12.0	12.6	12.9
19	-290.4	-286.8	-284.6	-242.6	-122.3	-27.1	7.2	16.3	18.5	19.2
18	-344.7	-338.9	-335.2	-278.4	-130.9	-27.5	9.3	22.4	25.8	26.5
17	-342.2	-330.3	-324.0	-270.6	-119.5	-22.4	13.7	30.4	34.3	34.5
16	-215.1	-210.5	-213.1	-180.2	-77.0	-15.8	19.3	38.9	42.9	42.6
15	-154.0	-156.4	-158.1	-144.7	-82.2	-21.0	24.0	46.5	50.5	50.0
14	-153.5	-163.5	-166.1	-160.8	-125.2	-27.6	29.8	53.1	57.1	56.3
13	-161.4	-180.4	-192.8	-194.8	-164.9	-45.2	35.2	58.4	62.3	61.1
12	-155.7	-191.1	-219.3	-232.3	-194.6	-73.1	43.8	62.6	65.5	63.9
11	-124.8	-190.7	-239.4	-266.1	-218.3	-90.6	35.7	61.7	66.2	64.9
10	-80.0	-180.1	-251.0	-292.5	-234.3	-92.2	30.4	62.1	71.6	74.9
9	-49.1	-162.7	-257.3	-307.7	-241.5	-76.9	30.1	59.6	72.8	82.6
8	-46.5	-137.5	-260.2	-313.4	-241.2	-50.3	29.4	55.4	72.3	74.7
7	-55.4	-115.4	-258.8	-310.9	-234.6	-30.8	23.3	38.7	38.4	.0
6	-66.2	-113.1	-247.3	-300.8	-221.9	-27.8	11.1	23.0	.1	.0
5	-74.7	-113.0	-223.4	-281.6	-202.4	-33.7	-3.8	6.3	.0	.0
4	-76.9	-101.4	-176.2	-244.3	-176.4	-43.9	-19.0	-7.5	.0	.0
3	-72.7	-86.9	-105.3	-112.8	-128.6	-57.3	-34.3	-13.5	.0	.0
2	-51.6	-52.8	-50.1	-43.7	-19.8	-23.6	-27.7	-1.7	.0	.0

Table E.4a. Numerical Data for Fuel Temperature (DTP) at Time 0.3 s

cycle= 6000 time= .30000000 dt= .00005000

********* tp *********

41	373.0	373.0	373.0	373.0	373.0	373.0	373.0	373.0	373.0	373.0
40	373.0	373.0	373.0	373.0	373.0	373.0	373.0	373.0	373.0	373.0
39	373.0	373.0	373.0	373.0	373.0	373.0	373.0	373.0	373.0	373.0
38	373.0	373.0	373.0	373.0	373.0	373.0	373.0	373.0	373.0	373.0
37	373.2	373.2	373.2	373.1	373.0	373.0	373.0	373.0	373.0	373.0
36	373.8	373.7	373.7	373.6	373.1	373.0	373.0	373.0	373.0	373.0
35	376.5	376.3	376.1	375.8	373.3	373.0	373.0	373.0	373.0	373.0
34	388.4	387.5	386.5	385.0	374.7	373.1	373.0	373.0	373.0	373.0
33	437.2	433.1	429.0	422.9	381.1	373.7	373.0	373.0	373.0	373.0
32	602.2	588.4	574.4	553.9	410.8	376.7	373.2	373.0	373.0	373.0
31	958.9	936.0	912.8	871.7	526.7	392.0	374.2	373.0	373.0	373.0
30	1333.5	1314.7	1296.4	1257.2	839.4	461.2	379.6	373.3	373.0	373.0
29	1554.0	1544.3	1536.0	1513.7	1246.2	694.6	407.0	374.5	373.0	373.0
28	1651.8	1647.4	1644.6	1634.2	1515.1	1103.4	522.1	381.2	373.2	373.0
27	1694.2	1692.2	1691.4	1686.7	1637.2	1435.9	833.5	413.7	374.1	373.0
26	1715.0	1714.0	1713.9	1711.4	1688.7	1600.7	1226.4	535.6	378.7	373.1
25	1726.9	1726.5	1726.5	1725.0	1712.3	1670.7	1484.4	822.3	398.1	373.3
24	1735.0	1734.8	1734.9	1733.7	1725.1	1701.8	1607.1	1156.3	460.9	374.3
23	1741.2	1741.2	1741.2	1740.3	1733.2	1717.3	1661.7	1382.6	594.4	377.4
22	1746.4	1746.5	1746.6	1745.7	1739.0	1725.9	1686.2	1495.8	763.5	383.9
21	1751.2	1751.4	1751.5	1750.8	1743.5	1730.7	1695.3	1535.7	866.0	390.9
20	1755.5	1755.7	1755.8	1755.3	1746.8	1731.7	1691.2	1516.0	839.3	390.1
19	1758.8	1759.0	1759.1	1758.8	1748.2	1725.2	1661.9	1400.7	666.2	381.2
18	1761.1	1761.3	1761.5	1761.2	1744.8	1692.7	1548.3	1065.3	458.3	374.7
17	1763.1	1763.3	1763.5	1763.4	1714.2	1530.3	1130.3	544.5	381.8	373.2
16	1764.8	1764.9	1765.1	1765.1	1361.1	845.8	463.3	380.6	373.3	373.0
15	1765.8	1765.8	1766.0	1766.1	948.1	400.6	374.3	373.1	373.0	373.0
14	1767.1	1767.0	1767.2	1767.3	1003.3	378.8	373.1	373.0	373.0	373.0
13	1768.7	1768.7	1768.8	1769.0	1171.9	373.8	373.0	373.0	373.0	373.0
12	1770.2	1770.3	1770.4	1770.4	1409.2	374.4	373.0	373.0	373.0	373.0
11	1770.7	1770.7	1770.7	1770.7	1426.1	374.4	373.0	373.0	373.0	373.0
10	1771.1	1771.1	1771.1	1771.0	1385.4	373.6	373.0	373.0	373.0	373.0
9	1771.5	1771.4	1771.4	1771.3	1267.7	373.1	373.0	373.0	373.0	373.0
8	1771.8	1771.8	1771.7	1771.6	967.7	373.0	373.0	373.0	373.0	373.0
7	1772.1	1772.0	1771.9	1771.8	377.7	373.0	373.0	373.0	373.0	373.0
6	1772.3	1772.2	1772.1	1772.0	376.6	373.0	373.0	373.0	373.0	373.0
5	1772.5	1772.4	1772.3	1772.1	375.9	373.0	373.0	373.0	373.0	373.0
4	1772.6	1772.5	1772.4	1772.3	375.4	373.0	373.0	373.0	373.0	373.0
3	1772.7	1772.7	1772.6	1772.5	375.0	373.0	373.0	373.0	373.0	373.0
2	1772.8	1772.8	1772.8	1772.7	374.8	373.0	373.0	373.0	373.0	373.0

Table E.4b.Numerical Data for Fuel Temperature (DTP) at Time 0.6 s

cycle= 12000 time= .60000000 dt= .00005000

********* tp *********

41	646.5	634.3	614.7	586.5	500.4	425.0	386.6	375.3	373.2	373.0
40	1458.4	1448.9	1432.0	1398.4	1261.2	990.1	640.8	431.7	379.8	373.4
39	1570.4	1565.4	1556.3	1535.6	1453.1	1258.8	903.3	530.8	393.9	374.3
38	1631.6	1629.3	1624.9	1613.3	1569.5	1457.5	1194.3	749.4	436.6	376.9
37	1662.8	1661.8	1659.7	1653.0	1629.7	1569.8	1411.1	1034.3	544.0	385.3
36	1679.7	1679.3	1678.3	1674.1	1660.9	1628.5	1540.4	1287.8	758.5	409.5
35	1689.8	1689.7	1689.2	1686.3	1677.9	1659.1	1610.1	1459.0	1022.2	469.8
34	1696.8	1696.8	1696.5	1694.3	1688.1	1675.9	1647.1	1558.5	1253.5	596.7
33	1702.2	1702.3	1702.1	1700.2	1694.9	1686.0	1667.4	1613.5	1414.6	796.8
32	1706.9	1707.0	1706.8	1705.1	1700.2	1692.7	1679.2	1644.0	1513.6	1001.6
31	1711.0	1711.2	1711.0	1709.5	1704.6	1697.5	1686.6	1661.3	1571.5	1168.6
30	1714.7	1714.8	1714.7	1713.4	1708.5	1701.4	1691.5	1671.5	1604.4	1284.0
29	1717.7	1717.8	1717.9	1716.9	1711.8	1704.6	1694.8	1677.3	1622.2	1353.1
28	1720.3	1720.4	1720.6	1719.9	1714.5	1706.9	1696.9	1679.9	1629.6	1384.5
27	1721.8	1721.9	1722.2	1721.8	1716.8	1708.4	1697.6	1679.7	1628.1	1382.3
26	1722.7	1722.8	1723.1	1722.9	1718.4	1708.9	1696.3	1675.9	1615.8	1343.1
25	1724.0	1723.9	1724.4	1724.1	1719.3	1708.2	1692.3	1666.4	1587.2	1255.1
24	1725.1	1725.2	1725.7	1725.5	1719.8	1705.0	1682.8	1645.8	1529.3	1104.4
23	1725.6	1725.9	1726.4	1726.2	1719.0	1696.9	1660.6	1599.6	1415.0	886.2
22	1725.3	1725.7	1726.2	1725.8	1715.3	1679.2	1608.1	1496.9	1206.4	640.4
21	1724.4	1725.0	1725.4	1724.8	1709.5	1639.9	1488.5	1289.4	903.7	453.1
20	1723.1	1723.8	1724.3	1723.7	1699.4	1557.7	1253.6	963.7	607.7	390.2
19	1721.2	1722.3	1722.9	1722.0	1689.1	1409.3	925.9	637.2	430.0	376.3
18	1718.0	1719.4	1720.2	1718.9	1682.9	1211.9	648.5	446.4	387.9	373.5
17	1714.2	1716.1	1717.0	1715.5	1677.5	1063.3	500.8	403.8	376.7	373.1
16	1708.9	1711.8	1712.8	1711.2	1667.5	1057.7	484.7	396.3	374.5	373.0
15	1700.9	1705.8	1706.8	1705.0	1665.6	1194.0	560.7	409.1	375.1	373.0
14	1688.3	1697.1	1697.7	1694.9	1672.6	1394.3	782.8	450.8	377.9	373.1
13	1667.4	1684.2	1683.7	1676.8	1678.7	1540.9	1075.9	586.0	390.6	373.3
12	1630.9	1664.2	1662.2	1644.2	1668.3	1482.0	1332.3	939.0	466.2	375.4
11	1568.1	1632.4	1629.2	1586.3	1608.2	1267.2	1227.5	1178.9	735.9	390.5
10	1463.7	1578.5	1577.3	1483.8	1406.5	973.4	951.7	1015.9	910.9	427.0
9	1326.0	1478.6	1491.4	1306.1	969.7	711.6	713.8	758.7	695.3	396.6
8	1164.6	1287.0	1341.2	1034.8	720.0	559.1	549.8	560.8	515.3	386.5
7	994.4	987.8	1082.4	726.1	512.7	461.7	461.0	470.3	456.9	386.9
6	825.6	704.3	716.5	482.2	425.9	424.0	427.0	434.9	433.1	389.1
5	656.3	485.7	465.4	409.1	404.9	408.9	411.9	418.2	420.6	391.8
4	499.7	417.3	399.6	390.4	396.7	400.7	403.9	407.2	411.9	394.2
3	424.2	390.9	385.2	382.6	386.8	393.4	398.5	402.5	404.9	395.4
2	379.3	378.4	377.6	377.1	378.1	381.5	390.7	398.3	401.4	394.9